2013

The Effect of Mechanical Cues on In Vitro Aging and Differentiation of Human Mesenchymal Stem Cells

Courtney Eileen LeBlon
Lehigh University

The Effect of Mechanical Cues on *In Vitro* Aging and Differentiation of Human Mesenchymal Stem Cells

by

Courtney Eileen LeBlon

Presented to the Graduate and Research Committee

of Lehigh University

in Candidacy for the Degree of

Doctor of Philosophy

in

Mechanical Engineering

Lehigh University

September 2013

Approved and recommended for acceptance as a dissertation in partial fulfillment of the requirements for the degree of Doctor of Philosophy

_____
Date

_____
Dr. Sabrina S. Jedlicka
Committee Chairman and Dissertation Advisor

_____
Accepted Date

Committee Members:

_____
Dr. John P. Coulter
Dissertation Co-Advisor

_____
Dr. Xuanhong Cheng

_____
Dr. Svetlana Tatic-Lucic

_____
Dr. Xiaohui Zhang

TABLE OF CONTENTS

List of Figures

List of Tables

Acknowledgments

First and foremost, I would like to thank my family and my boyfriend, Scott, for their constant support. I would like to thank my advisor, Dr. Sabrina Jedlicka, for her technical guidance and encouragement. I would also like to thank my committee members: Dr. John Coulter, Dr. Xiaohui Zhang, Dr. Svetlana Tatic-Lucic, and Dr. Xuanhong Cheng, for supporting my research and advising me. I'd especially like to acknowledge Dr. Xiaohui Zhang for the use of his atomic force microscope. I am very appreciative of the time he took to train me and assist me with my project. I would also like to thank Bill Muschock for his assistance with scanning electron microscopy, and Dr. Raymond Pearson for the use of his polymer characterization equipment. Last but not least, I'd like to thank my fellow graduate students who have helped me throughout this process, especially Meghan Casey, and the undergraduates who have assisted me with my research.

The research was supported by NSF Lehigh Valley STEM Partnership for GK-12 Teaching Fellows: Widening the Pipeline; Grant #0638664, NSF CMMI Grant #1014987, and the Lehigh University Faculty Innovation Grant (2009-2010). In addition, the qRT-PCR instrument was provided through an in-kind donation to Lehigh University from BD.

Abstract

Tissue engineering is a field that aims to replace or repair damaged tissue through the use of stem cells, biomaterials, and biomolecules. Human mesenchymal stem cells are multipotent adult stem cells that can be autologously transplanted. This work describes the effect of mechanical cues on human mesenchymal stem cells. An analysis on the age-related stiffening of these cells, and its effect on osteogenic and myogenic differentiation, is presented. This study gives insight to those using stem cells *in vitro* for extended periods of time. The effect of mechanical loading on stem cell differentiation is examined. Tensile and compressive loading are used to induce myogenic and osteogenic differentiation, respectively, in the absence of chemical cues. This study demonstrates that loading alone can accelerate differentiation. A 3-D cell culture method for cardiomyocyte differentiation is also explored. Numerous cardiomyocyte markers were observed, signifying that this method may be superior to chemical induction methods. A biodegradation study of four porous polymers is also presented, as scaffold choice is of great importance in the area of tissue engineering. This research provides guidance to those using human mesenchymal stem cells for tissue engineering.

Chapter 1: Introduction

1.1 Introduction to Tissue Engineering

The goal of tissue engineering is to replace or regenerate damaged tissue. This field combines stem cells, biomaterials, and biochemical factors. The stem cell type should be easy to obtain, expandable in culture, and should not cause an inflammatory response when implanted *in vivo*. There are three main classes of stem cells: embryonic stem cells (ESCs), induced pluripotent stem cells (iPSCs) and adult stem cells. ESCs are derived from the inner cell mass of a blastocyst. ECSs are not autologous, and therefore could elicit an immune response. ESCs are able to differentiate into all three germ layers [1,2], but are not easily obtained and have ethical concerns surrounding them. iPSCs are adult cells that have been reprogrammed using genetic engineering techniques [3]. The main concern with iPSCs is the risk of tumor formation after implantantion [4]. Adult stem cells include hematopoietic stem cells, which give rise to the blood cell lines [5], and mesenchymal stem cells (MSCs), which can differentiate into various lineages [6-18]. MSCs are of particular interest because of their relative ease of isolation, lack of ethical concern, and potential for autologous transplant.

MSCs are found in bone marrow [19], umbilical cord blood [20], adipose tissue [21], and other various tissues (Figure 1), although bone marrow MSCs are the most widely studied. MSCs classically differentiate into lineages from the mesoderm (bone, cartilage, fat, tendon, muscle), but may also be able to transdifferentiate into cells from other germ layers, including neurons [6-18]. By definition of the International Society of Cellular Therapy, MSCs are adherent cells that positively express cell surface

markers CD73 (SH2), CD90, and CD105 (SH3) and negatively express CD34, CD45, CD14 or CD11b, CD79α, or CD19 and HLA-DR, and are able to differentiate into osteoblasts, adipocytes, and chondrocytes [22]. While human MSCs (hMSCs) have the advantage that they can be autologously transplanted, they are also a potential candidate for safe allogenic transplant due to their immunosuppresive properties. Specifically, they lack the surface expression of human leukocyte antigen (HLA) class II molecules and the expression of costimulatory molecules for T cell induction (CD40, CD40 ligand, and the B7 molecules CD80 and CD86) [23].

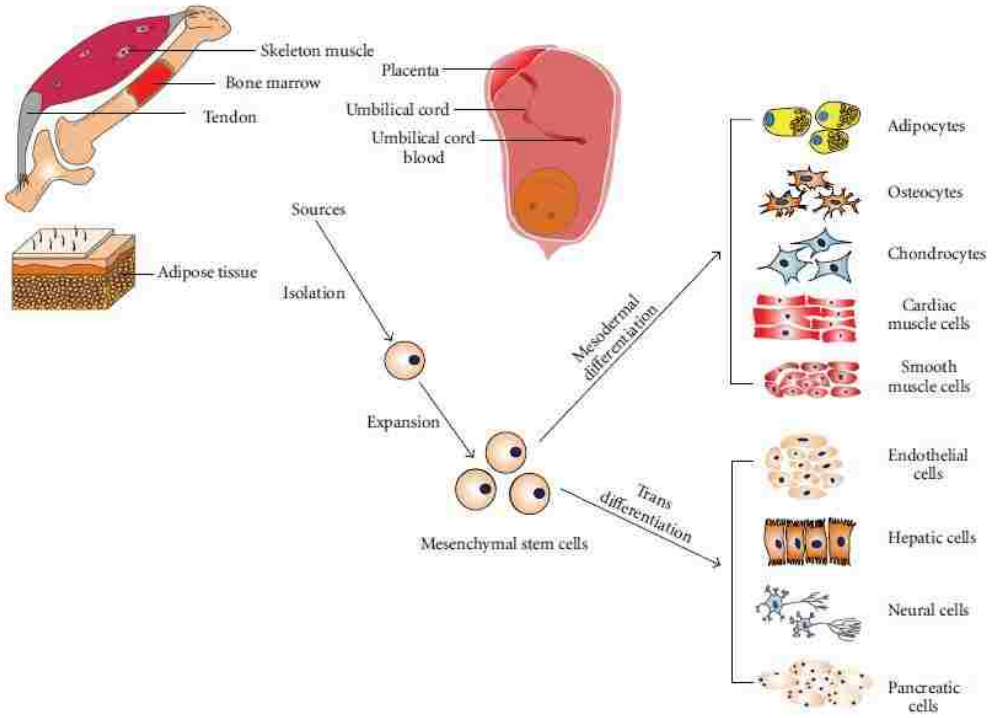

Figure 1: Isolation sites and lineages of MSCs [24]

hMSCs have been used in clinical trials for a variety of conditions, including osteogenesis imperfecta [25], cartilage repair [26], large bone defect [27], and improvement of cardiac function after a heart attack [28]. However, it is unclear whether the improvement of various conditions is due to differentiation after implantation, cell fusion, or the bioactive molecules secreted by hMSCs (which can stimulate angiogenesis and inhibit apoptosis), or a combination of these factors [29,30]. While the method of repair *in vivo* remains to be elucidated, it is apparent that hMSCs are of large significance to the tissue engineering field.

Besides cell choice, another important factor of tissue engineering is material choice. Stem cells can be grown on a natural or synthetic scaffold *in vitro* and then implanted in the body [31]. While cells can also be injected, a scaffold provides mechanical support for the cells. If a scaffold is chosen, it must be biodegradable and biocompatible. Common scaffold production methods include solvent casting/particulate leaching [32], electrospinning [33], and thermally induced phase separation [34]. Porous scaffolds have benefits over nonporous, as pores allow cell ingrowth and a 3-D environment. The mechanical properties and topographical features of the scaffold are of great importance, as cells can "feel" the substrate or extracellular matrix on which they reside [35].

1.2 Introduction to Mechanotransduction

The process by which cells sense and respond to mechanical signals is called mechanotransduction [36]. The cell's key players of mechanotransduction are the

extracellular matrix (ECM), cytoskeleton, transmembrane integrin receptors, and signaling molecules [37,38]. The ECM provides support for cells and is comprised of various proteins, including fibronectin, collagen, laminin, hyaluronic acid, and numerous proteoglycans [39]. The cytoskeleton is made up of actin filaments, intermediate filaments, and microtubules, and is responsible for cell shape, motility, division, and intracellular trafficking. Integrins are a family of heterodimers comprised of α and β subunits. There are at least 18 α and 8 β subunits, which can produce 24 different heterodimers, each of which binds to specific ligands [40]. Cells attach to substrates by forming focal adhesions, where integrins cluster and attach to actin filaments by proteins such as talin, tensin, and vinculin (Figure 2) [41].

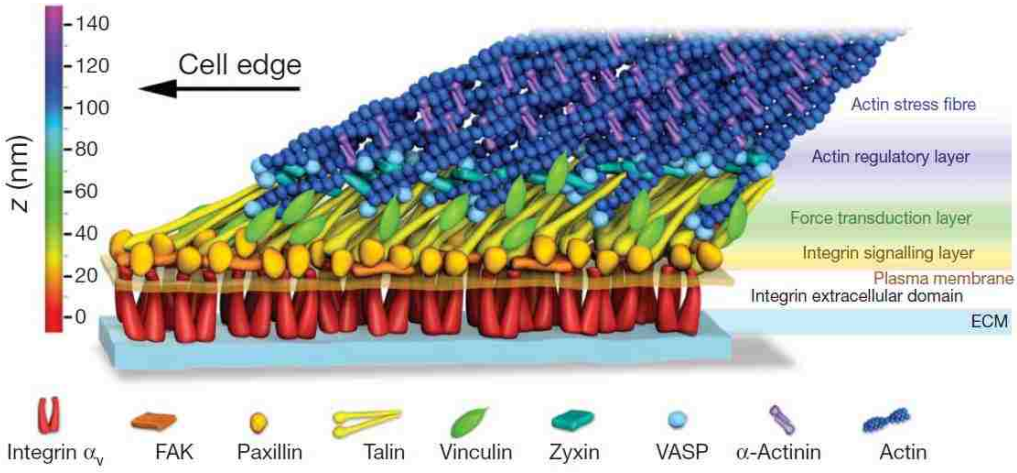

Figure 2: Schematic of the nanoscale architecture of a focal adhesion [42]

In vitro, mechanical cues can direct many aspects of cell function, including cell migration [43-45], proliferation [46], the regulation of disease states [37], and stem cell

differentiation [47,48]. One cue that can direct cells is substrate stiffness, which has been shown to dictate differentiation, functionality, and the cells' own mechanical properties. Engler et al. showed that myoblasts and cardiomyocytes organize and function optimally on substrates that have similar elasticity to their native tissue [47,49]. Engler et al. also differentiated hMSCs into neurogenic, myogenic, and osteogenic cells solely based on matrix stiffness [48]. However, it should be noted that differentiation also depends on ligand presentation. hMSCs were able to differentiate into osteoblasts on stiff polyacrylamide gels (80 kPa) when they were coated with collagen 1 (the main collagen type present in bone), but not with collagen IV, fibronectin, or laminin [50]. In opposition to stiffness-mediated differentiation, MSCs were able to remain quiescent on substrates with a stiffness that mimics bone marrow (250 Pa) [51]. Additionally, the mechanical properties of cells can also be modulated by the substrate. hMSCs exhibited lower elastic modulus values when grown on polydimethylsiloxane (PDMS) ($E \approx 3$ MPa) vs. TCPS ($E \approx 2$ GPa) [52].

Another mechanical cue that can be used to direct stem cell differentiation and alignment is topography at the nano- and micro-scale. hMSCs were grown on PDMS with microprinted collagen I features in both square and rectangular shapes. It was found that not only did the rectangular collagen I features elongate the cells, but they also caused the upregulation of myogenic markers (as muscle cells are typically elongated) [53]. At the nano-scale, Yim et al. used 350nm gratings on PDMS to align and stimulate neuronal differentiation of hMSCs. The expression of neuronal markers was higher in the cells on the nano-features compared to chemical induction on

unpatterned surfaces [54]. Therefore, both nano- and micro-sized features can guide hMSCs.

Differentiation can also be controlled by cell shape, which is modulated by cytoskeletal tension. hMSCs in mixed adipogenic/osteogenic media that are confined to a round shape by micropatterned fibronectin displayed lipid droplets (a marker of adipocytes). On the other hand, hMSCs that were able to spread on larger, square patterns and form stress fibers displayed alkaline phosphatase, a marker of osteoblasts [55]. Additionally, hMSCs were more likely to exhibit an adipogenic phenotype on micropatterns with rounded edges (flower shape) and an osteoblastic phenotype on a micropattern with straight edges (star shape) when grown in mixed osteogenic/adipogenic media, due to differences in cytoskeletal tension [56]. The impact of cell shape in differentiation is largely controlled by the Rho GTPase RhoA, as a rounded cell decreases RhoA and induces adipogeneis, while a spread cell increases RhoA and induces osteogenesis [55]. Gao et al. examined the effect of transforming growth factor β (TGF-β) (which can induce both chondrogenesis and myogenesis) and cell shape on hMSC differentiation. Cells on round micropatterns upregulated a chondrogenic marker, collagen II. Conversely, cells on larger, square micropatterns, as well as cells on unpatterned surfaces, were allowed to spread and upregulated a smooth muscle marker, calponin (Figure 3) [57]. These studies demonstrate the effect of cell shape on lineage determination between adipogenesis, chondrogenesis, osteogenesis, or myogenesis in hMSCs.

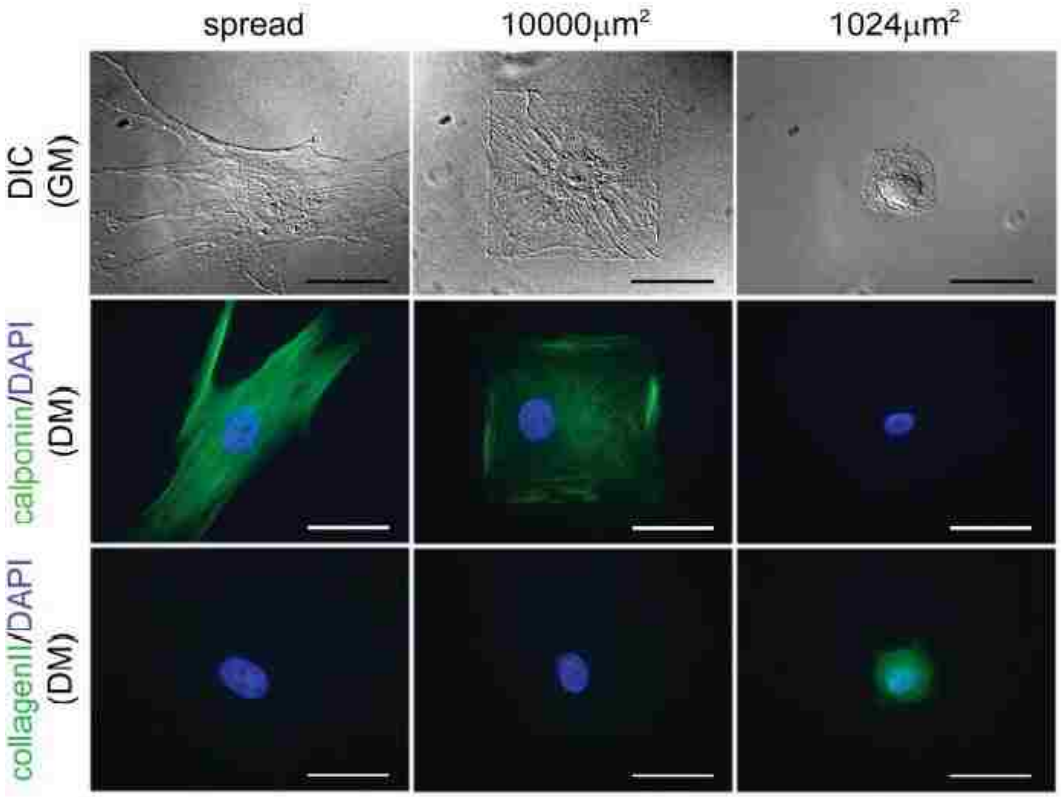

Figure 3: Expression of myogenic marker, calponin, when confined to a square shape, and to a higher degree, when allowed to spread and elongate. Conversely, a chondrogenic marker, collagen II, was expressed when cells were confined to a round shape [57]

The Rho GTPases play a large role in cell signaling and cytoskeleton arrangement. Of the Rho GTPases, Cdc42, Rac1, and RhoA are the most widely studied. Cdc42 affects filopodia (small cell projections), Rac1 controls lamellopodia (projections at the leading edge of the cell), and RhoA controls stress fibers (bundles of actin) [58]. These Rho GTPases seem to play large roles in the lineage specification of MSCs (Figure 4). As previously mentioned, Rho may play a role in the adipogenesis/myogenesis cell fate decision, as reduced Rho activity leads to adipogenesis, while increased Rho activity leads to myogenesis [55,59]. RhoA's

downstream effector Rho Kinase (Rock) mediates cytoskeletal tension, and was shown to induce osteogenesis in hMSCs independent of cell shape [55]. Additionally, Rac1, which tends to oppose the action of RhoA, has been implicated in chondrogenesis and adipogenesis [57,60]. In conclusion, Rho, Rac1, and Rock mediate cell fate in MSCs.

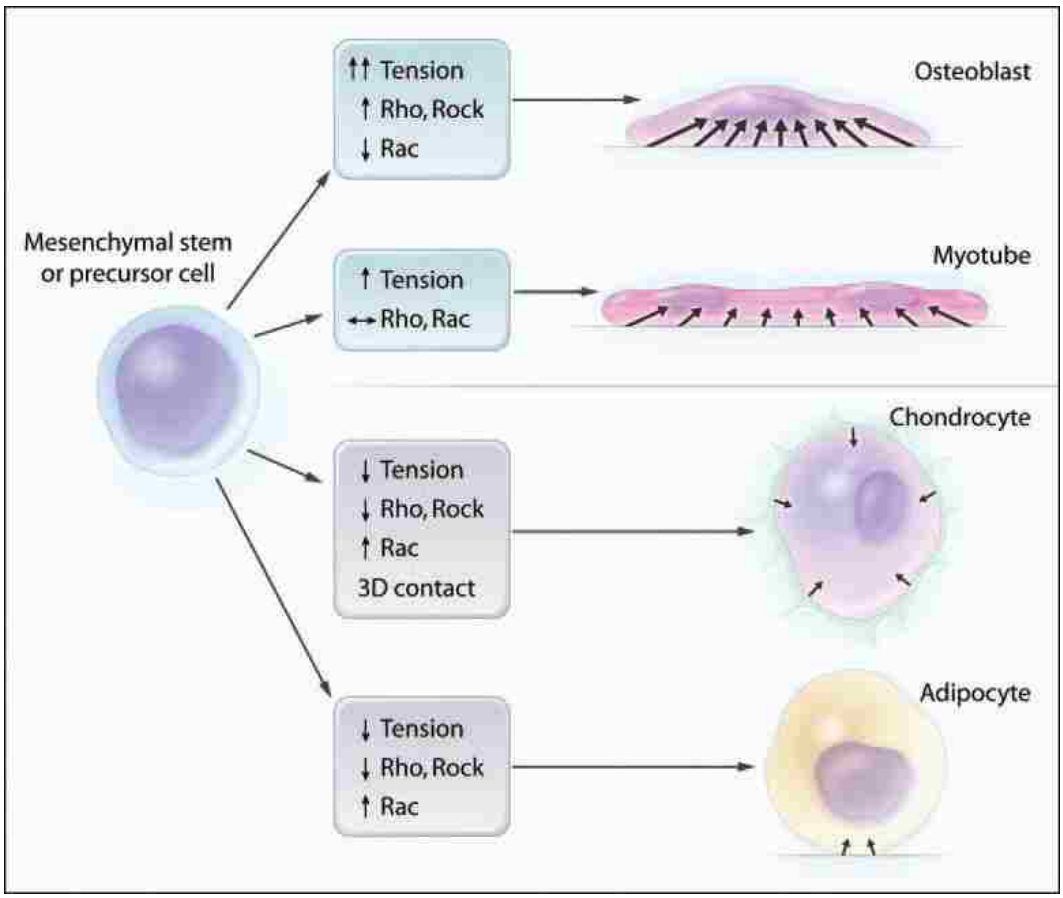

Figure 4: Involvement of Rho GTPases in MSC lineage determination [61]

1.3 Systems for biomechanical measurements

Many systems have been developed for measurements of cellular mechanical properties, including optical tweezers [62], micropipette aspiration [63], and atomic force microscopy (AFM) [64]. The chosen method depends on the amount of force and deformation required, the type of cell, and level of force application (cell population, single cell, or single molecule). Further, the chosen model depends on the technique and the cell type, i.e. some techniques/models are better suited for nonadherent cells, such as erythrocytes, as opposed to adherent cells. Models for cell mechanics are generally grouped as continuum models or micro/nano-structural models. Examples of continuum models are elastic and viscoelastic solid models. On the other hand, an example of a micro/nano-structural model is tensegrity, where actin filaments and intermediate filaments are assumed to be in tension, and microtubules oppose compressive forces [65]. The methods and models most relevant to hMSCs are discussed below.

Micropipette aspiration is a technique used to measure time-dependent deformation of living cells [63]. A cell is pulled into a micropipette and the extension of the cell is measured by optical microscopy (Figure 5). The diameter of the glass tube is chosen relative to the cell size and the applied pressure can range from 0.1-1000 Pa. The force (F) can be calculated, using the pressure, radius of the micropipette, and the velocities of the cells in the presence and absence of pressure. Micropipette aspiration has the benefits of loading an entire cell and eliminating the cell-matrix interactions. Both linear elastic and viscoelastic solid models have been applied to micropipette

aspiration. A linear elastic solid model neglects the time factor, and can be modeled as a spring, by the equation:

$$\sigma = E\varepsilon \tag{1}$$

Where σ is the applied stress, ε is the resulting strain, and E is the elastic modulus. When the micropipette radius is much smaller than the radius of the cell, the cell can be considered an incompressible half space, and the projection length is:

$$L = \frac{R\Phi_p \Delta p}{2\pi G} \tag{2}$$

Where G is the shear modulus and Φ_p is a function of the pipette geometry (wall thickness and radius) [66].

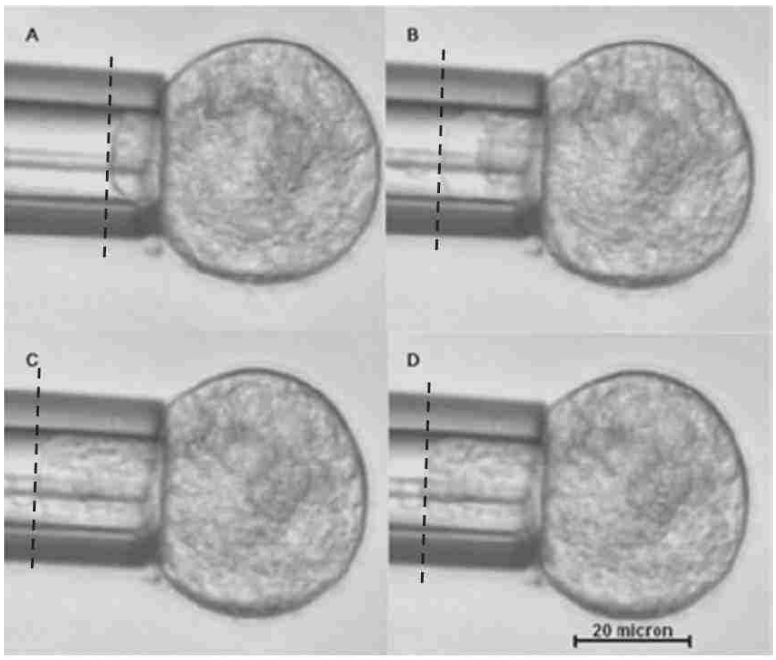

Figure 5: Micropipette aspiration of hMSCs at A) 1s, B) 15s, C) 100s, and D) 200s [67].

However, a linear elastic model is generally inadequate to describe cell mechanics and a viscoelastic model may be a more suitable choice, as cells are inherently viscoelastic. A homogeneous viscoelastic standard linear solid model was proposed to study the response of human leukocytes to micropipette aspiration [68]. It is modeled as a spring and dashpot in series that are parallel to another spring (Figure 6).

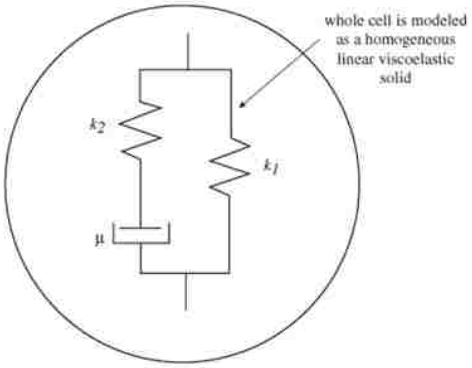

Figure 6: Homogenous standard linear solid model can be applied to a cell [69]

This model has the constitutive equation:

$$\frac{d\varepsilon}{dt} = \frac{\frac{k_2}{\eta}\left(\frac{\eta\, d\sigma}{k_2\, dt} + \sigma - k_1\varepsilon\right)}{k_1 + k_2} \tag{3}$$

Where k_1 and k_2 are elastic constants, and η is a viscous constant. The creep compliance is given by:

$$J(t) = \left(\frac{1}{k_1+k_2}\right) + \frac{k_2}{k_1}\left(\frac{1}{k_1+k_2}\right)\left(1 - e^{-\frac{t}{\tau}}\right) \tag{4}$$

The exponential time constant is:

$$\tau = \frac{\eta(k_1+k_2)}{k_1 k_2} \tag{5}$$

Using the following substitution relating creep compliance and shear modulus, the aspiration length using the standard linear solid model can be derived from the elastic solution:

$$J(t) = \frac{1}{2G} \tag{6}$$

$$L(t) = \frac{R\Phi_p \Delta p}{\pi k_1}\left[1 - \frac{k_2}{k_1 + k_2} e^{-\frac{t}{\tau}}\right] \quad (7)$$

The instantaneous Young's modulus (E_0) and equilibrium Young's modulus (E_∞) can be calculated as:

$$E_0 = \frac{3}{2}(k_1 + k_2) \quad (8)$$

$$E_\infty = \frac{3}{2} k_1 \quad (9)$$

Besides the standard linear solid model, various liquid drop models have also been applied to micropipette aspiration. These models represent the cell membrane as a shell and the cytoplasm as a viscous liquid [70]. Liquid drop models are most appropriate for cells that demonstrate liquid behavior (i.e. leukocytes, neutrophils) [63]. While micropipette aspiration is a tool commonly used for non-adherent cells, it may also be used to determine the mechanical properties of adherent cells in suspension.

AFM is a technique that can be used to indent living cells with pN forces. It is reviewed in great detail in Section 2.3.2. In general, values of elastic modulus are found to be higher with AFM compared to micropipette aspiration. For example, reported modulus values of hMSCs with AFM are 1-40 kPa [71-73] and <1 kPa with micropipette aspiration [74]. The AFM also determines local cell properties (and underlying effects of the nucleus, stress fibers, etc.), while micropipette aspiration reflects whole cell properties in a suspended state. The Hertz elastic contact model is frequently used to find the elastic modulus of a cell, and is based on indenter radius (R),

force applied (F), indentation depth (δ), and Poission's ratio (ν) (assumed to be 0.5 for cells) [75]:

$$F = \frac{4E\delta^{\frac{3}{2}}\sqrt{R}}{3(1-\upsilon^2)} \tag{10}$$

The classical model relates the indentation of two spheres, but this model has also been extended to indenters of conical shapes (where α is the half opening angle of the tip) [76]:

$$F = \frac{2E\delta^2 \tan\alpha}{\pi(1-\upsilon^2)} \tag{11}$$

While this model makes many assumptions which are not valid for cells (isotropic, linearly elastic, and infinitely deep), it fits well at small deformations. However, precautions must be taken when using this model. The sample indentation should be <10% to neglect the effect of the cell substrate [77] and slow indentation speeds (<10 um/s) should be utilized to minimize viscous effects [78]. Variations of the Hertz model have been created for different cell shapes [79] and for thin samples [80]. While the elastic Hertz model may not be entirely suitable for cells, some improvements have been made to account for cell shape and height.

A viscoelastic solution to the Hertz model has also been derived, assuming small indentations of an isotropic, incompressible surface by a hard, spherical indenter [81]:

$$F(t) = \frac{4E_R\sqrt{R}{\delta_0}^{\frac{3}{2}}}{3(1-\upsilon)}\left(1 + \frac{\tau_\sigma - \tau_\varepsilon}{\tau_\varepsilon}e^{-\frac{t}{\tau_\varepsilon}}\right) \tag{12}$$

Where E_R is the relaxed modulus, τ_σ is the time of relaxation of deformation under constant load, and τ_ε is time of relaxation of load under constant deformation. Darling et al. performed 60 s relaxation tests on cells, and applied the Hertz model to the approach to determine the elastic behavior and the above equation to the relaxation data to determine the viscoelastic behavior. Fitting the above equation to the force-displacement curve provides three parameters that describe a standard linear solid viscoelastic model (Figure 6), where k_1 and k_2 are elastic constants and η is a viscous constant:

$$k_1 = E_R \tag{13}$$

$$k_2 = E_R\left(\frac{\tau_\sigma - \tau_\varepsilon}{\tau_\varepsilon}\right) \tag{14}$$

$$\eta = E_R(\tau_\sigma - \tau_\varepsilon) \tag{15}$$

The instantaneous modulus (E_0) and Young's modulus (E_Y) can then be calculated:

$$E_0 = E_R\left(1 + \frac{\tau_\sigma - \tau_\varepsilon}{\tau_\varepsilon}\right) \tag{16}$$

$$E_Y = \frac{3}{2}E_R \tag{17}$$

Therefore, the viscoelastic behavior of cells can be found by AFM using the appropriate tests and model.

Optical tweezers are a tool that uses a laser beam with an objective lens of high numerical aperture to apply forces to cells [82]. This method was used to determine the

membrane tether length in hMSCs [83]. Fluorescent polystyrene beads (diameter=0.5 μm) were attached to cells using an anti-CD29 (MSC cell surface marker) antibody. An elastic spring equation was used to determine the force applied to the bead by the optical tweezers:

$$F = -kx \tag{18}$$

where k is the stiffness of the optical tweezers and x is the displacement of the bead. The bead was pulled from the membrane until the bead escaped, and the tether length and escape force were recorded. The average tether length and escape force for hMSCs was 10.6±1.1 μm and 9.7±0.7 pN, compared to 3.0±0.5 μm and 8.8±0.5 pN for fibroblasts, respectively. This difference was attributed to increased membrane reservoir in hMSCs [83]. Suspended hMSCs were also examined using optical stretching, a variation of optical tweezers (Figure 7) [71]. The best fit was found with the offset power law (compared to 3 and 4 element viscoelastic models):

$$\varepsilon(t) = At^{a_S} + B \ (t_0 \leq t \leq t_1) \tag{19}$$

$$\varepsilon(t) = \varepsilon(t_1) - C(t - t_1)^{a_R} \ (t_1 < t \leq t_2) \tag{20}$$

where cells were stretched from t_0 to t_1, and allowed to recover until t_2. A and C are fitted prefactors, B is the offset constant, and a_S and a_R are the exponents for stretching and recovery, respectively. Results show that hMSCs exhibit power law rheology during both stretching and recovery, where A, B, and C were 3.45, -1.32, and 0.79, respectively. The stretching and recovery could be described by a single exponent, a_S and a_R = 0.256. Interestingly, this study showed that while differences in mechanical properties (increased elastic modulus) were observed during extended passaging in

adherent cells, no changes in creep behavior were observed in suspended cells during extended passaging [71].

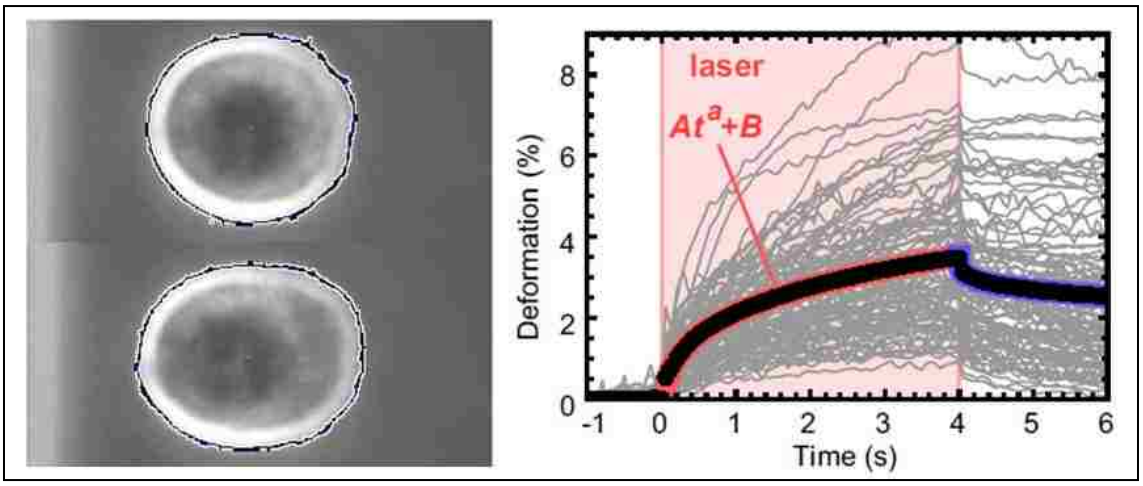

Figure 7: Optical stretching of hMSCs (left). Deformation during stretching and recovery (right) [71].

The use of these techniques has been complemented by the use of reagents to disrupt or stabilize components of the cytoskeleton. For example, cytochalasin D is a reagent that disrupts actin fibers. When hMSCs were treated with 20 µM cytochalasin D, instantaneous modulus and elastic modulus decreased by 42–66% and viscosity increased by 95%. This caused a significant increase in aspiration length during micropipette aspiration (Figure 8) [67]. Titushkin et al. subjected hMSCs to cytochalasin D or nocodazole (which prevents microtubule polymerization), and found the elastic modulus using AFM. The elastic modulus decreased more than 75% when actin fibers were disrupted, but no statistically significant difference was observed when microtubules were disrupted [72]. Methyl-b-cyclodextrin was used in the aforementioned study of hMSC tether length by optical tweezers. Methyl-b-

cyclodextrin depletes cholesterol, which is known to decrease membrane stiffness. After treatment, the membrane tether length increased from was 10.6±1.1 μm to 16.6±1.9 μm [83]. The use of these reagents gives insight into the effect of various cytoskeletal components on mechanical properties.

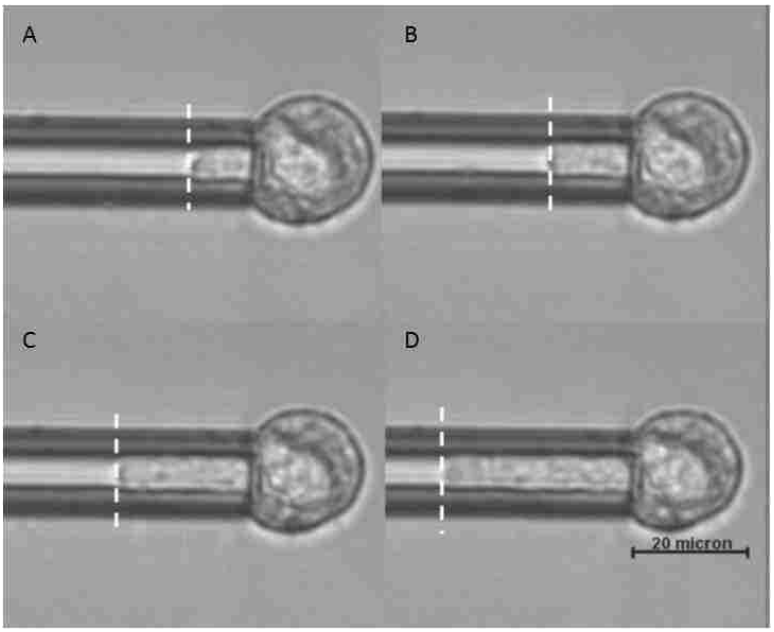

Figure 8: Micropipette aspiration of hMSCs treated with μM cytochalasin D at at A) 1s, B) 15s, C) 100s, and D) 200s. The disruption of actin filaments causes a significant increase in aspiration length compared to control [67].

1.4 Outline of Dissertation

Chapter 2 is an investigation of the change in elastic moduli of hMSCs during *in vitro* aging, and how this change relates to differentiation capacity. *In vitro* aging is an important subject since hMSCs are routinely cultured for extended periods of time on

tissue culture polystyrene (TCPS), and there are currently no standards for this practice. This study illustrates the effects of long-term culture on hMSC mechanical properties and differentiation.

Chapter 3 explores the effects of cyclic mechanical loading on hMSC differentiation. Chemical induction is the most common method of hMSC differentiation, but mechanical forces may more accurately mimic the *in vivo* environment. Cells were grown on 3-D porous polymer scaffolds and subjected to tensile and compressive loading to stimulate myogenesis and osteogenesis, respectively. Results demonstrate that differentiation can be accelerated by short-term loading.

Chapter 4 describes the use of a 3-D cell culture method for hMSC cardiomyocyte differentiation. In line with the previous chapter, there is a need for differentiation methods that do not require chemical induction. This chapter uses a cell aggregation method that can produce aligned cells that express cardiomyogenic markers, and may provide a clinical alternative to current methods.

Chapter 5 is an *in vitro* biodegradation study of 4 polymers commonly used in tissue engineering and biomedical applications. The study was conducted on 3-D porous foams, as there was a lack of knowledge about the effects of porosity on biodegradation. Common polymer characterization methods were used to examine the mechanical, thermal, chemical, and morphological characteristics during a 16 week period. Results may be useful to the tissue engineering community that requires different degradation time lengths for different applications.

Chapter 6 provides a conclusion of the dissertation, which includes a summary of the conducted research, as well as a description of future recommended studies.

Chapter 2: Effect of *In Vitro* Aging on Mechanical Properties and Differentiation Capacity of Human Mesenchymal Stem Cells

2.1. Chapter Overview

hMSCs are an attractive cell source for tissue regeneration, given their self-renewal and multilineage potential. hMSCs were cultured and routinely passaged on TCPS to investigate the correlation between cell stiffening and differentiation capacity during *in vitro* aging. Local cell elastic modulus was measured at every passage using AFM indentation. At each passage, osteogenic and myogenic differentiations were carried out. Gene and protein expression was examined using quantitative reverse transcriptase polymerase chain reaction (qPCR) and immunofluorescent staining, respectively, for osteogenic (osteocalcin, osteonectin, osteopontin, alkaline phosphatase, Runx2, collagen 1) and myogenic (tropomyosin, sarcomeric actin, smooth muscle α actin, β-myosin heavy chain, calponin 1, troponin T, desmin) markers. Results show that the success of myogenic differentiation is highly reliant on the elastic modulus of the undifferentiated cells, and peaks when the elastic modulus of the undifferentiated cells is closest to that of native muscle. The success of osteogenic differentiations appears to be somewhat dependent on the cell elastic modulus, as differentiations were more successful in earlier passages, when cells exhibited a lower endogenous elastic modulus. This is the first study that links the average elastic modulus of a population of hMSCs to their differentiation success in long-term culture, as well as the first report of myogenic potential during aging. This study elucidates some of the age-related changes

of hMSCs, and provides guidance for those utilizing adult stem cells for tissue engineering.

2.2. Introduction

hMSCs are adult stem cells that can differentiate into different lineages, including bone, cartilage, fat, tendon, muscle, and possibly neurons [6-18]. They have the ability to proliferate in culture while retaining their multilineage potential. Because of their multipotency, hMSCs have great potential for regenerative medicine and tissue engineering. However, MSCs only represent 0.001% to 0.01% of cells in bone marrow [84]. To have an adequate amount for therapeutic use, hMSCs must be expanded *in vitro*.

TCPS is the standard growth substrate in cell culture laboratories and has an elastic modulus is approximately 3 GPa. This is several orders of magnitude stiffer than values for cells, which are typically in the kPa range [71,72,85,86]. Therefore, this substrate may not be ideal for stem cell maintenance. It is known that hMSCs are subject to *in vitro* aging, which is hallmarked by telomere shortening, slowed proliferation, and decreased differentiation capacity [71,87-91]. Bonab et al. studied the osteogenic and adipogenic differentiation potential of expanded hMSCs. By the 10th passage *in vitro*, 20% and 60% of the samples lost their osteogenic and adipogenic differentiation potential, respectively [87]. Aging *in vitro* is accompanied by changes in the mechanical properties of hMSCs, most likely due to stiff *in vitro* culture substrates, as it has been shown that the elasticity of hMSCs can be modulated by growth substrate

[52]. AFM indentation is commonly used to measure the elasticity of live cells [64,77,92]. Maloney et al. used AFM to indent hMSCs maintained on TCPS over 17 population doublings and saw the elastic modulus increase from approximately 2 kPa to 8 kPa [71]. That study also found that the differentiation potential for both osteogenic and adipogenic differentiation reduced between population doublings 4 and 14. It seems evident that cell culture conditions contribute to the *in vitro* aging effects of cell stiffening and decreased differentiation capacity.

This study examines how differentiation capacity changes with elastic modulus of undifferentiated hMSCs in extended culture. AFM was used to quantify cell elastic modulus over many *in vitro* passages. At each passage, osteogenic and myogenic differentiations were carried out. While most aging studies have used mineralization assays to assess osteogenic differentiation success [10,87,88,90,93,94], this study examines the protein and mRNA expression of various lineage-specific markers at each passage. Additionally, the success of myogenic differentiation over various passages has not been studied until now. Our results show that the average elastic modulus of a population of hMSCs dictates their osteogenic and myogenic differentiation success in extended culture.

2.3.Experimental Details

2.3.1. Cell culture

Adult hMSCs (PT-2501, Lonza, Walkersville, MD) were cultivated on TCPS dishes in Mesenchymal Stem Cell Basal Medium supplemented with Mesenchymal

Stem Cell Growth Media (MSCGM) SingleQuots (Lonza). When cells reached 70% confluency, they were passaged at a 1:6 dilution (approximately 1000 cells/cm^2). Cells were directed down the osteogenic and myogenic lineages from passage 4 (P4) to P9. To induce osteogenic differentiation, hMSCs were incubated in osteoinductive media for 4 weeks. Osteoinductive media contained Dulbecco's Modified Eagle Medium (DMEM) Low Glucose with L-glutamine, glucose, and sodium pyruvate (HyClone Laboratories, Logan, UT) supplemented with 10% fetal bovine serum (FBS) (HyClone Laboratories), 0.1μM dexamethasone (EMD Millipore, Billerica, MA), 10 mM β glycerol phosphate (Sigma Aldrich, St. Louis, MO), and 0.05 mM ascorbic acid (Acros Organics, Morris Plains, NJ). To induce myogenic differentiation, 5 mM 5-azacytidine (MP Biomedicals, Solon, OH) was added to media (DMEM Low Glucose, 10% FBS) once a week for 24 hours. This procedure was repeated for 4 weeks.

2.3.2. AFM indentation

The AFM was developed in 1986 [95], and was originally used as a tool to characterize the topography of surfaces. It can also be used for force spectroscopy, to measure the mechanical properties of biological specimens and adhesive forces between molecules. The AFM utilizes a cantilever with a tip that can indent or scan surfaces. A piezoelectric translator allows for vertical movement with sub-nanometer resolution. The cantilever deflection is measured by focusing a laser on the cantilever. The light is reflected off the cantilever and detected by a photodetector (Figure 9). The photodetector records the voltage as a function of piezoelectric displacement. Silicon or

silicon nitride probes are commonly used. For indentation of biological samples, probes with a spring constant of 10-200 pN/nm are preferred [96].

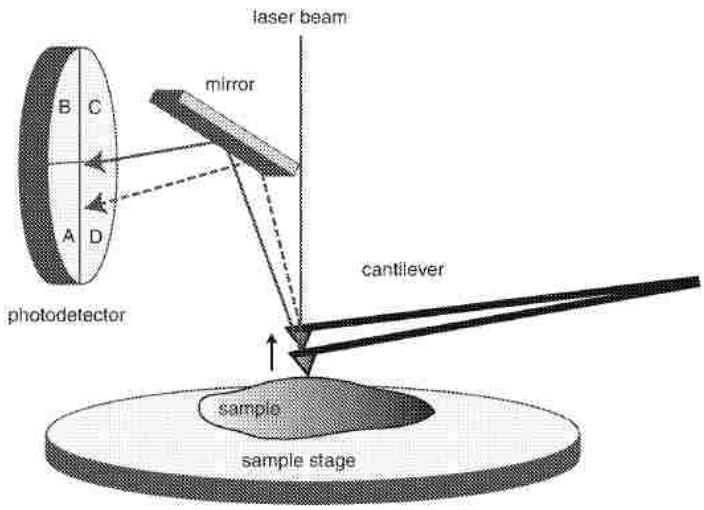

Figure 9: Diagram of the AFM [97]

Prior to indentation, the optical lever sensitivity and spring constant of the tip must be calibrated. The cantilever sensitivity (C) (m/V) is found by pressing the tip onto a hard surface and measuring the slope of the force-distance curve (Figure 10). A typical slope (C) is $1*10^{-7}$, or 100nm/V.

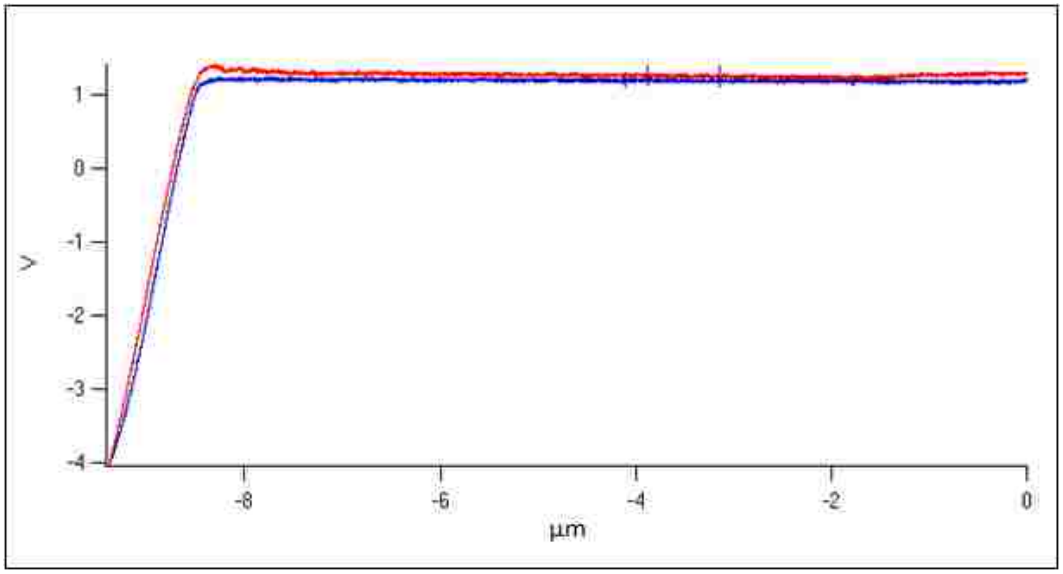

Figure 10: Cantilever sensitivity

The spring constant is calculated by submerging the cantilever in buffer (or other media used during force spectroscopy) and finding the thermally induced fluctuation. To do this, a sample scan is recorded (Figure 11).

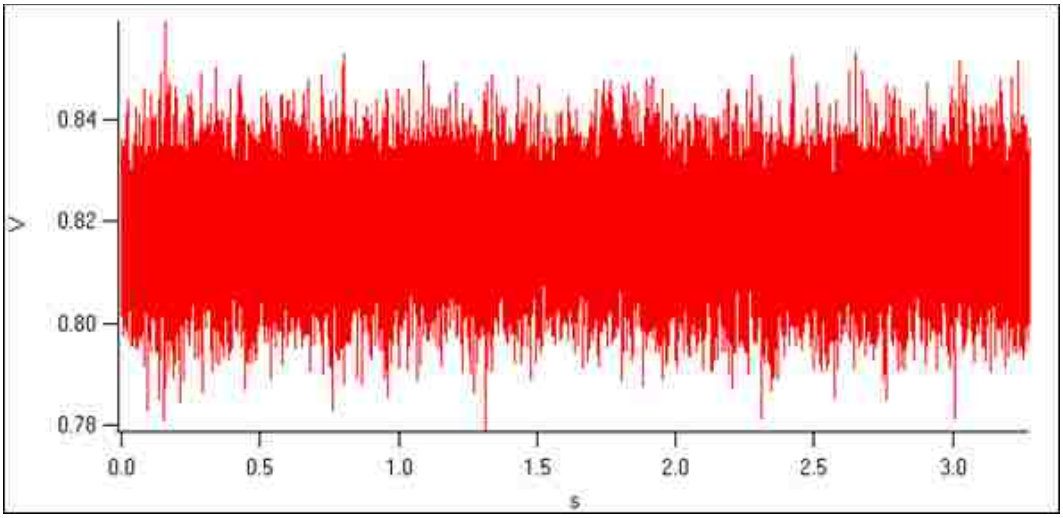

Figure 11: Sample scan to record thermal fluctuation.

From the sample scan, a power spectral density can be calculated (Figure 12). The area of the spectral density is equal to the mean square displacement of the cantilever.

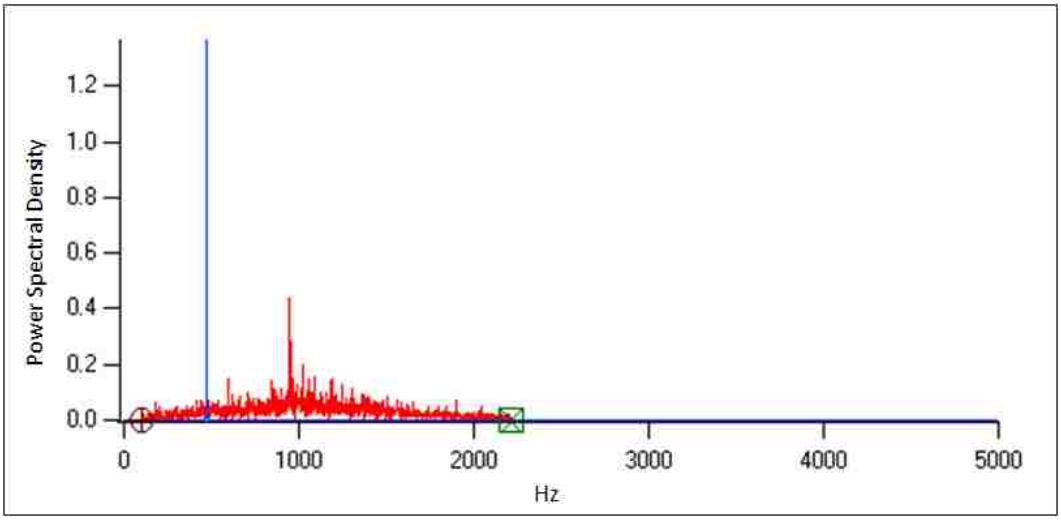

Figure 12: Power spectral density

The equipartition theorem can be applied to equate the elastic potential energy to the thermal energy, if it is assumed that cantilever response is linear and with one degree of freedom.

$$\frac{k_c\langle\chi^2\rangle}{2} = \frac{k_B T}{2} \tag{21}$$

The spring constant (k_c) can then be calculated, where k_b is Boltzmann's constant, T is temperature, and $\langle\chi^2\rangle$ is the mean square displacement of the cantilever [98]:

$$k_c = \frac{k_B T}{\langle\chi^2\rangle} \tag{22}$$

As a cell is indented, the displacement of the cantilever is recorded as a force-distance curve (Figure 13).

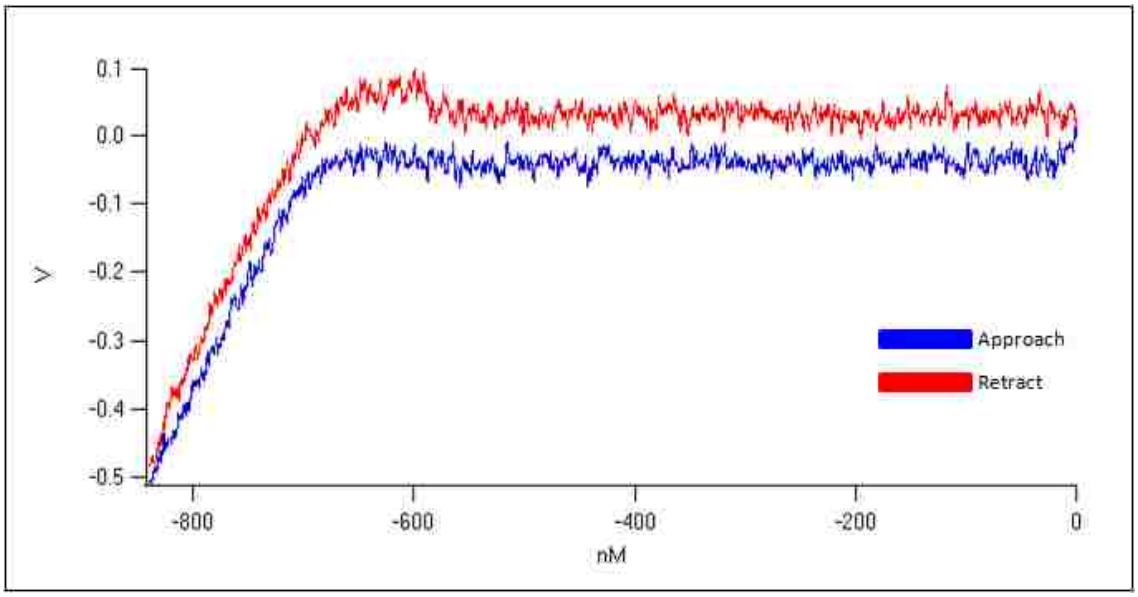

Figure 13: Force-distance curve recorded during cell indentation.

The force (F) can be calculated through Hooke's Law (Figure 14), as the cantilever behaves as a spring for small deflections (d):

$$F = k_c d \tag{23}$$

The displacement is equal to:

$$d = C\Delta V \tag{24}$$

where C (m/V) is the cantilever sensitivity and ΔV is the change in voltage.

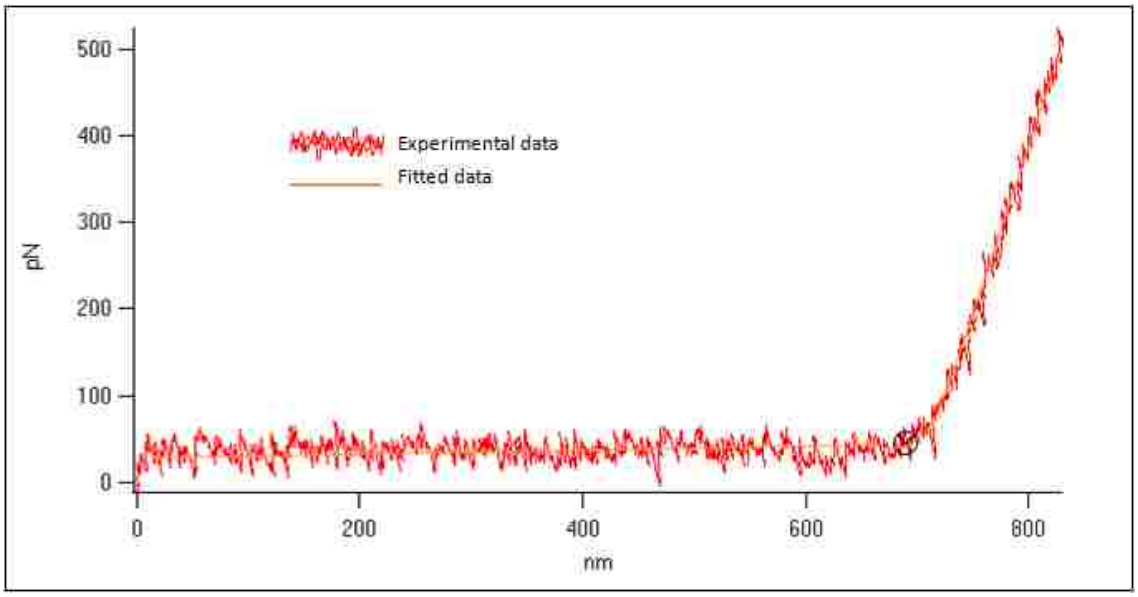

Figure 14: Force-distance curve of approach

The indentation depth (δ) can be found by subtracting the deflection (d) from the position of the probe (z) (Figure 15):

$$\delta = z - d \tag{25}$$

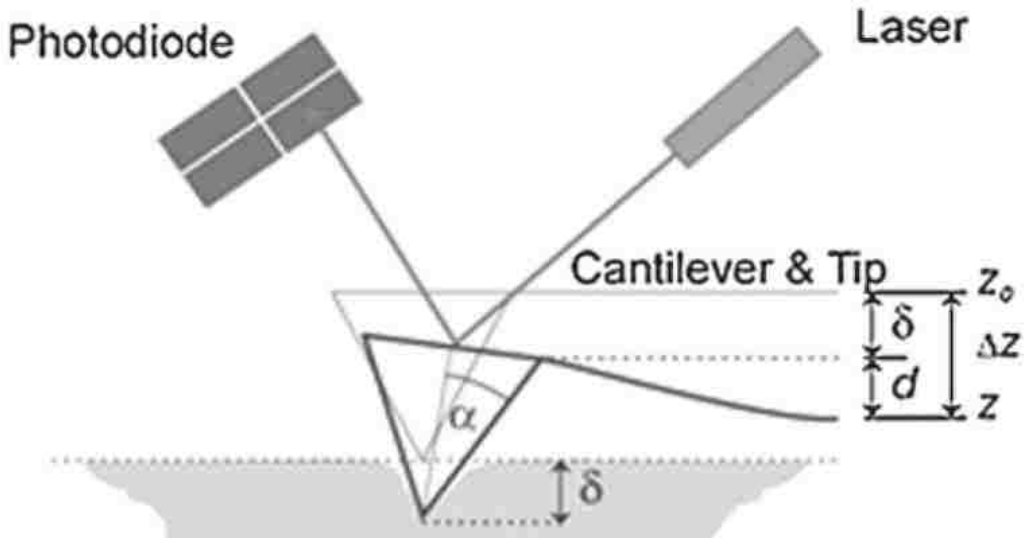

Figure 15: Deflection of the cantilever as a sample is indented [99]

The Hertz contact theory can be applied to find the elastic modulus of the indented surface [75]. While the classical theory involves two spheres, Sneddon applied the Hertz contact theory to conical probes, with the assumptions that the sample is semi-infinitely large (compared to indenting tip), perfectly flat, homogeneous, linearly elastic, and isotropic [76]. For a conical tip, the indentation force equals:

$$F = \frac{2E^*\delta^2 \tan\alpha}{\pi} \tag{26}$$

Where E* is the relative elastic modulus that depends on the elastic moduli and Poisson's ratio (ν) between the indenter and the sample:

$$\frac{1}{E^*} = \frac{1-\nu_1^2}{E_1} + \frac{1-\nu_2^2}{E_2} \tag{27}$$

$$E_1 \ll E_2 \tag{28}$$

$$E^* = \frac{E_1}{1-\nu_1^2} \tag{29}$$

Therefore, the force on the sample is equal to:

$$F = \frac{2E_1\delta^2 \tan\alpha}{\pi(1-\nu_1^2)} \tag{30}$$

Where E_1 and ν_1 are the elastic modulus and Poisson's ratio of the indented sample, respectively. The Poisson's ratio is generally assumed to be 0.5 for cells, and α is the half opening angle of the cone tip.

2.3.2.1.AFM Experimental Conditions

AFM indentations were performed on a home-built system (Figure 16). Local cell elastic modulus of undifferentiated cells was measured at every passage from P3 to P11 using AFM indentation. Fully differentiated osteogenic and myogenic cells were indented at the most successful passage (P4 and P7, respectively). A Basal Locke Buffer was used during indentation to maintain pH. Fifty cells were indented per passage, and cells were indented in 2 spots (1 on the edge of the cell and 1 in the cytoplasm). Silicon nitride cantilevers (MLCT, Bruker Nano, Camarillo, CA) with a nominal tip radius of 20nm were used (Figure 17).

Figure 16: Home-built AFM system

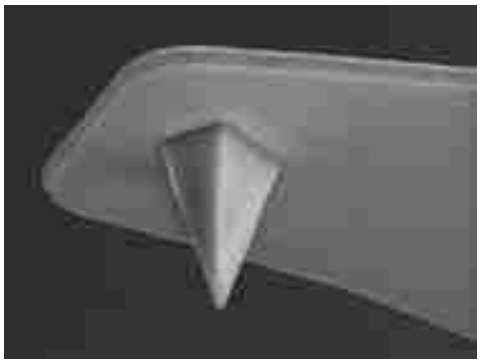

Figure 17: Silicon nitride probe used for cell indentation

The spring constants (0.01 N/m) of the calibrated cantilevers agreed with the values specified by the manufacturer. The tip had a half opening angle (α) of 35°. A maximum signal of 500 mV was used. Typical forces were approximately 500pN:

$$F = k_c d = k_c C \Delta V = \left(0.01 \frac{N}{m}\right)\left(1X10^{-7} \frac{m}{V}\right)(0.5V) = 500pN \quad (31)$$

The sample rate was 8 kHz. The elastic moduli were found using the Hertz model, as previously discussed. Data was analyzed with a custom-made program written in IgorPro (WaveMetrics, Portland, OR), using a least square analysis.

2.3.3. Actin stress fiber measurements

The average stress fiber diameter was measured at every passage from P3 to P11 using fluorescence microscopy. hMSCs were fixed in 10% formalin and stained with rhodamine phalloidin (Cytoskeleton, Inc., Denver, CO) to view actin stress fibers. The images were analyzed using the NIH program, ImageJ. A line was drawn perpendicular to the plane of most stress fibers (Figure 18, top). The plot profile was used to find the diameter of each stress fiber (Figure 18, bottom). Fifty cells were analyzed for every passage. The experiment was repeated.

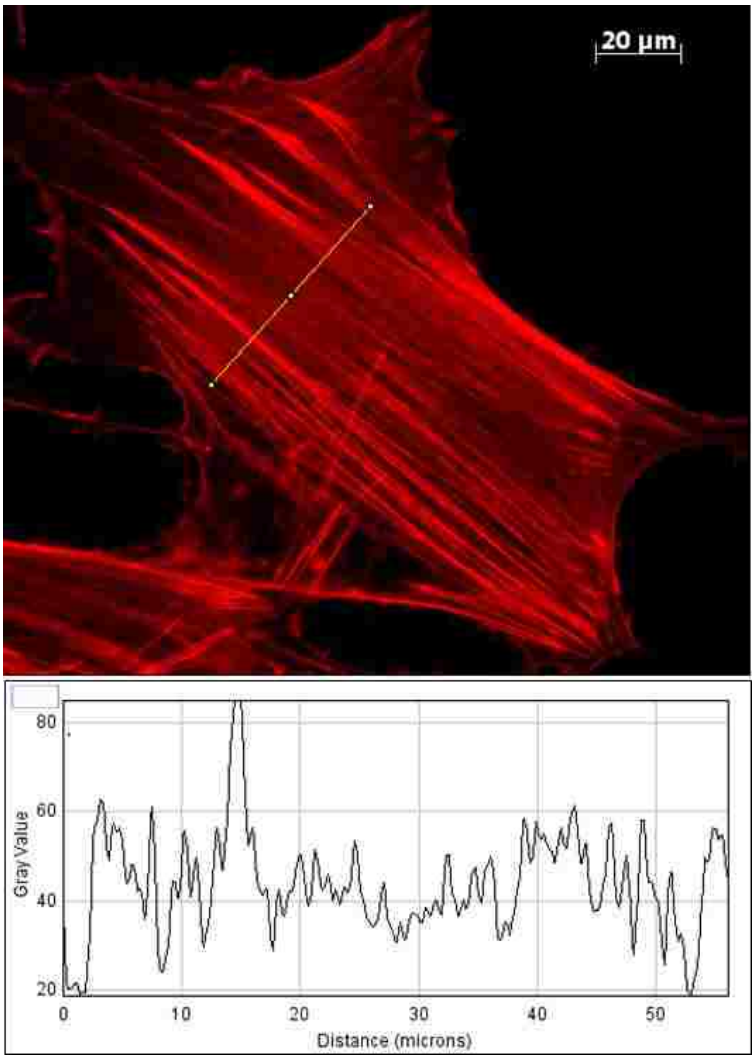

Figure 18: An hMSC stained with rhodamine phallodin to view stress fibers (top). ImageJ was used to find the plot profile (bottom).

2.3.4. Immunocytochemistry

Immunocyochemistry is a technique that uses antibodies tagged with fluorescent molecules to visualize the antigen of interest. Fixation and immunocytochemical processing for osteogenic and myogenic markers was conducted using standard

protocols. Briefly, cells were fixed with 10% formalin in 1 x PBS for 15 minutes. The samples were then treated with 100% methanol for 7 minutes. Non-specific binding sites were blocked for 30 minutes with agitation at room temperature with 1% bovine serum albumin (BSA). Primary antibodies were incubated for 1h at 37°C, followed by incubation with appropriate secondary antibodies (Alexa Fluor 488, Alexa Fluor 546, Alexa Fluor 555, 1:1000, Invitrogen) for 1h at room temperature. The nuclei were then counterstained with Hoechst dye (0.002 mg/ml in 1 x PBS) for 5 minutes. The monoclonal antibodies mouse anti-osteopontin (OP) (MPIIIB10(1), 1:500), developed by Michael Solursh and Ahnders Franzen, and anti-osteonectin (ON) (AON-1, 1:500), developed by John D. Termine, were obtained from the Developmental Studies Hybridoma Bank developed under the auspices of the NICHD and maintained by The University of Iowa, Department of Biology, Iowa City, IA 52242. Phycoerythrin-conjugated mouse anti-osteocalcin (OC) (1:500) was purchased from R&D (Minneapolis, MN). Sheep polyclonal anti-tropomyosin (1:500) was purchased from Millipore (Billerica, MA). Mouse monoclonal anti-sarcomeric actin (1:250) was purchased from Invitrogen (Carlsbad, CA).

2.3.5. qPCR

qPCR a technique that exponentially amplifies target DNA sequences for genetic analysis [100]. RNA from the sample of interest is isolated and converted to cDNA by reverse transcription. Short DNA sequences that are complementary to the target sequence (“primers”) are used for each gene of interest. This method uses

thermal cycling. In the first step, the temperature is raised to ~95°C to melt the DNA strands (denaturation step). The temperature is then lowered (~60°C), and primers bind to the ends of the target sequence (annealing step). The third step is extension, where DNA polymerase synthesizes new complementary strands. The temperature of this step depends on the DNA polymerase used. A fluorescent dye that binds to double stranded DNA, such as SYBR Green, is used to measure the amount of amplified sequence. The thermal cycling sequence is repeated for approximately 40 cycles, and the fluorescence signal is measured after each cycle. A gene sequence that is present in approximately the same amount in all cells is used as a "housekeeping gene." Examples of housekeeping genes are glyceraldehyde-3-phosphate dehydrogenase (GAPDH), β actin, and major histocompatibility complex I. The amplification curves of each gene of interest are compared by setting a threshold value (commonly 20% above the baseline). The cycle number at which the amplification curve crosses the threshold is called the threshold cycle (Ct) (Figure 19).

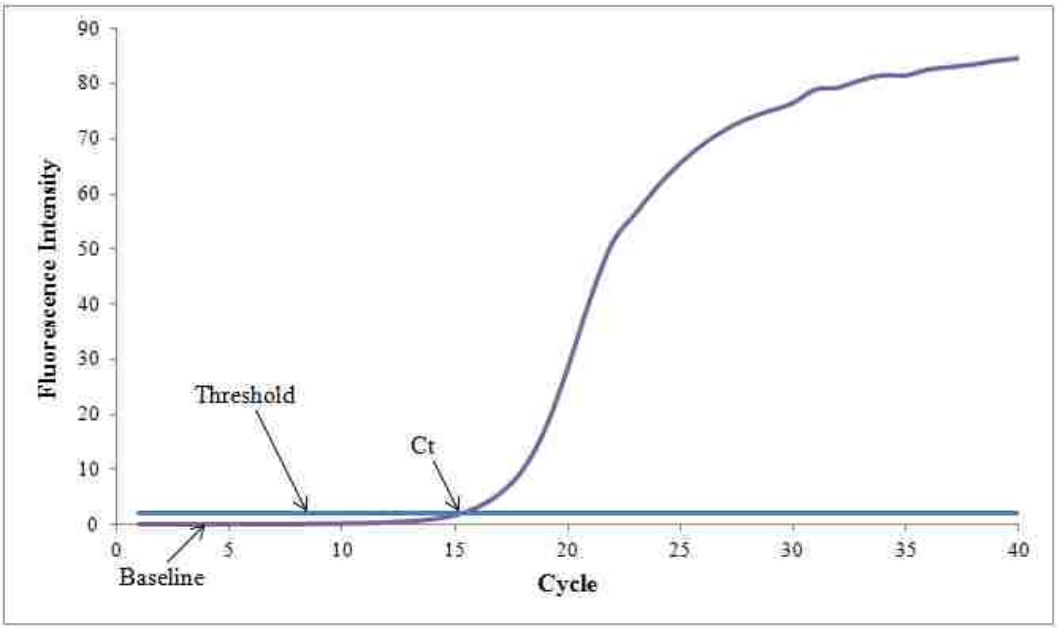

Figure 19: Typical amplification curve of qPCR

qPCR was performed on undifferentiated and differentiated cells from P4 to P9 to assess mRNA expression. Total RNA was isolated using RNeasy Plus Micro kits (Qiagen, Valencia, CA). RNA was converted to cDNA using a Qiagen Omniscript RT Kit. Cycles were optimized for the amplicon size and primer Tm on a Qiagen Rotor-Gene qPCR system. A SYBR green qPCR kit from Qiagen was used to assess gene expression. Primers can be seen in Table 1.

Analysis of the qPCR data was completed using the ΔCt method [101], with a threshold value of 20% above the background. Primer efficiency values were empirically derived from undifferentiated hMSCs for the housekeeping gene (GAPDH), osteogenic hMSCs for bone markers, and myogenic hMSCs for muscle markers. The

copy rate of each primer was found using the slope of the efficiency curve, where r is the copy rate and x is the slope:

$$r = \sqrt[x]{10} \tag{32}$$

Fold changes were determined through ΔCt comparison, and all data was subject to normalization to the housekeeping gene (GAPDH) corresponding to each experimental condition and specimen. The ΔCt was calculated using the Cts of both the housekeeping gene (HKG) and the gene of interest (GOI):

$$\Delta Ct = 2^{Ct_{HKG} - Ct_{GOI}} \tag{33}$$

Table 1: qPCR primers

Target/control gene	Primer Sequence (5'-3')	Amplicon Size	Melting Temperatures
GAPDH	F- CGGATTTGGTCGTATTGG R- TCAAAGGTGGAGGAGTGG	861	F Tm = 53.2 R Tm = 55.7
Collagen 1 (Col 1)	F- ATCCAGCTGACCTTCCTGCG R- TCGAAGCCGAATTCCTGGTCT	323	F Tm = 62.3 R Tm = 61.5
Runx2	F- CCACCCGGCCGAACTGGTCC R- CCTCGTCCGCTCCGGCCCACA	258	F Tm = 67.7 R Tm = 71.1
Osteocalcin (OC)	F- GAAGCCCAGCGGTGCA R- CACTACCTCGCTGCCCTCC	70	F Tm = 60.0 R Tm = 62.1
Alkaline Phosphatase (ALP)	F- ACGTGGCTAAGAATGTCATC R- CTGGTAGGCGATGTCCTTA	476	F Tm = 55.5 R Tm = 55.9
Osteonectin (ON)	F- ATGAGGGCCTGGATCTTCTT R- GCTTCTGCTTCTGAGTCAGA	580	F Tm = 58.1 R Tm = 57.3
Smooth muscle α actin (SMAA)	F- GTGTTGCCCCTGAAGAGCAT R- GCTGGGACATTGAAAGTCTCA	109	F Tm = 60.6 R Tm = 58.2
Calponin 1 (CNN1)	F- CAACCACCACGCACACAACTA R- GGTCCAGCCAAGAGCAGCAG	97	F Tm = 61.3 R Tm = 63.4
β-Myosin Heavy Chain (β-MHC)	F- GATCACCAACAACCCCTACG R- ATGCAGAGCTGCTCAAAGC	528	F Tm = 58.3 R Tm = 58.8
Desmin	F- CCAACAAGAACAACGACG R- TGGTATGGACCTCAGAACC	408	F Tm = 54.4 R Tm = 55.7

2.3.6. Von Kossa staining

Mineralization in the osteogenic samples was assessed with Von Kossa staining. The samples were incubated under a UV light in 5% silver nitrate (MP Biomedicals) for 30 min. The samples were then rinsed 3 times with ddH20, followed by incubation with 5% sodium thiosulfate (Sigma Aldrich) for 2 min [102]. ImageJ was used to

quantify the percentage of staining in 30 images per experiment. All experiments were repeated.

2.3.7. Statistical analysis

Statistical significance was evaluated with a paired Student's t-test for comparison of t-dependent groups. T-tests were used to analyze data between all passages for the AFM indentation, stress fiber diameter measurements, and Von Kossa staining. Subsequent passages for undifferentiated and differentiated cells were analyzed for the qPCR data. All values are reported as means ±SE unless otherwise stated.

2.4. Results and Discussion

2.4.1. Cell proliferation

hMSCs were received at P2. Each passage corresponded to approximately 2 population doublings. Experiments on undifferentiated cells (AFM indentation, stress fiber analysis) began at P3. Differentiations began at P4 and were carried out at each passage until P9, when differentiations were considered unsuccessful. Undifferentiated cells were analyzed until P11, at which point senescence occurred. During extended culture, cells showed signs of aging, including slowed proliferation, increased cell debris, and a change in appearance, from spindle-shaped to a broad, flattened morphology (Figure 20), as previously described [87,88,103].

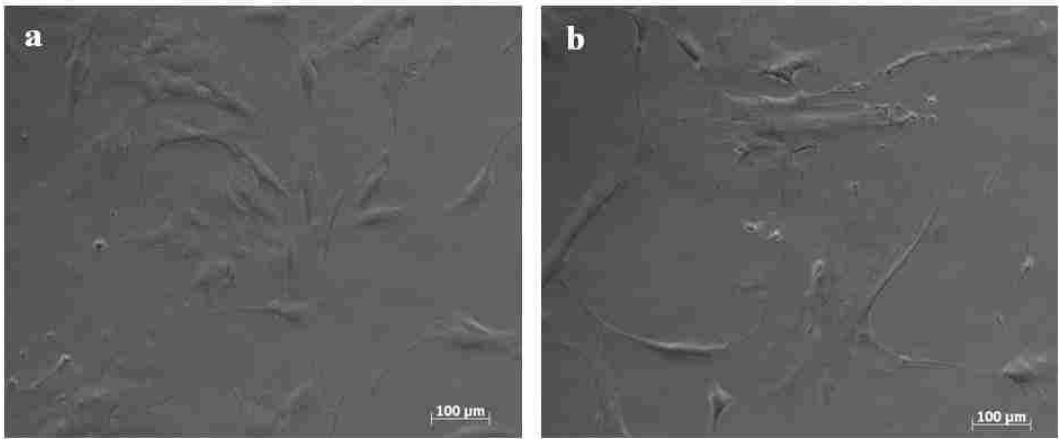

Figure 20: Phase contract images of hMSCs at a) P4 and b) P9. Cells at P4 are small and spindle-shaped, compared to larger, flattened cells at P9.

2.4.2. AFM indentation

Prior to differentiation, the average elastic modulus of hMSCs on TCPS was analyzed (Figure 21). The elastic modulus of undifferentiated hMSCs remained fairly constant from P3 to P5 (approximately 6 kPa). Significant increases ($P<0.05$) were observed from P6 (7.95±0.83 kPa) to P7 (10.93±1.04 kPa), and from P7 to P8 (14.89±1.20 kPa). After P8, the average elastic modulus value was 16 kPa. The initial average elastic modulus of a stem cell population is likely dependent on donor age [104,105]. These results are generally consistent with other studies [71-73,86,106,107], with any differences attributed to donor, AFM tip geometry [78,108], and location of indentation, as elastic modulus values vary widely in a single cell [107].

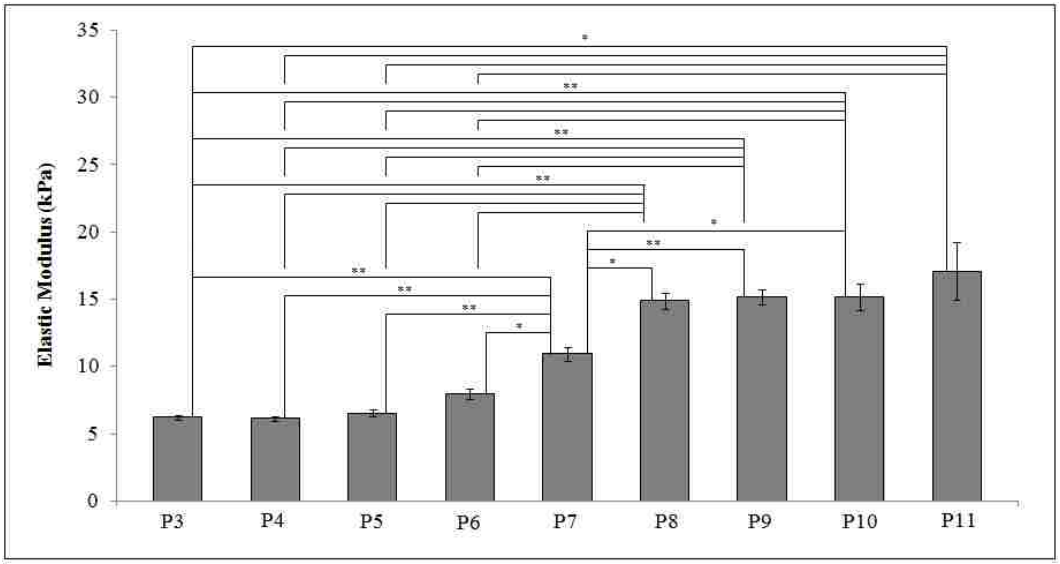

Figure 21: Change in elastic modulus from P3 to P11. (*P<0.05, **P<0.01)

2.4.3. Actin stress fiber measurements

The actin stress fiber diameters of undifferentiated cells on TCPS can be seen in Figure 22. Slight increases occurred at every passage, with very significant (P<0.01) increases between each passage from P5 to P9. It has previously been reported that hMSC elastic modulus is primarily dependent on actin fibers [72,109,110]. Titushkin et al. found that the elastic modulus decreased more than 75% when actin fibers were disrupted, but saw no statistically significant difference when microtubules were disrupted [72]. Similar findings have been reported for skeletal myocytes [109] and osteoblasts [110]. Therefore, it is evident that the increases in stress fiber diameter led to the changes in cell elastic modulus.

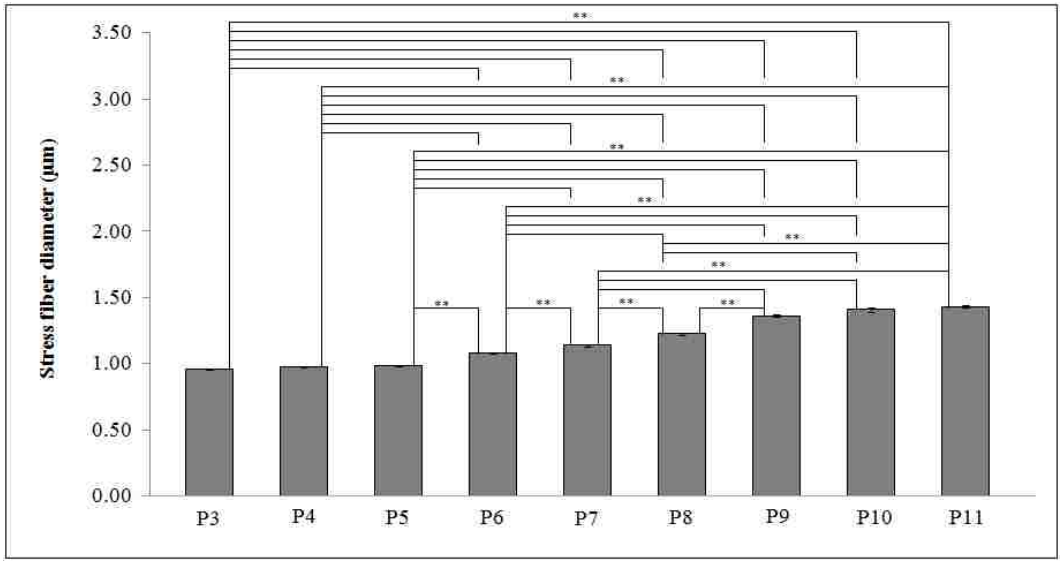

Figure 22: Change in actin stress fiber diameters from P3 to P11 (P<0.01)**

2.4.4. Myogenic differentiations

Myogenic differentiations were carried out at every passage from P4 to P9. The protein expression of two myogenic markers, tropomyosin and sarcomeric actin, were assessed with immunocytochemistry (Figure 23). Tropomyosin is a protein that regulates muscle cell contraction. Tropomyosin interacts with actin and the troponin complex to control the attachment of crossbridges to actin [111]. The appearance of sarcomeric actin coincides with the appearance of contraction in cardiac and skeletal muscle cells [112,113]. Protein levels of tropomyosin and sarcomeric actin peaked at P7, but were barely visible prior to P6 and after P8. At the passage of peak expression, P7, the average elastic modulus value of the undifferentiated cell population was 10.93±1.04 kPa. It appears that this value may be most conducive to myogenic

differentiation of hMSCs. The elastic modulus of fully differentiated hMSCs at passage 7 was 14.71±0.98 kPa. Engler et al. previously reported that the elasticity of skeletal muscle is approximately 12kPa [47]. Similar values have been reported for human skeletal muscle [114], murine myoblasts [109], and murine skeletal myocytes [115]. Therefore, it appears that hMSCs most easily differentiate down the myogenic lineage when their elastic modulus is most similar to that of native muscle. This novel finding may guide those using adult stem cells for muscle regeneration.

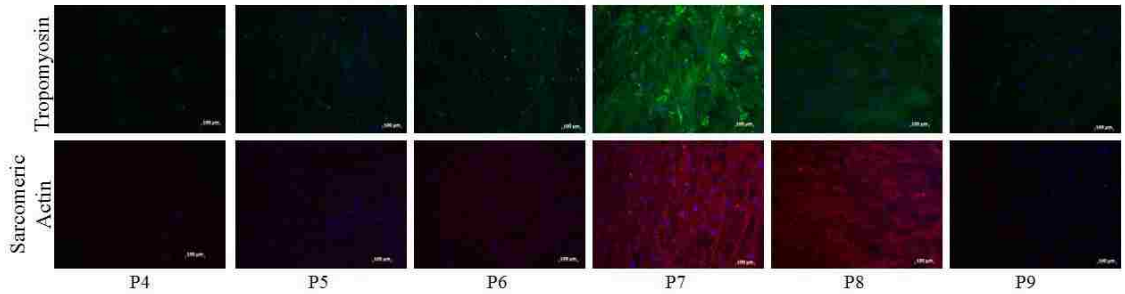

Figure 23: Expression of myogenic markers in differentiated hMSCs from P4 to P9. Tropomyosin can be seen in green, sarcomeric actin in red, and nuclei in blue.

mRNA expression in differentiated hMSCs on TCPS was investigated using qPCR (Figure 24Figure 28). The myogenic markers desmin, SMAA, CNN1, β-MHC, and troponin T were examined. Desmin is a muscle-specific intermediate filament that appears in the early formation of cardiac, skeletal, and smooth muscle. Desmin is thought to be involved in myofibrillogenesis and provides mechanical support for muscle cells [116]. SMAA, the primary actin isotype found in vascular smooth muscle cells, is also transiently expressed in the development of cardiac and skeletal muscle [117]. CNN1 is a protein that interacts with F-actin and tropomyosin to control the

contraction of smooth muscle cells [118]. The mRNA expression of β-MHC was also investigated. Myosin is the main component of thick filaments in sarcomeres. Type II myosin, found in muscle cells, has two heavy chains and four light chains. The heavy chains are each comprised of a globular head domain and a coiled tail domain [119]. In this study, a cardiac muscle-specific MHC isoform was used. Troponin T is a component of the troponin complex (along with troponin C and I) that binds to tropomyosin to form the tropomyosin-troponin complex [111]. The troponin T isoform used in this study is cardiac-muscle specific. It is interesting to note that the cells express markers associated with all types of muscle. However, CNN1, a marker associated with smooth muscle, was much more upregulated than the cardiac muscle-specific marker β-MHC.

In general, endogenous levels of myogenic markers increased until P7, then decreased. This trend has been reported before, as Siegel et al. reported peak intrinsic expression of myogenic markers troponin I and myosin light chain in hMSCs at P7 [120]. In this study, a similar trend was observed in the differentiated cells, with peak expression at P7. It seems evident that the increased upregulation of myogenic markers in undifferentiated cells from P4 to P7, as well as the stiffening of cells to an optimal elasticity (approx. 11kPa), both contribute to the success of the myogenic differentiation at P7.

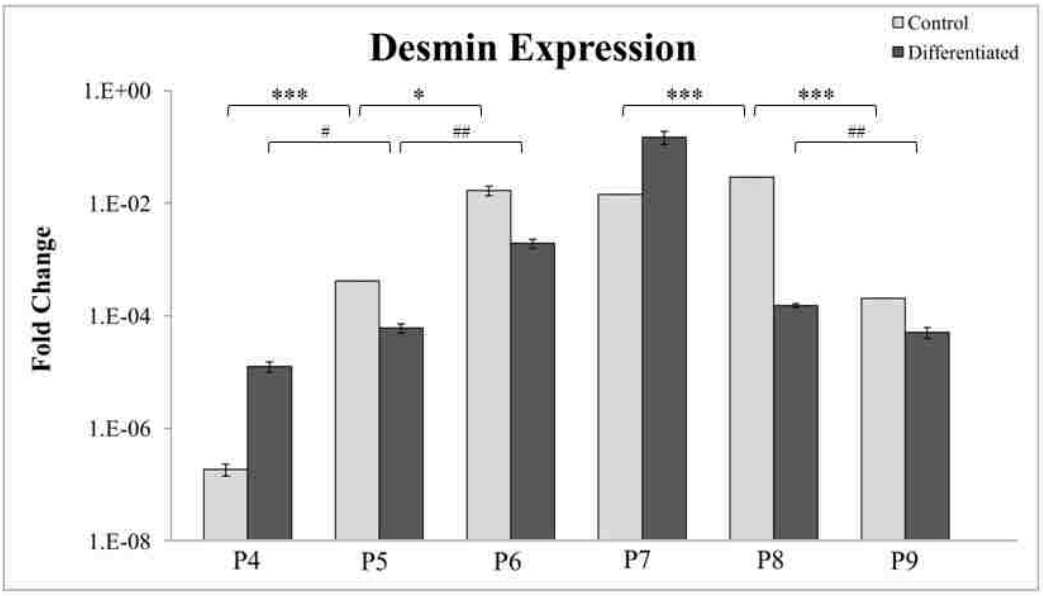

Figure 24: Fold change (ΔCt) of desmin compared to housekeeping gene (GAPDH) for hMSCs from P4 to P9 (*P<0.1, **P<0.05, ***P<0.01 between subsequent passages of control samples, $^{\#}$P<0.1, $^{\#\#}$P<0.05, $^{\#\#\#}$P<0.01 between differentiated samples)

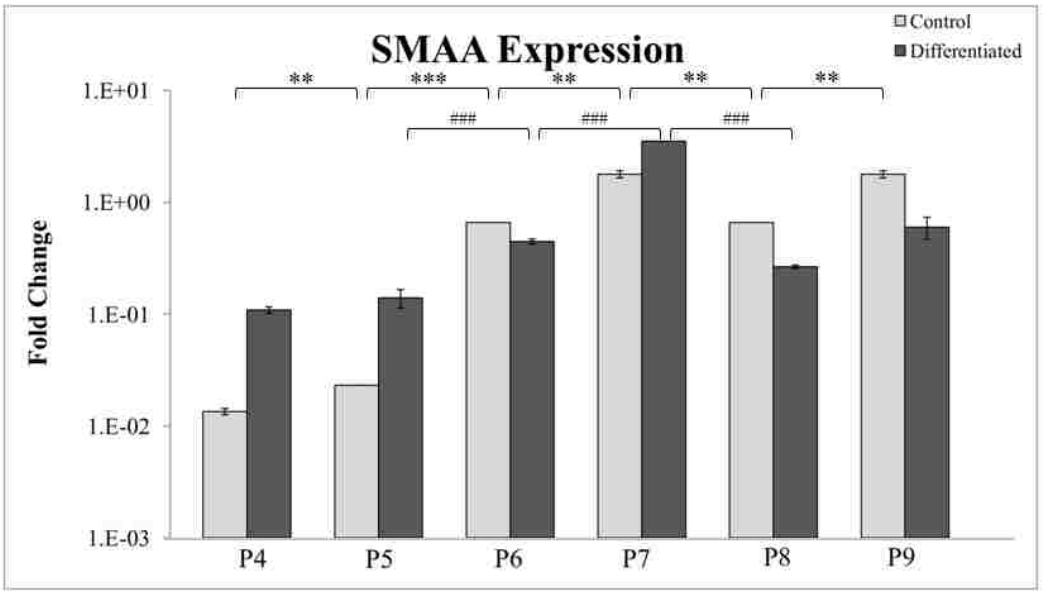

Figure 25: Fold change (ΔCt) of SMAA compared to housekeeping gene (GAPDH) for hMSCs from P4 to P9 (*P<0.1, **P<0.05, ***P<0.01 between subsequent passages of control samples, $^{\#}$P<0.1, $^{\#\#}$P<0.05, $^{\#\#\#}$P<0.01 between differentiated samples)

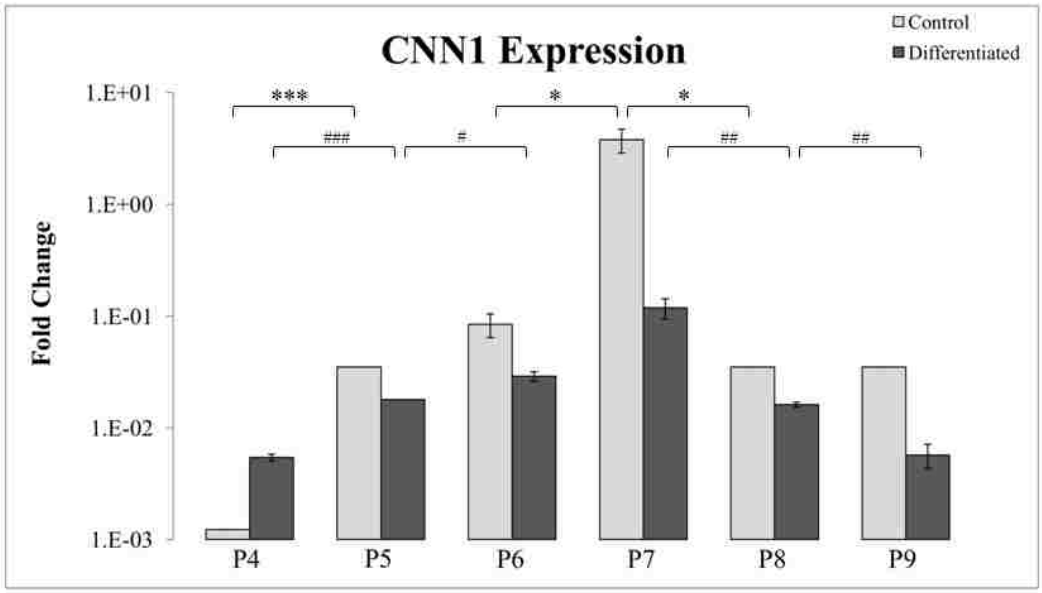

Figure 26: Fold change (ΔCt) of CNN1 compared to housekeeping gene (GAPDH) for hMSCs from P4 to P9 (*P<0.1, **P<0.05, ***P<0.01 between subsequent passages of control samples, $^{\#}$P<0.1, $^{\#\#}$P<0.05, $^{\#\#\#}$P<0.01 between differentiated samples)

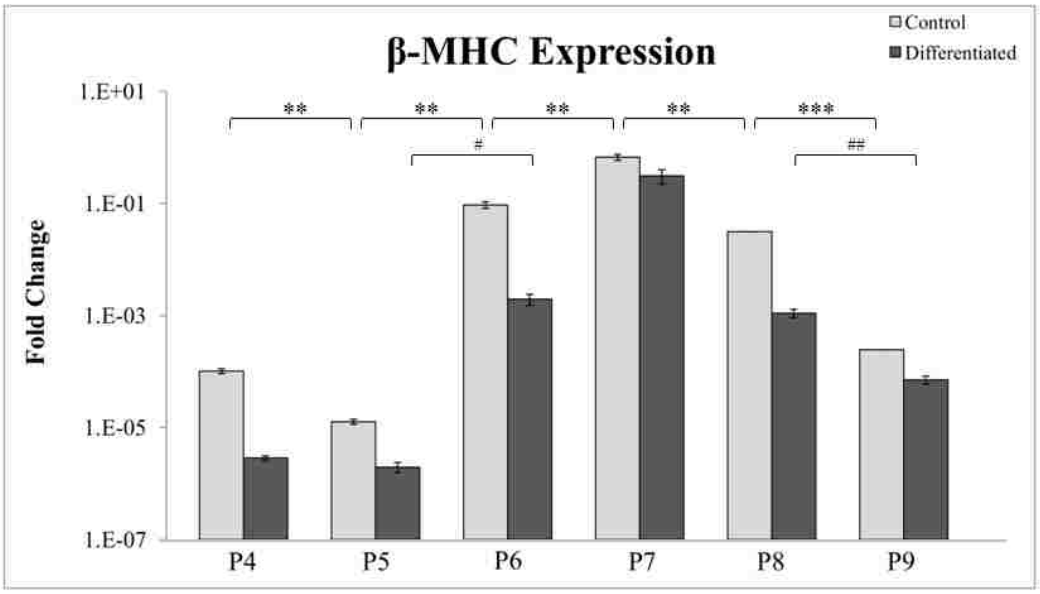

Figure 27: Fold change (ΔCt) of β-MHC compared to housekeeping gene (GAPDH) for hMSCs from P4 to P9 (*P<0.1, **P<0.05, ***P<0.01 between subsequent passages of control samples, $^{\#}$P<0.1, $^{\#\#}$P<0.05, $^{\#\#\#}$P<0.01 between differentiated samples)

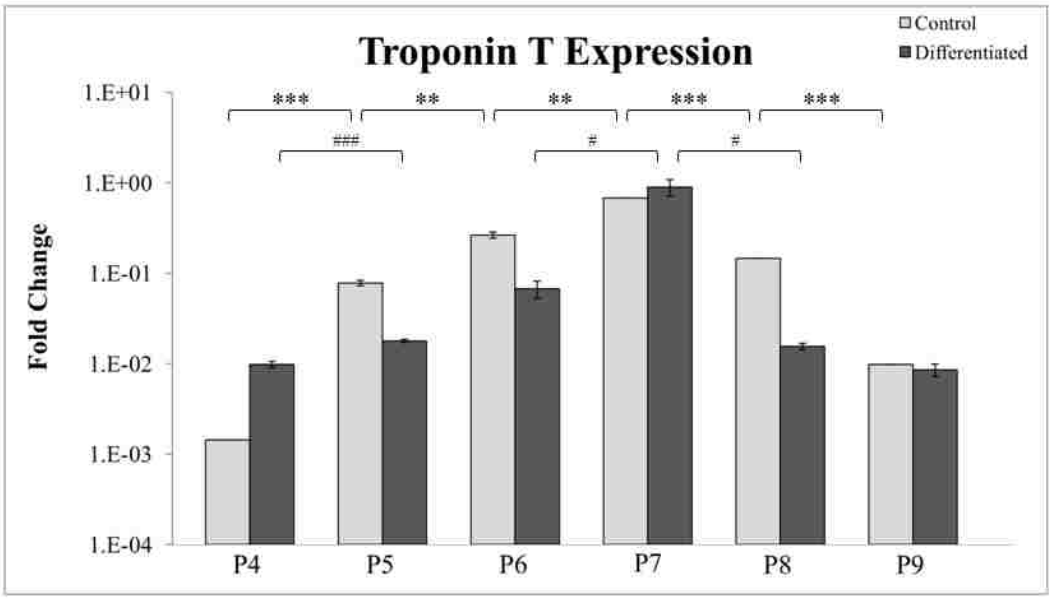

Figure 28: Fold change (ΔCt) of Troponin T compared to housekeeping gene (GAPDH) for hMSCs from P4 to P9 (*P<0.1, **P<0.05, ***P<0.01 between subsequent passages of control samples, $^{\#}$P<0.1, $^{\#\#}$P<0.05, $^{\#\#\#}$P<0.01 between differentiated samples)

2.4.5. Osteogenic differentiations

Osteogenic differentiations were carried out at every passage from P4 to P9. ON, OP, and OC expression were assessed with immunocytochemistry (Figure 29). ON is an extracellular matrix glycoprotein that initiates mineralization through binding to collagen and hydroxyapatite [121]. ON protein expression appears to decrease after P4, with no expression at P9. OP is a protein that regulates mineralization by binding to hydroxyapatite, while OC is involved in regulation of mineral deposition and is a marker of mature osteoblasts [122]. OP expression was minimal from P7 to P9, while OC expression was minimal at P8 and P9. Since both OP and OC are expressed in the

later stages of differentiation, the lack of expression after P7 indicates unsuccessful differentiations.

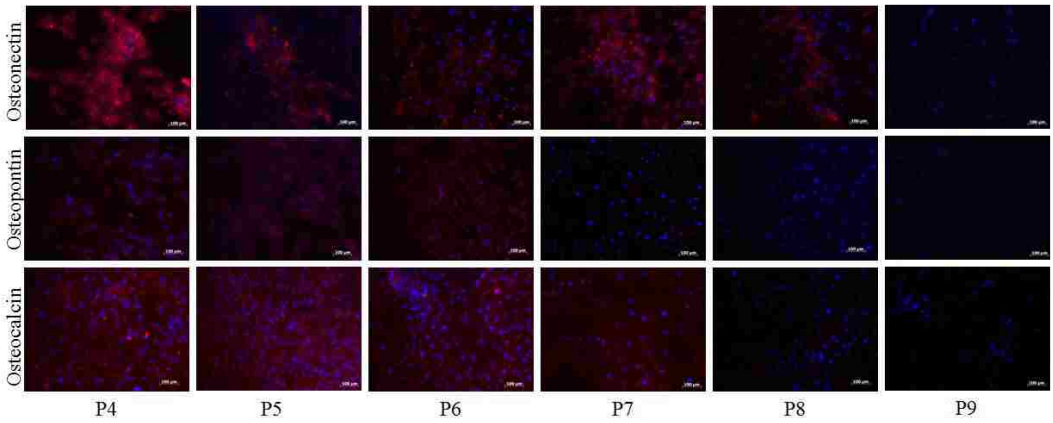

Figure 29: Expression of osteogenic markers in differentiated hMSCs from P4 to P9. ON, OP, and OC can be seen in red and nuclei in blue.

qPCR results for osteogenic hMSCs on TCPS can be seen in Figure 30-Figure 34. The osteogenic markers ALP, Col 1, Runx2, OC, and ON were examined. ALP is a metalloenzyme that initiates mineralization and peaks at day 14 of differentiation [123]. ALP generally decreased after extended culture in differentiated cells, with a significant ($p<0.1$) decrease from P8 to P9, with downregulation at P9 compared to undifferentiated cells. This may indicate the cells' inability to produce a mineralized matrix in P8-P9. Col 1 is the main collagen protein in the bone matrix, and its gene expression typically peaks in the first 2 weeks of differentiation [124]. Significant ($P<0.05$) decreases in Col 1 expression in differentiated cells were observed between P7 and P9, accompanied by downregulation after P7. Runx2 is an essential transcription factor in osteogenesis that regulates OC and OP expression [125]. Interestingly,

significant ($p<0.01$) increases were seen in undifferentiated cells from P7 to P9, although differentiations at these passages were generally considered unsuccessful because of the lack of osteogenic protein expression. Significant ($P<0.05$) decreases were detected in OC expression in differentiated cells from P7 to P9, with downregulation after P7 compared to undifferentiated cells. Additionally, very significant ($P<0.01$) decreases in ON expression was observed from P5 to P6 in undifferentiated cells, and from P6 to P7 in differentiated cells. A large increase in cell elastic modulus was observed from P7 (10.93±1.04 kPa) to P8 (14.89±1.20 kPa), which are the passages where several key players in osteogenesis are downregulated. hMSCs undergoing osteogenesis have been shown to soften by approximately 33% early in differentiation, which was attributed to the actin network reorganization during differentiation [72]. This suggests that hMSCs may have more differentiation success in earlier passages, when they exhibit reduced endogenous cell stiffness.

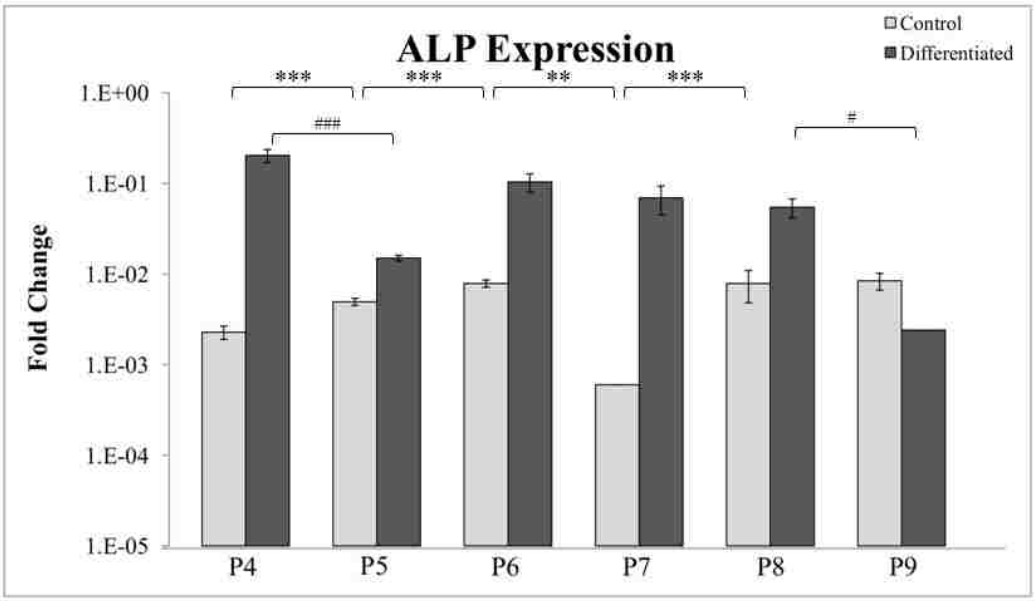

Figure 30: Fold change (ΔCt) of ALP compared to housekeeping gene (GAPDH) for hMSCs from P4 to P9 (*P<0.1, **P<0.05, ***P<0.01 between subsequent passages of control samples, $^{\#}$P<0.1, $^{\#\#}$P<0.05, $^{\#\#\#}$P<0.01 between differentiated samples)

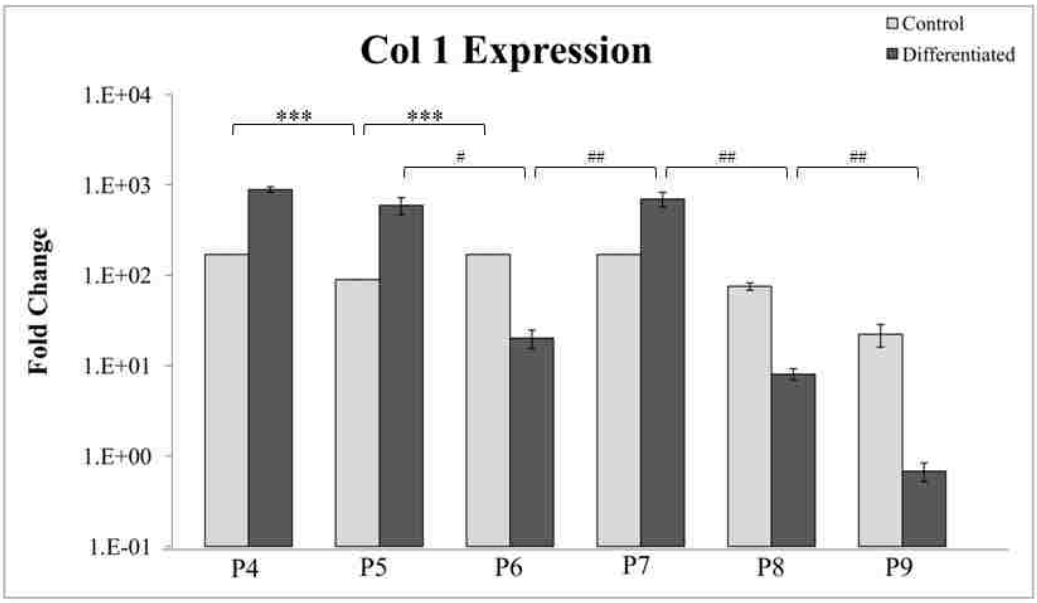

Figure 31: Fold change (ΔCt) of Col 1 compared to housekeeping gene (GAPDH) for hMSCs from P4 to P9 (*P<0.1, **P<0.05, ***P<0.01 between subsequent passages of control samples, $^{\#}$P<0.1, $^{\#\#}$P<0.05, $^{\#\#\#}$P<0.01 between differentiated samples)

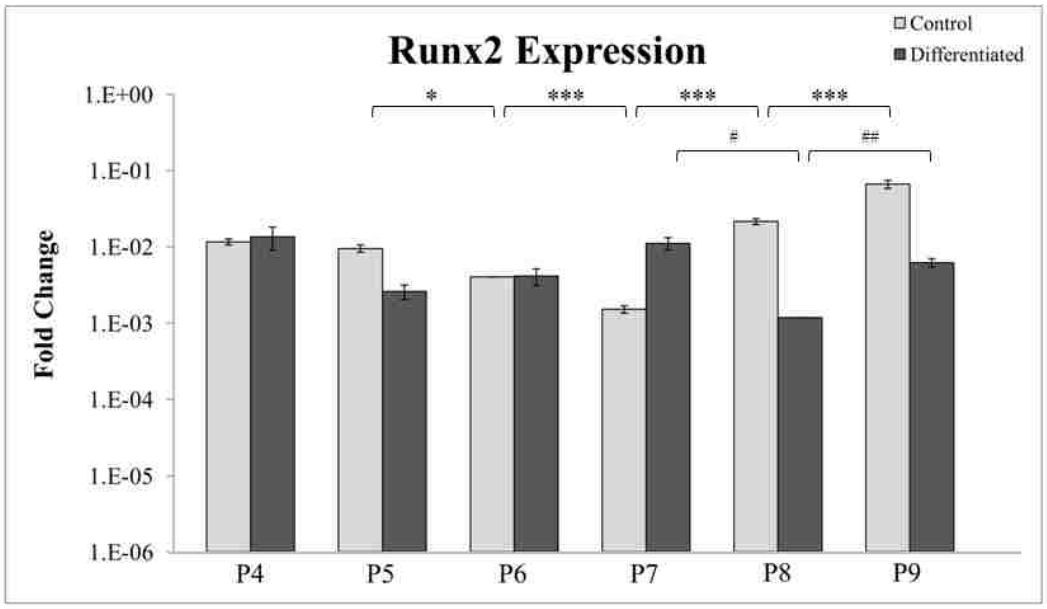

Figure 32: Fold change (ΔCt) of Runx2 compared to housekeeping gene (GAPDH) for hMSCs from P4 to P9 (*P<0.1, **P<0.05, ***P<0.01 between subsequent passages of control samples, $^{\#}$P<0.1, $^{\#\#}$P<0.05, $^{\#\#\#}$P<0.01 between differentiated samples)

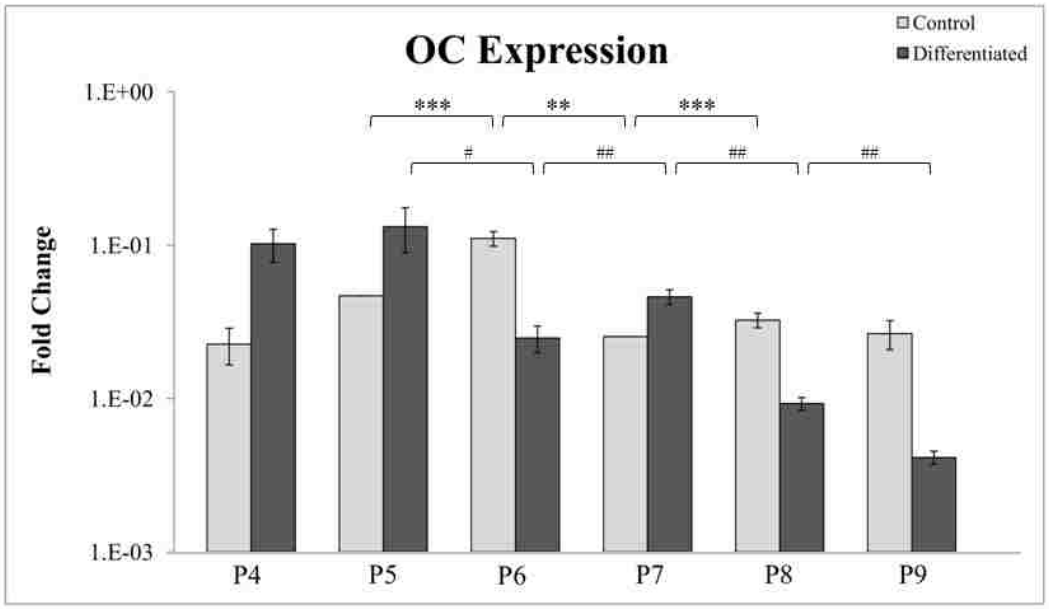

Figure 33: Fold change (ΔCt) of OC compared to housekeeping gene (GAPDH) for hMSCs from P4 to P9 (*P<0.1, **P<0.05, ***P<0.01 between subsequent passages of control samples, $^{\#}$P<0.1, $^{\#\#}$P<0.05, $^{\#\#\#}$P<0.01 between differentiated samples)

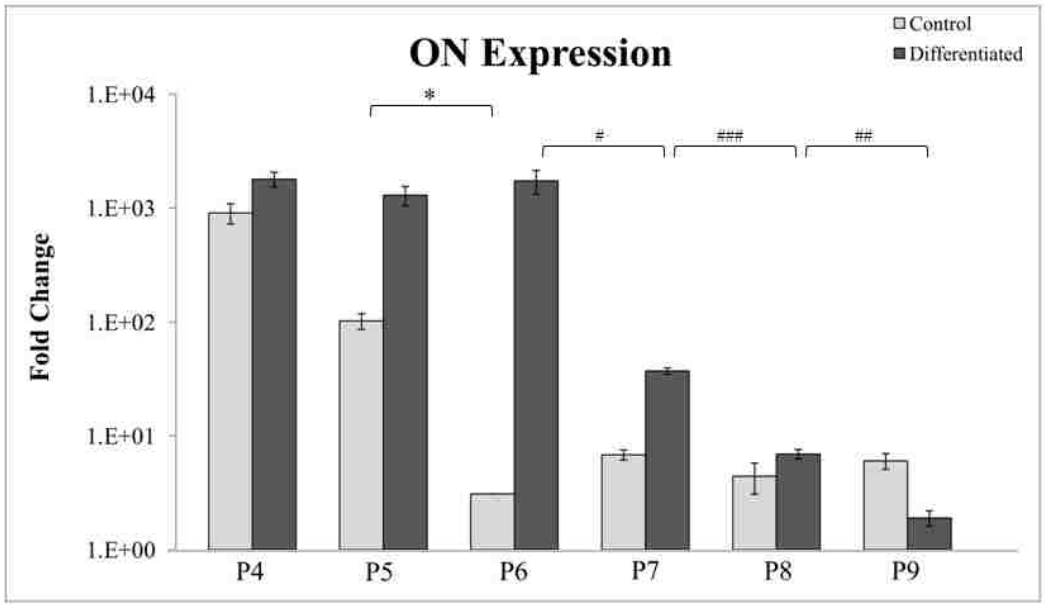

Figure 34: Fold change (ΔCt) of ON compared to housekeeping gene (GAPDH) for hMSCs from P4 to P9 (*P<0.1, **P<0.05, ***P<0.01 between subsequent passages of control samples, $^{\#}$P<0.1, $^{\#\#}$P<0.05, $^{\#\#\#}$P<0.01 between differentiated samples)

2.4.6. Von Kossa staining

A mineralized matrix is a hallmark of successful osteogenesis. The mineralization in osteogenic samples was quantified using Von Kossa staining. Calcium deposits appear in black after treatment with silver nitrate. The amount of calcium deposits is decreased in higher passages compared to lower passages (Figure 35). The percentage of matrix mineralization was quantified with ImageJ (Figure 36). Significant decreases between subsequent passages were observed from P5 to P6 and from P7 to P8. The large decline in mineralization from P5 to P6 (approximately 66%) signifies that the differentiations had the highest success in P4 and P5. These results agree with the immunocytochemistry and qPCR data, which depict the decreases in ON

and ALP, both which are crucial for mineralization. ON protein expression appears to decrease after P4, with no expression at P9, while ON mRNA expression decreased from P6 to P7. Additionally, ALP mRNA expression generally declined during extended passaging, with a significant ($P<0.1$) decrease from P8 to P9.

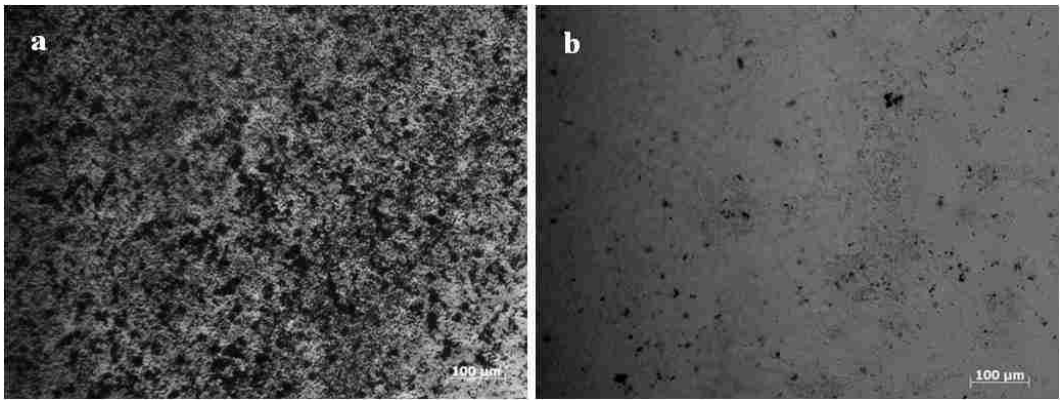

Figure 35: Von Kossa staining in a) P5 and b) P8 osteoblasts shows a decrease in higher passages

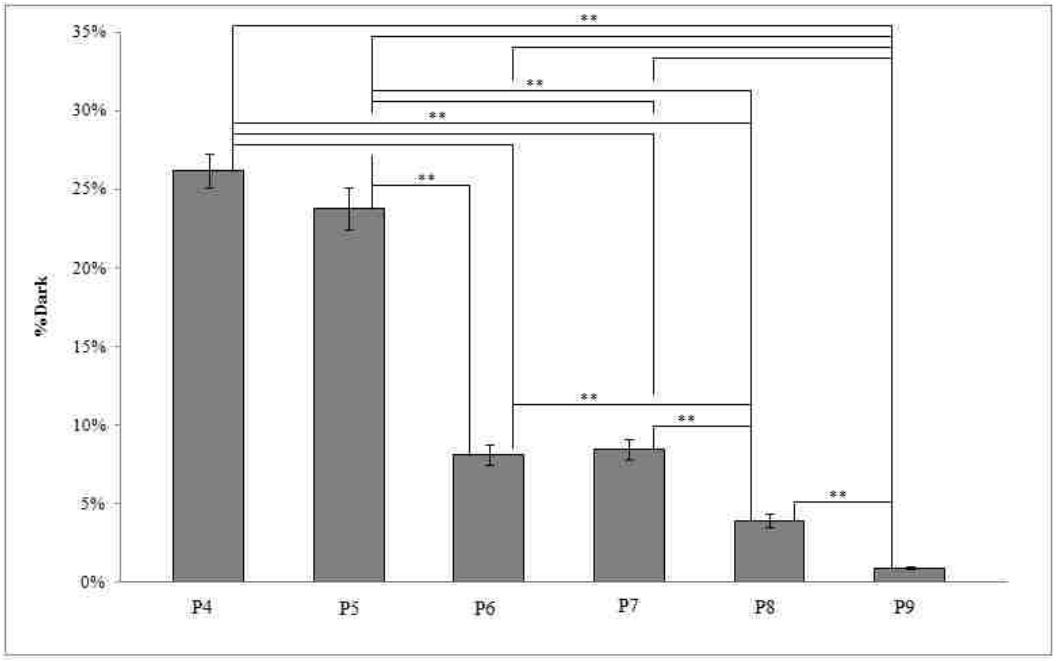

Figure 36: Von Kossa staining in osteogenic samples from P4 to P9. (P<0.01)**

We report that the average local elastic modulus of the hMSC population increases as cells age *in vitro*, and that this change in elastic modulus dictates differentiation success. Osteogenic differentiations were more successful in the earlier passages (P4 to P6), when cells exhibited a lower elastic modulus value. While it has previously been reported that hMSCs lose their osteogenic potential after long term *in vitro* culture, most studies have confirmed osteogenic decline by mineralization assays [10,87,88,90,93,94]. Few studies have examined osteogenic markers during *in vitro* aging [126,127], which revealed some of the trends that led to decreased differentiation capacity. While osteogenic differentiations were most successful from P4 to P6, myogenic differentiation success peaked at P7, due to an elastic modulus value matching native muscle. The myogenic potential of aging hMSCs had not been

explored until the present study. While much of the focus on aging hMSCs has been on the osteogenic, chondrogenic, and adipogenic lineages [87,88,93,128,129], the myogenic lineage is one that may be very useful for regenerative medicine. Further investigation must be done to elucidate the mechanisms behind cell stiffening during aging, as well as how it relates to chondrogenic and adipogenic differentiation in extended culture.

It is known that stem cell fate can be modulated by cell shape and cytoskeletal tension [55,57]. Additionally, the mechanical properties of adipose-derived stem cells have been shown to reflect their differentiation potential [130]. Here we show how stem cell fate is reliant on the average elastic modulus of an aging population. While this study verifies stiffness-related changes during aging, it calls attention to the need for a stem cell culture substrate that does not induce rapid cell stiffening. It also demonstrates the need for analysis of lineage-specific markers prior to differentiation.

A mechanism that may play a role in the decrease of osteogenic potential and peak of myogenic potential is the GTPase RhoA. Studies have shown that RhoA activity, along with Rho-associated protein kinase Rock, can induce osteogenesis in hMSCs [55,131]. On the contrary, Beqaj et. al showed that RhoA levels were downregulated in smooth muscle myogenesis and that upregulation of RhoA delays myogenesis in embryonic MSCs [132]. Likewise, Kim et al. reported downregulated RhoA and upregulated Rac1 during cardiomyogenic differentiation of hMSCs [133]. RhoA was also downregulated during the skeletal muscle differentiation of avian myoblasts and mouse satellite cells [134]. Therefore, the endogenous levels of active

RhoA may be higher in earlier passages (P3-P6), and decrease at P7, which would lead to the peak myogenic differentiation at this passage.

2.5. Conclusions

Cells passaged on TCPS were subject to cell stiffening. The average elastic modulus of undifferentiated cells remained constant (approximately 6 kPa) from P3 to P5. Significant increases ($P<0.05$) were observed from P6 (7.95±0.83 kPa) to P7 (10.93±1.04 kPa) and P8 (14.89±1.20 kPa). After P8, the average elastic modulus value was 16 kPa. These increases in cell elastic modulus were likely a result of increases in actin stress fiber diameters. Elastic modulus values of hMSCs largely dictated the success of myogenic differentiation. Highest expression of myogenic markers was observed at P7, where the elastic modulus was 10.93±1.04 kPa, which is comparable to previously reported values for muscle cells. Osteogenic differentiations were more successful in earlier passages (P4 through P6), which may suggest that hMSCs more easily differentiate when in a softer state. This is the first report that correlates the average elastic modulus of an aging cell population to its differentiation success, as well as the first study of myogenic potential during *in vitro* aging. This study illustrates the importance of mRNA and protein analysis during extended culture, while demonstrating a need for a more suitable substrate for the extended culture of hMSCs.

Chapter 3: Mechanical Loading on Polymeric Foams: Effect on hMSC Differentiation

3.1.Chapter Overview

This chapter describes the use of mechanical loading for the differentiation of hMSCs. Chemical cues are commonly used for differentiation, but mechanical cues may more accurately mimic *in vivo* conditions. Tensile (5-20%) and compressive (2.5-10%) loading were used to induce myogenic and osteogenic differentiation, respectively, on 3-D porous polymer scaffolds. Results show that 10% tensile stretch upregulates myogenic markers. All compressive loading conditions upregulated osteogenic markers, while the cells loaded at 2.5% expressed the highest amount of late-stage differentiation marker. This study demonstrates that loading alone can accelerate differentiation on 3-D scaffolds.

3.2. Introduction

hMSCs are adult stem cells that can differentiate into various lineages, including bone, cartilage, fat, tendon, muscle, and potentially neurons [6-18]. Because of their multipotency, hMSCs have great potential for regenerative medicine and tissue engineering. Differentiation is usually induced by chemical induction (i.e. growth factors, glucocorticoids). However, mechanical loading may be a better approach to replicate *in vivo* conditions, and therefore, would control the differentiation more effectively than chemical induction and may be more clinically relevant.

It is known that mechanical cues are crucial to development and morphogenesis [135-137]. Further, in most mechanosensitive tissues, lack of mechanical loading can lead to tissue degradation or impaired function. For example, strain is crucial for the contractile phenotype of vascular smooth muscle cells [138]. Additionally, lack of loading or microgravity can lead to severe bone loss [139]. Many attempts have been made to reproduce *in vivo* body conditions in *in vitro* cell culture using mechanical stimulation. MSCs have been stimulated by cyclic stretch [140,141], compressive forces [142-145], 4-point bending [146], shear flow [147,148], perfusion [149,150], and cyclic hydrostatic pressure [151]. Mechanical loading can promote or inhibit cell proliferation [152], alignment [141,152-155] and differentiation [141-145,150,152-154,156-167]. Depending on the amount of strain, frequency, and loading time, tensile loading can promote myogenesis [141,152-154,168], osteogenesis [140,163-166,169,170], or tenogenesis [171] and compressive loading can promote osteogenesis [145,150,160] or chondrogenesis [142-144,156-159,161,172-180] of MSCs.

While studies have examined the differentiation of hMSCs by compressive or tensile loading, many different loading conditions, times, and substrates have been used. Most studies have used a 2-D substrate, such as polydimethylsiloxane (PDMS), but a 3-D substrate more accurately represents *in vivo* conditions. The mechanical properties of the chosen material must be considered, as stiffness alone can induce differentiation of hMSCs [48]. Additionally, scaffolds must be able to withstand loading. In this study, porous scaffolds were made out of polyurethane resin (PUR) and poly-DL-lactic acid (PLA)/polycaprolactone (PCL) blend with compressive moduli of 30 kPa and 140 kPa,

respectively [181]. PURs have been used in many biomedical applications, including pacemaker lead insulation and catheters [182]. Because of their elastomeric properties, PURs are commonly used for soft tissue engineering applications, such as skeletal muscle [183] and heart valves [184]. PCL and PLA are commonly used as a blend or a copolymer. PLA/PCL blends and copolymers have been used for tissue-engineered bone [185-187], among other applications. The purpose of this study was to assess the capability of hMSCs to differentiate solely with tensile or compressive cyclic loading in 3-D porous foams. hMSCs were grown on 3-D porous PUR or PLA/PCL scaffolds and subjected to continuous tensile (5-20%) or compressive loading (2.5-10%), respectively, for 3 days. The mRNA levels of various osteogenic and myogenic markers were investigated to assess differentiation. Comparable upregulation of myogenic markers was observed with 10% stretch and static culture on PUR. All levels of compressive loading appeared to enhance osteogenesis, with 2.5% compression producing the most mature cells.

3.3.Experimental Details

3.3.1. Preparation of scaffolds

PUR (Texin 950) was purchased from Bayer MaterialScience (Pittsburgh, PA). PDLLA 3051D was purchased from Natureworks (Minnetonka, MN). PCL was purchased from Sigma Aldrich. PLA/PCL (50:50) blend was synthesized using microwave radiation [188]. The porous samples were prepared by a solvent casting/salt leaching method [189]. Polymers were dissolved in solvent to yield a solution of 5%

(w/v). The solvents used for the PLA/PCL blend and Texin 950 were chloroform (VWR, West Chester, PA) and THF (Acros Organics, Morris Plains, NJ), respectively. NaCl particles (>125μm) (90% w/v) (Chemicals Inc., Gibbstown, NJ) were added to each solution. The solution was cast into individual molds. The scaffolds were air-dried for 48 h to allow the solvent to evaporate. They were subsequently removed from the mold and immersed in distilled deionized water at 60˚C for 48 h to leach out the salt. Sample dimensions of PUR scaffolds were 100x20x1 mm. The PLA/PCL blend scaffolds had a diameter of 15mm and thickness of 1 mm.

3.3.2. Remote actuated bioreactors

For continuous stimulation, a remote actuation mechanism was made. The remote actuator consisted of a motor (Part # WGB234607, Global Industrial Charlotte, NC), a cam, and a swinging frame. The swinging frame has an angular reciprocation inside a fixed frame. This mechanism activates one or more coaxial cables. The cables can be connected in to mechanism at 4 different places, which results in 4 different displacements (Figure 37).

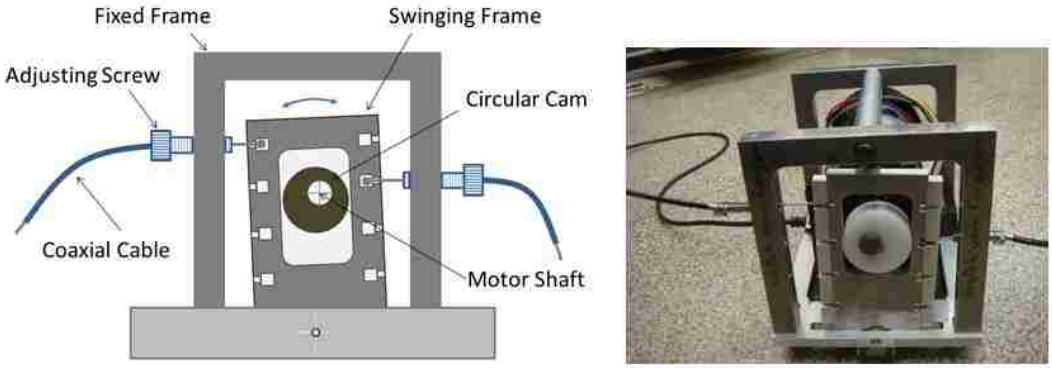

Figure 37: Remote actuator

The tensile and compressive loading devices are shown in Figure 38 and Figure 39, respectively. The tensile loading device contained clamps to hold the PUR scaffold in place, and put tensile cyclic force on one side of the scaffold. In the compressive loading device, the PLA/PCL blend scaffold was held in place while the bottom stage moved up and down to compress the scaffold. These devices are placed inside the incubator and run by cables.

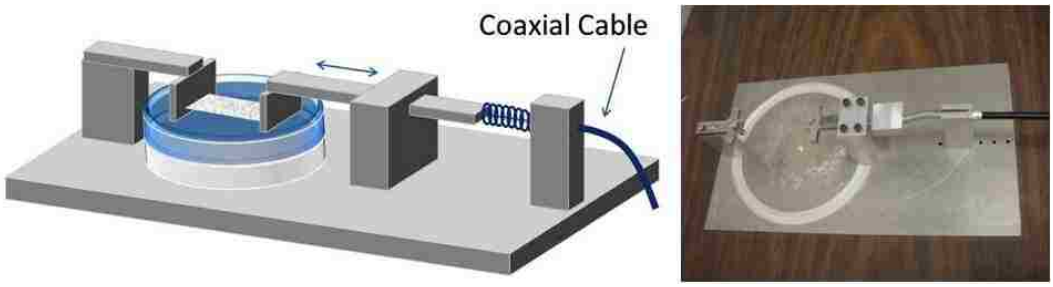

Figure 38: Remote actuated tensile loading device

Figure 39: Remote actuated compressive loading device

3.3.3. Cell culture

hMSCs (PT-2501, Lonza, Walkersville, MD) were cultivated on TCPS dishes in Mesenchymal Stem Cell Basal Medium supplemented with MSCGM SingleQuots (Lonza). Scaffolds were UV sterilized for 48 h and then incubated in media for 24 h prior to seeding. Approximately $5x10^5$ and $2x10^5$ cells (passages 5-7) were seeded onto the PUR and PLA/PCL blend scaffolds, respectively. Cells were allowed to adhere for 24 h prior to the start of loading. The scaffolds were then subjected to compressive or tensile loading on PLA/PCL blend or PUR scaffolds, respectively, for 3 days. hMSCs grown for 3 days on PLA/PCL blend or PUR scaffolds without loading were used as negative control samples. Positive control samples for compressive and tensile loading were grown in osteogenic or myogenic media, respectively, in TCPS dishes for 3 days (period of loading) or 28 days (full differentiation). Osteoinductive media contained DMEM Low Glucose with L-glutamine, glucose, and sodium pyruvate (HyClone Laboratories, Logan, UT) supplemented with 10% fetal bovine serum (FBS) (HyClone

Laboratories), 0.1μM dexamethasone (EMD Millipore, Billerica, MA), 10 mM β glycerol phosphate (Sigma Aldrich), and 0.05 mM ascorbic acid (Acros Organics, Morris Plains, NJ). To induce myogenic differentiation, 5 mM azacytidine (MP Biomedicals) was added to media (DMEM Low Glucose, 10% FBS) once a week for 24 hours, for 4 weeks.

3.3.4. qPCR

Total RNA was isolated after 3 days of loading using RNeasy Plus Micro kits (Qiagen, Valencia, CA). RNA was converted to cDNA using a Qiagen Omniscript RT Kit. Cycles were optimized for the amplicon size and primer Tm on a Qiagen Rotor-Gene qPCR system. A SYBR green qPCR kit from Qiagen was used to assess gene expression. Primers used for tensile and compressive loading are shown in Table 2 and Table 3, respectively. Fold changes were determined through ΔΔCt comparison to the negative control (undifferentiated hMSCs). Primer efficiency values were empirically derived from undifferentiated hMSCs for the housekeeping gene (GAPDH) and from osteogenic and myogenic hMSCs for differentiation markers. The copy rate for each primer was found using the slope of the efficiency curve. Fold changes were determined through ΔΔCt comparison, and all data was subject to normalization to the housekeeping gene (GAPDH) corresponding to each experimental condition and specimen. The ΔΔCt was calculated using the Ct of both the housekeeping gene (HKG) and the gene of interest (GOI) for the experimental and control conditions:

$$\Delta\Delta Ct = \frac{2^{Ct_{HKG_{Exp}} - Ct_{GOI_{Exp}}}}{2^{Ct_{HKG_{control}} - Ct_{GOI_{control}}}} \quad (34)$$

Statistical significance was evaluated with a paired Student's t-test for comparison of t-dependent groups.

Table 2: qPCR primers for tensile loading

Target/control gene	Primer Sequence (5'-3')	Amplicon Size	Tm
GAPDH	F- CGGATTTGGTCGTATTGG R- TCAAAGGTGGAGGAGTGG	861	F Tm = 53 R Tm = 56
β-Myosin Heavy Chain (β-MHC)	F- GATCACCAACAACCCCTACG R- ATGCAGAGCTGCTCAAAGC	528	F Tm = 58 R Tm = 59
Smooth muscle A-actin (SMAA)	F- GTGTTGCCCCTGAAGAGCAT R- GCTGGGACATTGAAAGTCTCA	109	F Tm = 61 R Tm = 58
Calponin 1 (CNN1)	F- CAACCACCACGCACACAACTA R- GGTCCAGCCAAGAGCAGCAG	97	F Tm = 61 R Tm = 63
Collagen 1 (Col 1)	F- ATCCAGCTGACCTTCCTGCG R- TCGAAGCCGAATTCCTGGTCT	323	F Tm = 62 R Tm = 61

Table 3: qPCR primers for compressive loading

Target/control gene	Primer Sequence (5'-3')	Amplicon Size	Tm
GAPDH	F- CGGATTTGGTCGTATTGG R- TCAAAGGTGGAGGAGTGG	861	F Tm = 53 R Tm = 56
Runx2	F- CCACCCGGCCGAACTGGTCC R- CCTCGTCCGCTCCGGCCCACA	258	F Tm = 68 R Tm = 71
Osteocalcin (OC)	F- GAAGCCCAGCGGTGCA R- CACTACCTCGCTGCCCTCC	70	F Tm = 60 R Tm = 62
Col 1	F- ATCCAGCTGACCTTCCTGCG R- TCGAAGCCGAATTCCTGGTCT	323	F Tm = 62 R Tm = 61
Collagen II (Col II)	F- GAAACCATCAATGGTGGCTTCC R- CGATAACAGTCTTGCCCCACTT	301	F Tm = 60 R Tm = 62

3.4. Results and Discussion

3.4.1. Tensile Loading qPCR Results

hMSCs on porous PUR scaffolds were stretched at 5%, 10%, 15%, and 20% for 3 days and mRNA expression was examined. hMSCs stretched at 20% underwent extensive cell death, and therefore, the mRNA could not be analyzed. hMSCs on PUR were compared to cells in myogenic media for 3 days (MM 3d) and 28 days (MM 28). Both smooth and cardiac muscle markers were used, as tensile loading has been shown to induce both types of muscle [141,152-155,162,190]. The mRNA expression of β-MHC, a cardiac specific isoform, was investigated (Figure 40). Myosin is the main component of thick filaments in sarcomeres. Type II myosin, found in muscle cells, has two heavy chains and four light chains. The heavy chains are each comprised of a globular head domain and a coiled tail domain [119]. β-MHC is downregulated compared to undifferentiated cells in all conditions, suggesting that hMSCs do not take on a cardiomyogenic phenotype, although the samples stretched at 10% displayed comparable levels to cells treated with 5-aza for 4 weeks.

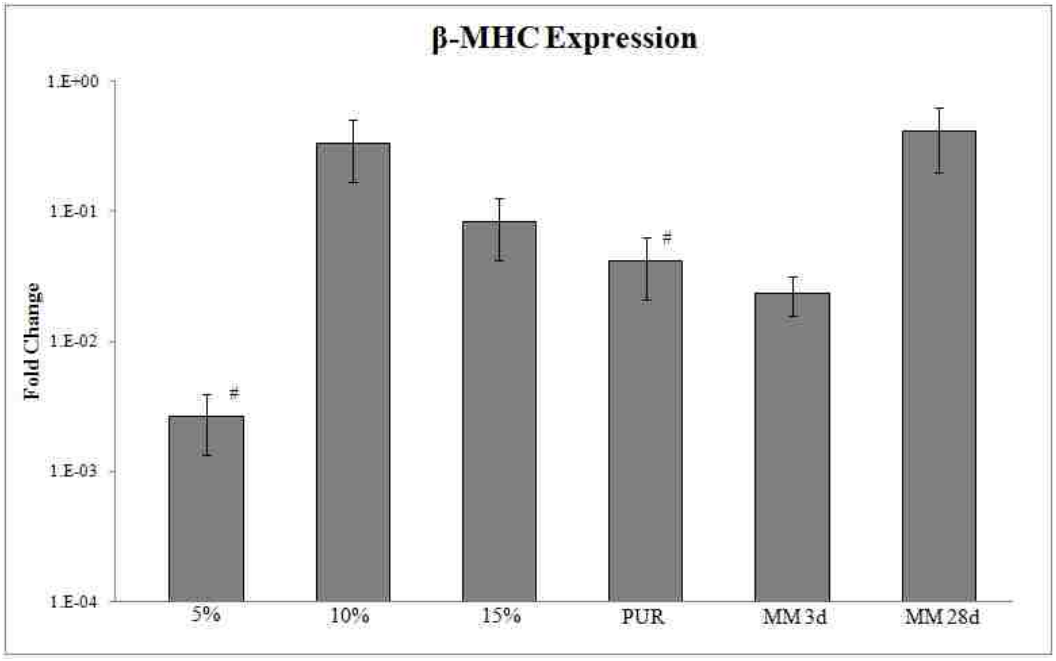

Figure 40: Fold change (ΔΔCt) of β-MHC compared undifferentiated hMSCs (*P<0.1, **P<0.05, ***P<0.01 compared to MM 3d, #P<0.1, ##P<0.05, ###P<0.01 compared to MM 28d)

The mRNA levels of SMAA and CNN1, two smooth muscle markers, were also examined. SMAA is the primary actin isotype found in vascular smooth muscle cells, and is also transiently expressed in the development of cardiac and skeletal muscle [117]. Comparable levels of upregulation of SMAA were observed in 10%, 15%, and static culture on PUR, and all three conditions were significantly upregulated compared to MM 3d and MM 28d (Figure 41). Because SMAA is considered an early marker for smooth muscle, it is especially significant that these conditions had upregulated mRNA expression compared to MM 3d, indicating that they may accelerate smooth muscle myogenesis. CNN1 is a protein that interacts with F-actin and tropomyosin to control the contraction of smooth muscle cells, and is considered an intermediate marker [118].

hMSCs on PUR had the most significant upregulation ($P<0.05$) compared to MM 3d and MM 28d (Figure 42). An upregulation was observed with 10% stretch, but was not considered significant ($P<0.15$ compared to MM 3d, MM 28d). Downregulation of CNN1 was detected with 5% and 15% stretch. The levels of CNN1 in MM 3d and MM 28d were also downregulated, due to the fact that peak expression most likely occurs in the first 2 weeks. While upregulation of SMAA mRNA was observed for 10%, 15%, and PUR, the upregulated mRNA levels of CNN1 in 10% and PUR may indicate that the cells are more mature, as CNN1 is an intermediate marker.

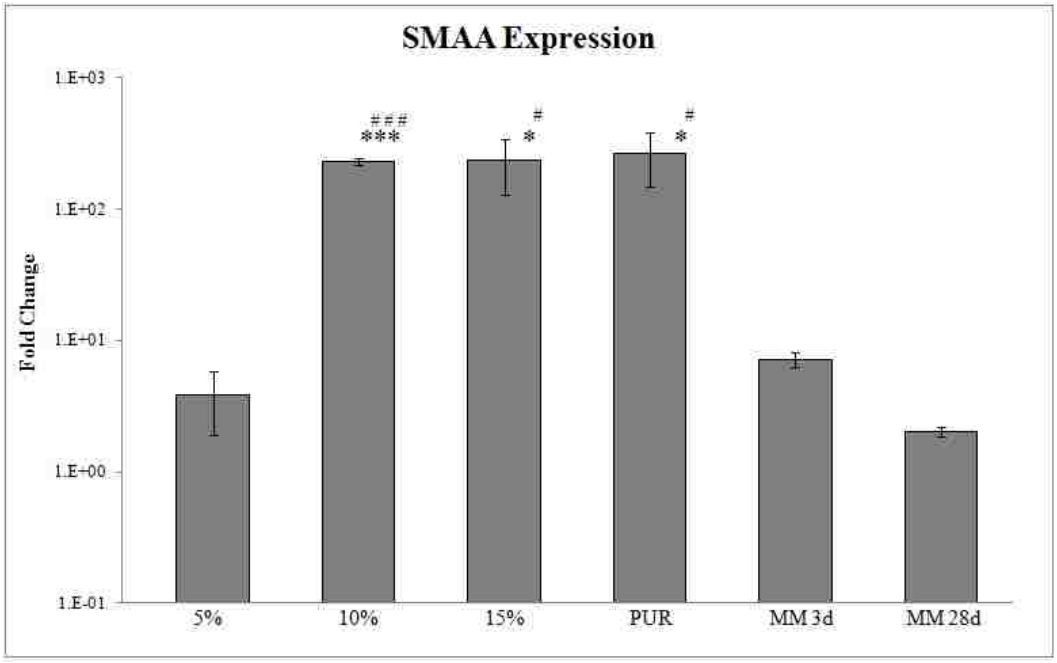

Figure 41: Fold change (ΔΔCt) of SMAA compared undifferentiated hMSCs (*P<0.1, **P<0.05, ***P<0.01 compared to MM 3d, #P<0.1, ##P<0.05, ###P<0.01 compared to MM 28d)

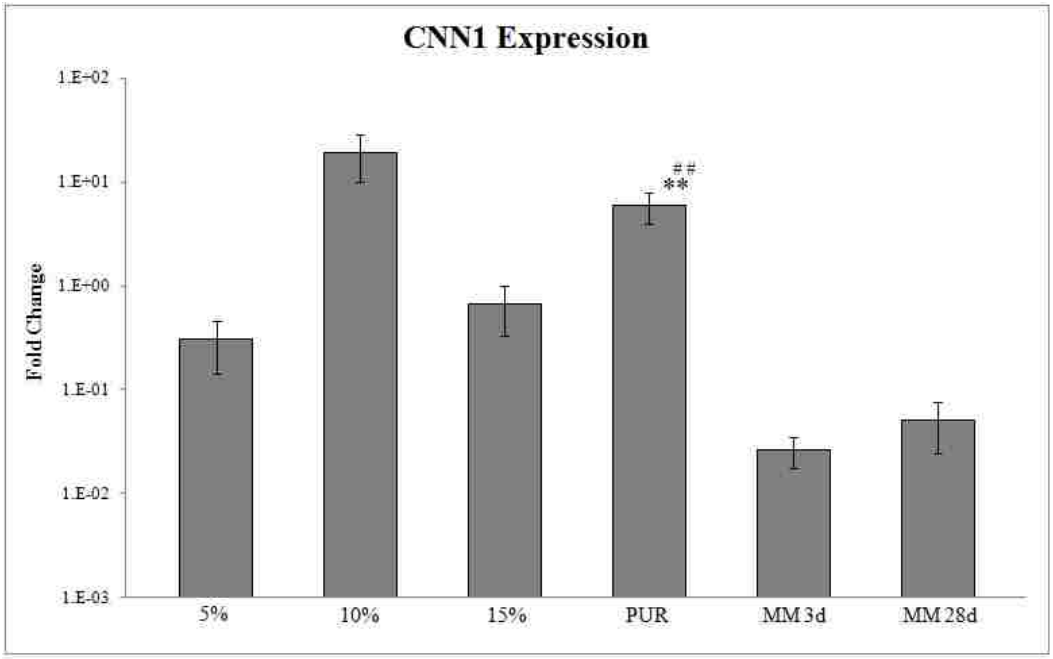

Figure 42: Fold change (ΔΔCt) of CNN1 compared undifferentiated hMSCs (*P<0.1, **P<0.05, ***P<0.01 compared to MM 3d, #P<0.1, ##P<0.05, ###P<0.01 compared to MM 28d)

Col 1 is present in vascular smooth muscle, where it is indicative of a synthetic (immature) phenotype, but can help to promote a contractile phenotype and proliferation [191]. It is also the main protein component of bone [124], and therefore, is frequently used as an osteoblast marker. Significant (P<0.1) upregulation of Col 1 was observed with 10% stretch and PUR, while 5% and 15% loading downregulated Col 1 (Figure 43). While the upregulation of Col 1 could also be indicative of osteogenic differentiation, the same trends that are seen in Col 1 expression were observed with CNN1 expression. Therefore, it is believed that cells exposed to 10% loading and PUR (no loading) are developing a myogenic phenotype.

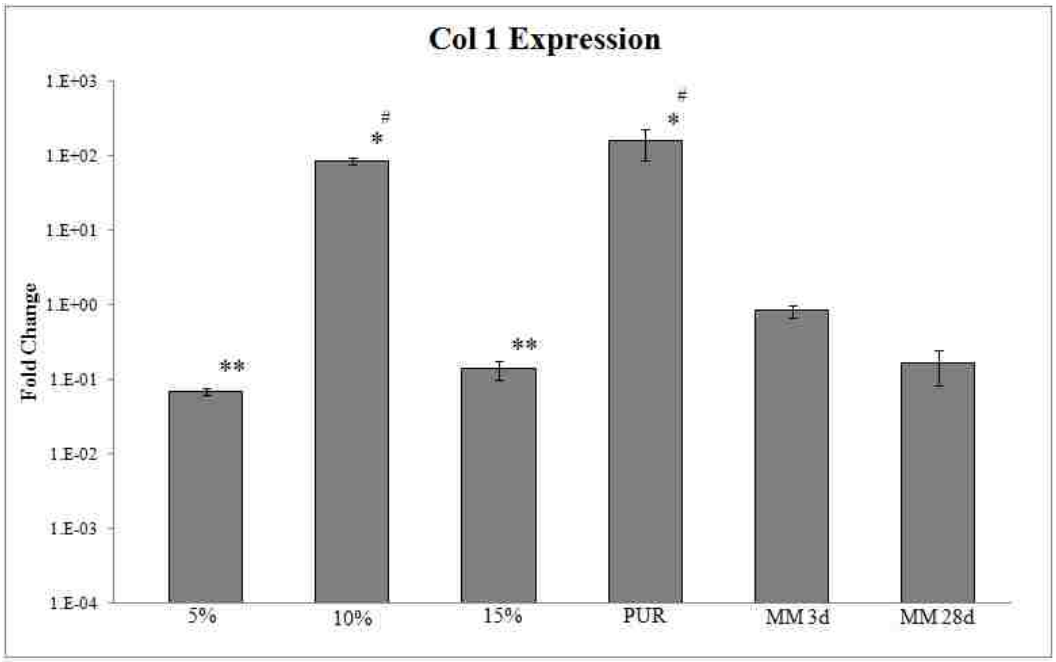

Figure 43: Fold change (ΔΔCt) of Col 1 compared undifferentiated hMSCs (*P<0.1, **P<0.05, ***P<0.01 compared to MM 3d, #P<0.1, ##P<0.05, ###P<0.01 compared to MM 28d)

In vivo, aortic smooth muscle cells undergo 9-12% strain [192]. *In vitro* studies typically stretch at 10% to induce myogenesis, but most studies have been conducted on 2-D PDMS substrates [141,152,155,193]. Park et al. stretched hMSCs on PDMS at 10% and 1 Hz [141]. Smooth muscle markers (SMAA and SM-22α) were upregulated after 1 day of loading, but expression decreased as cells oriented themselves perpendicularly to the direction of strain, demonstrating the need for the cells to remain parallel to strain, as in native blood vessels. In previous studies, MSCs stretched on 2-D substrates generally oriented perpendicularly to direction of applied strain [141,152,155], while MSCs stretched on 3-D substrates oriented parallel to strain [154].

Rat MSCs in a 3-D fibrin gel not only oriented parallel to strain (10%, 1 Hz for 6 days), smooth muscle markers SMAA and CNN1 were also upregulated [154]. However, there was a need for a 3-D study to be carried out with hMSCs.

This study stretched hMSCs at 5%, 10%, 15%, and 20% at 1 Hz on 3-D PUR scaffolds for 3 days. Both 10% stretch and PUR upregulated SMAA, CNN1, and Col 1. When t-tests were done to compare these upregulations, no statistical significance was found. Therefore, the material alone may accelerate myogenic differentiation as well as 10% cyclic stretch. However, tensile loading has been shown to promote cell alignment. In the native blood vessel, smooth muscle cells are oriented parallel to the direction of strain. In previous studies, MSCs stretched on 2D substrates generally oriented perpendicularly to direction of applied strain [141,152,155], while MSCs stretched on 3D substrates oriented parallel to strain [154]. More studies must be done to investigate the effects of 10% loading in a 3-D porous PUR scaffold on cell alignment.

3.4.2. Compressive Loading qPCR Results

hMSCs on porous PLA/PCL blend scaffolds were compressed at 2.5%, 5%, 7.5%, and 10% for 3 days and mRNA expression was examined. hMSCs on PLA/PCL were compared to cells in osteogenic media for 3 days (OM 3d) and 28 days (OM 28). Various osteogenic markers (Runx2, OC, Col 1) as well as an additional extracellular matrix (ECM) marker (Col II), were investigated. Runx2 is an essential transcription factor in osteogenesis that regulates OC, among other genes [125]. It is expressed prior

to an osteoblast phenotype and may regulate the inhibition of proliferation, which is necessary for differentiation [194]. All loading conditions, as well as static culture on PLA/PCL, upregulated Runx2 compared to OM 3d (Figure 44). This is significant as Runx2 is an early osteogenic marker. Compressive loading at 7.5% had the highest upregulation ($P<0.05$), followed by static culture on PLA/PCL ($P<0.05$).

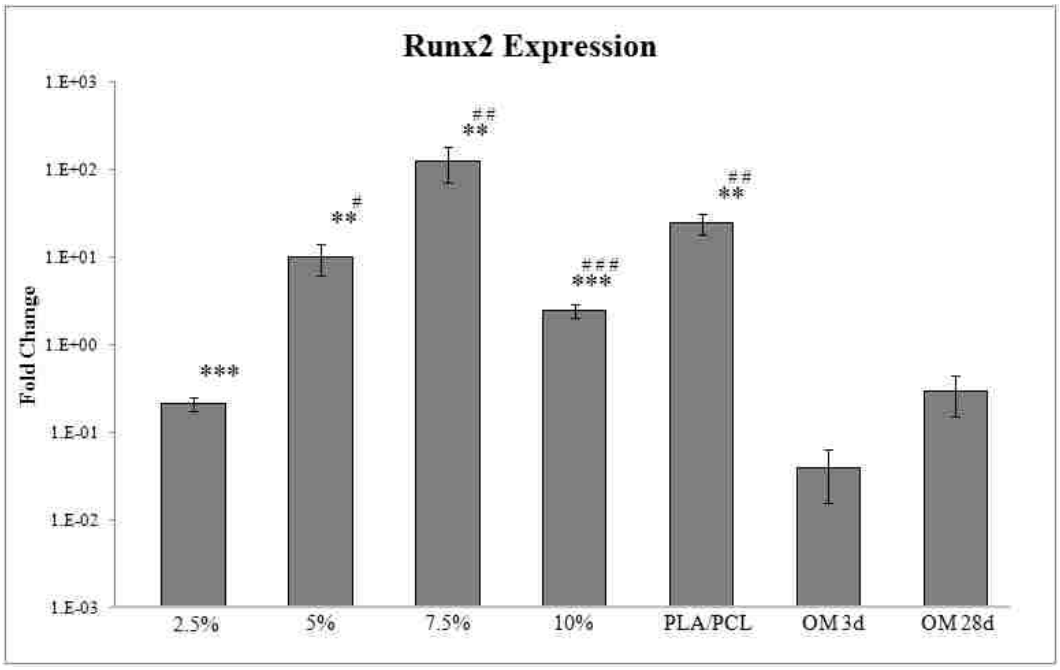

Figure 44: Fold change (ΔΔCt) of Runx2 compared undifferentiated hMSCs (*P<0.1, **P<0.05, ***P<0.01 compared to OM 3d, #P<0.1, ##P<0.05, ###P<0.01 compared to OM 28d)

Col 1 is the main collagen protein in the bone matrix, and its gene expression typically peaks in the first 2 weeks of differentiation, during the matrix maturation phase of osteogenesis [124]. Col 1 mRNA expression was upregulated with 7.5% ($P<0.1$) and 5% (not significant, $P<0.15$) loading, and was downregulated with 2.5%

loading and static culture on PLA/PCL scaffolds (Figure 45). Corresponding to the results of Runx2 mRNA expression, it appears that 7.5% compressive loading accelerates an early stage of osteogenesis.

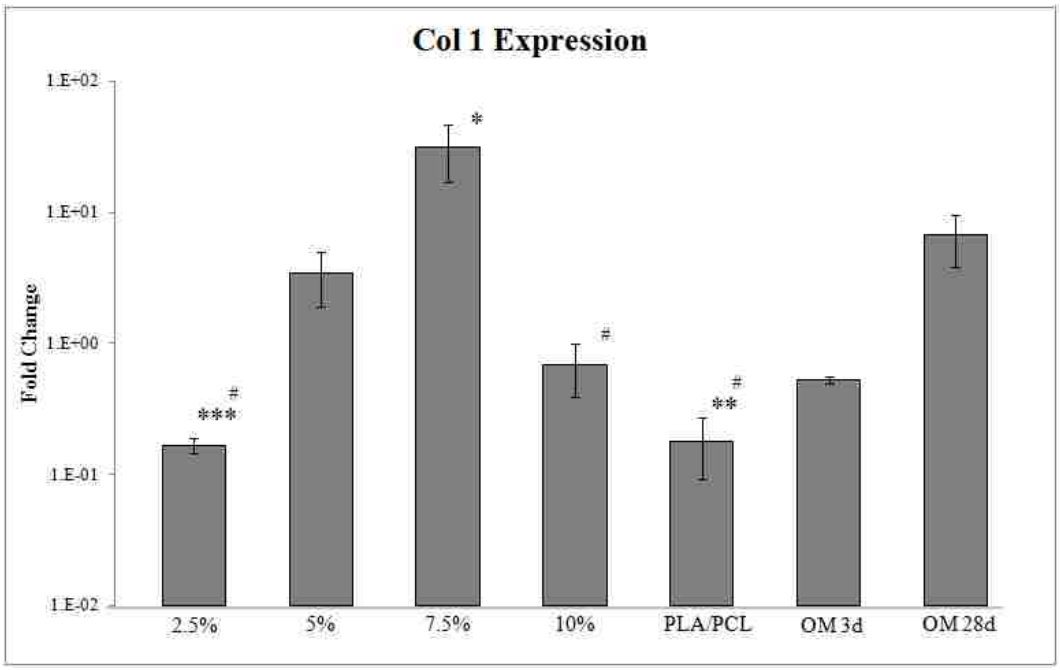

Figure 45: Fold change (ΔΔCt) of Col 1 compared undifferentiated hMSCs (*P<0.1, **P<0.05, ***P<0.01 compared to OM 3d, #P<0.1, ##P<0.05, ###P<0.01 compared to OM 28d)

A marker of mature osteoblasts, OC, was also investigated. OC is involved in regulation of mineral deposition and peaks in the fourth week of osteogenesis [122]. OC was significantly upregulated in all conditions compared to OM 3d (Figure 46). Loading at 2.5% significantly upregulated (P<0.1) OC compared to OM 28d. This is noteworthy because OC peaks during the mineralization phase of osteogenesis, and is

necessary for successful differentiation. Therefore, 2.5% compressive loading accelerated the upregulation of a late-stage osteogenic marker.

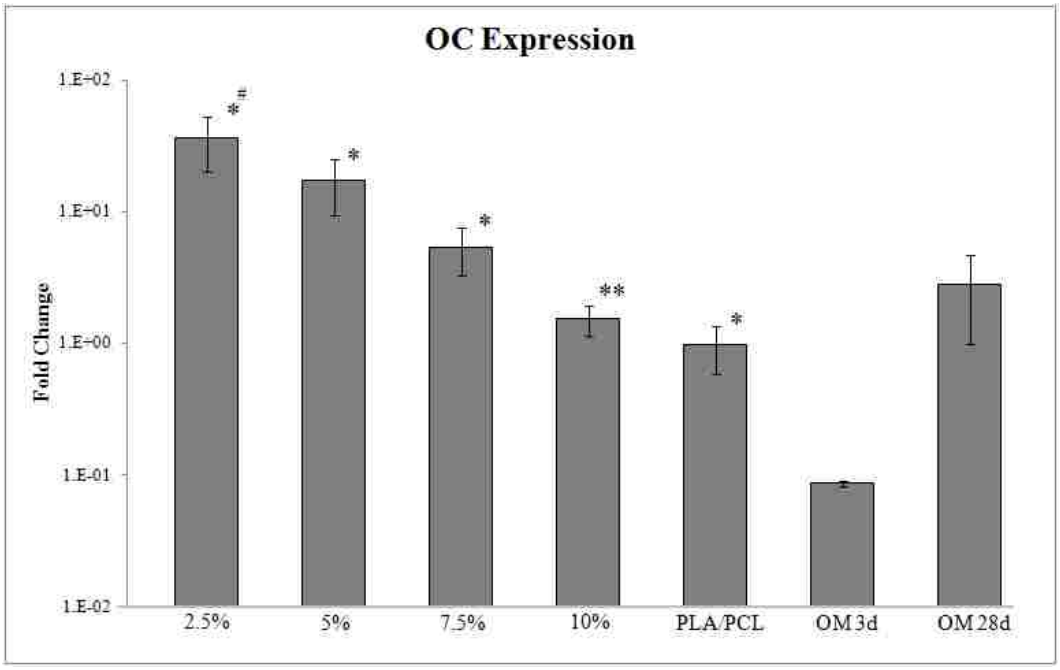

Figure 46: Fold change (ΔΔCt) of OC compared undifferentiated hMSCs (*P<0.1, **P<0.05, ***P<0.01 compared to OM 3d, #P<0.1, ##P<0.05, ###P<0.01 compared to OM 28d)

Col II expression was also investigated, as compressive loading can also induce chondrogenesis [142-144,156-159,161,172-180]. Col II is typically a marker of matrix formation in chondrogenesis [195]. While Col II mRNA expression was upregulated in some conditions (Figure 47), the levels were not significantly higher than OM 3d. Therefore, the loading conditions seem to have upregulated the mRNA expression of an ECM protein that is intrinsically expressed by hMSCs.

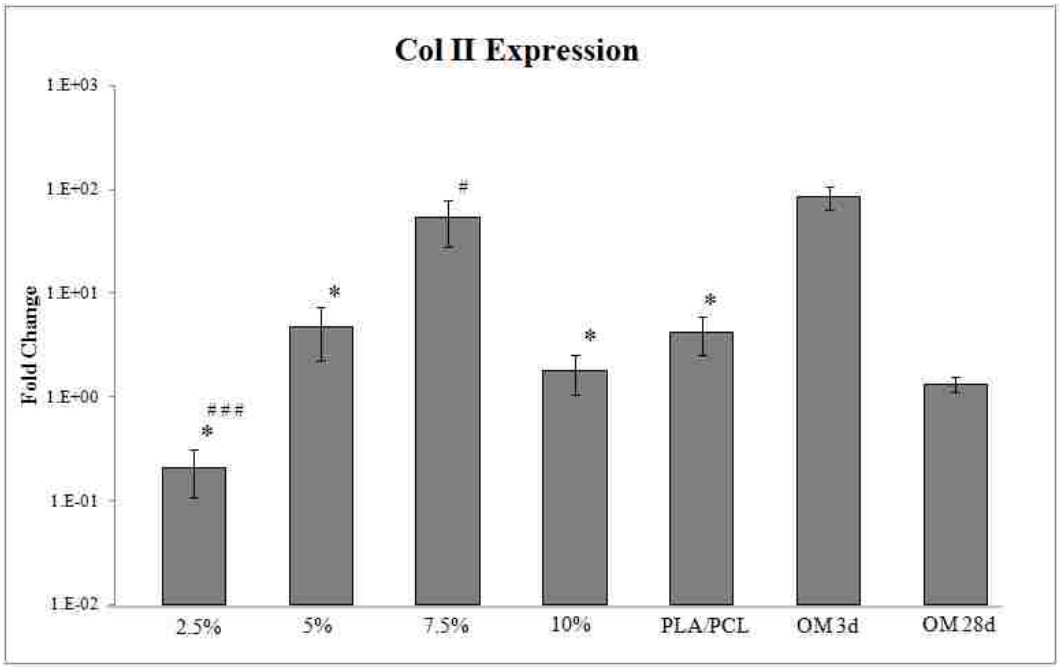

Figure 47: Fold change (ΔΔCt) of Col II compared undifferentiated hMSCs (*P<0.1, **P<0.05, ***P<0.01 compared to OM 3d, #P<0.1, ##P<0.05, ###P<0.01 compared to OM 28d)

Due to the large variations in compressive loading conditions, it is difficult to compare results from various studies. While typical strains on bone *in vivo* are 0.3-5% [196], *in vitro* studies frequently use larger strains of 10%. Additionally, many different loading regimens (from minutes per day to continuous loading), experiment lengths (from hours to weeks), and frequencies (typically 0.5-1 Hz) have been used. The following is a summary of relevant studies.

In conjunction with osteogenic media (typically ascorbic acid, β-glycerol phosphate, and dexamethasone), compressive loading has been shown to upregulate osteogenic markers [145,150]. hMSCs on glass were loaded at 1 Hz twice a day (10

minutes each) for 7 days with a pressure of 5 kPa [145]. A significant increase in ALP and calcium deposition was seen in the stimulated group compared to the group with no stimulation. hMSCs have also been grown on bovine spongiosa disks and subjected to perfusion and cyclic compression of 10% at 0.5 Hz for 21 days [150]. The cells subjected to both perfusion and compression had the highest amount of OC expression (compared to perfusion alone and static culture). While the addition of loading to the osteogenic media enhances osteogenesis, it is necessary to determine if loading alone can have similar effects.

To assess the effect of loading without dexamethasone, hMSCs on a PUR foam were loaded using a protocol deemed successful with mature osteoblasts (5% strain at 1 Hz for 2 hours on day 9 and then every 5 days up to and including day 19) [160]. The combination of loading and dexamethasone generally had the highest expression of all osteogenic markers tested. However, the amounts of collagen and calcium at day 24 were comparable between the group of loading alone and loading and dexamethasone, suggesting that the cells could mature equally in both groups. Another study loaded hMSCs on collagen-alginate scaffolds at 10% compression for 4 hours a day for 21 days and found upregulation of Runx2 compared to static controls, although no other osteogenic markers were assessed [197]. While Runx2 is an essential transcription factor in osteogenesis, its upregulation is not enough to confirm osteogenesis.

The present study evaluates the mRNA expression of various osteogenic markers in the absence of differentiation media. Four different loading conditions were used: 2.5%, 5%, 7.5%, and 10%, all at 1 Hz for 3 days. While 5-10% strain has been

used in previous studies, a smaller amount of strain may more accurately match *in vivo* conditions. All loading conditions, as well as static culture on PLA/PCL, upregulated an essential transcription factor in osteogenesis (Runx2) compared to OM 3d, with the highest levels observed in 7.5% loading and PLA/PCL. Additionally, Col 1 mRNA was upregulated with 5% and 7.5% compressive loading, indicating that the matrix maturation phase had begun. OC was significantly upregulated in all conditions compared to OM 3d, and 2.5% upregulated OC compared to OM 28d. These results indicate that the cells subjected to all loading conditions may have accelerated osteogenesis. However, cells compressed at 2.5% may be the most mature, as OC, a late-stage marker, was upregulated compared to OM 28d. The mRNA levels of Runx2 and Col 1 in cells loaded at 2.5% may have been already upregulated, and then consequently downregulated, as OC levels rose. These observations seem to agree with *in vivo* loading conditions, as 2.5% compressive loading is within the physiological range [196].

While it is evident that mechanical loading can regulate the differentiation of hMSCs, the mechanisms behind this regulation still remain elusive. Several possibilities include integrins [198], stretch activated cation channels [199], and focal adhesion proteins, such as vinculin and talin [200]. It is hypothesized that during mechanical loading, protein deformation occurs, which signals biochemical signaling [201]. Stretch activated ion channels (SACs) are mechanotransducers present in the membrane that respond to tension and fluid flow. They have been implicated in the chondrogenic differentiation response of hMSCs to tensile strain [202] and therefore,

are of great interest. In compressive loading, the SACCs may also be activated due to the fluid flow of media induced by the loading. More studies must be done to determine the role of SACs in loading-induced differentiation to osteoblasts and myocytes.

3.5. Conclusions

Mechanical loading as a means of differentiation may be a suitable replacement for chemical induction in the near future. hMSCs were cyclically stretched at 5%, 10%, 15%, and 20% on PUR. Cell death was observed with 20% stretch. mRNA levels of MHC were downregulated in all conditions, indicating a cardiomyogenic phenotype was not acquired. Highest levels of SMAA, CNN1, and Col 1 were observed with 10% stretch and static culture on PUR, indicating these conditions can accelerate smooth muscle myogenesis. hMSCs were also compressed at 2.5%, 5%, 7.5%, and 10% on PLA/PCL blend scaffolds. While all loading conditions seemed to enhance osteogenesis to an extent, cells compressed at 2.5% seemed to mature the fastest, with a significant increase in OC compared to OM 28d. This study indicates that tensile and compressive loading alone can induce myogenesis and osteogenesis, respectively, in hMSCs on 3-D porous scaffolds.

Chapter 4: Cardiogenic Potential of hMSCs by Embryoid Body Formation

4.1. Chapter Overview

hMSCs are considered a potential cell source for cardiac tissue engineering, due to their transdifferentiation potential and homologous availability. Current differentiation methods are varied, but many use 5-azacytidine (5-aza) for differentiation. 5-aza use may be clinically discouraged, due to the potential for harmful demethylation activity. Another method for transdifferentiation of hMSCs into cardiomyocytes is embryoid body culture, commonly used with embryonic stem cells. This method has been explored for potential in hMSC cardiomyocyte differentiation. However, the RNA expression of embryoid body-derived hMSCs has not been examined. In this study, hMSCs were grown using the hanging drop method to form embryoid bodies. Cellular differentiation was quantified by assessing cell outgrowth and cardiac marker expression. Cells were positive for various cardiac markers (sarcomeric actin, tropomyosin, troponin T, myosin heavy chain, α-actinin), including the adherens junction protein, N-cadherin. The genes GATA4, α-cardiac actin, β-myosin heavy chain, troponin T, and desmin were upregulated compared to undifferentiated cells. The cells also contained organized myofibrils and some Z bands, which are generally not observed after 5-aza treatment. Therefore, the embryoid body method may be viable clinical alternative for cardiac differentiation of hMSCs.

4.2. Introduction

Damage to heart muscle, whether is it acute or chronic, can often lead to heart failure. In the United States, almost 300,000 people die from heart failure every year [203]. Because cardiomyocytes cannot significantly proliferate, the heart primarily responds to injury through ventricular remodeling and scar tissue formation, which leads to a decline in contractile function [204-206]. Cardiac tissue engineering aims to repair, regenerate, or replace injured myocytes and improve cardiac function after myocardial infarction. Because the heart has limited resident stem cells [207-210], another cell source, such as skeletal myoblasts, embryonic stem cells, or MSCs, may be chosen.

Bone marrow MSCs are a potential cell source for repair after myocardial infarction. They are adult stem cells that can differentiate into different lineages, including bone, cartilage, fat, tendon, muscle, and possibly neurons [6-19]. They have the ability to proliferate in culture while retaining their multilineage potential. Several groups have used hMSCs to aid in the repair of infarcted myocardium [211-216], but it is debated whether hMSCs fully differentiate after implantation [18,217]. Additionally, the safety of undifferentiated MSCs has been questioned. There have been several reports of calcification after transplantation of bone marrow MSCs into an infracted heart [218,219]. Therefore, some researchers have suggested that it may be beneficial to differentiate the hMSCs prior to implantation [220,221].

The demethylation agent 5-aza is commonly used to induce differentiation in hMSCs [222,223]. However, it has been reported that the frequency of differentiation

using this method is very low [224] or even unsuccessful [225]. Additionally, the demethylation action of 5-aza may be nonspecific [226]. Other methods to differentiate hMSCs include co-culture with cardiomyocytes [120,227-229], electrical stimulation [230,231], medium enriched with insulin, dexamethasone, and ascorbic acid [120,220], transforming growth factor (TGF) β1 [221], and a combination of 5-aza and oxytocin [232]. A combination of retinoic acid, activin A, alpha thrombin, interleukin-6, and a variety of growth factors has also been used to induce cardiac transcription factors while maintaining the proliferative state prior to implantation [233]. Cardiomyocyte-differentiated hMSCs generally display cardiac markers, but lack the ability to contract *in vitro.* Therefore, a method that can produce functional cardiomyocytes, preferably without chemical induction, is needed.

Embryoid body (EB) formation is commonly used in the differentiation of stem cells, specifically ESCs [1,2,234,235] and embryonal carcinoma cells [236]. EBs are three-dimensional aggregates that contain multiple cell types that display a similar gene pattern to the developing embryo [112,237,238]. EB formation may be superior to 2D culture because it provides an environment that mimics *in vivo* conditions [239]. While EB formation has not been used extensively for hMSCs, it has been used to enhance osteogenic [240-245] and adipogenic differentiation [240,243], to create neural stem cell-like cells [246], and to enhance the anti-inflammatory properties of hMSCs [247]. Potapova et al. used hMSC EBs to produce cardiomyogenic cells that displayed the cardiac markers α-actinin, troponin T, atrial natiuretic peptide, cardiotin, and Ca_v 1.2 (a voltage gated calcium channel). Immunocytochemistry was performed at 4-7 days post

plating, at which point approximately 50% of the cells were positive for the cardiac markers.

This study was conducted to further investigate the characteristics of hMSC-derived cardiomyocytes produced by EB formation. The differentiation was carried out to 18 days post plating to examine whether or not the additional time would allow all cells to display cardiac proteins. Several key proteins involved in cardiomyocyte contraction (tropomyosin, sarcomeric actin, and myosin heavy chain), as well as an adherens junction protein (N-cadherin) were examined. Additionally, quantitative polymerase chain reaction (qPCR) was used to evaluate mRNA expression in EB-derived cardiomyocytes, which had not been previously investigated.

4.3. Experimental Details

4.3.1. Cell culture and differentiation

hMSCs were cultivated on TCPS dishes in Mesenchymal Stem Cell Basal Medium supplemented with MSCGM SingleQuots (Lonza, Walkersville, MD). Cells were committed to a cardiac lineage by cultivating hMSCs (passages 6-7) into EBs using the hanging drop method as reported by Potapova et al. [248]. Approximately 25 drops (40 µl each) of cell suspension in media (DMEM High Glucose with L-glutamine, glucose, and sodium pyruvate, HyClone Laboratories, Logan, UT) supplemented with 30% FBS were cultivated for 3 days on the lids of bacteriological grade petri dishes (Figure 48). Each drop contained approximately $2.5x10^5$ cells [248]. The EBs were transferred to tissue culture treated glass coverslips and grown for an

additional 18 days. Cell counts were performed at days 0, 5, 10, and 18. The cells were detached from the glass using trypsin (HyClone Laboratories) and counted using a hemocytometer. Statistical significance was evaluated with a paired Student's t-test for comparison of t-dependent groups. The experiment was completed a total of three times.

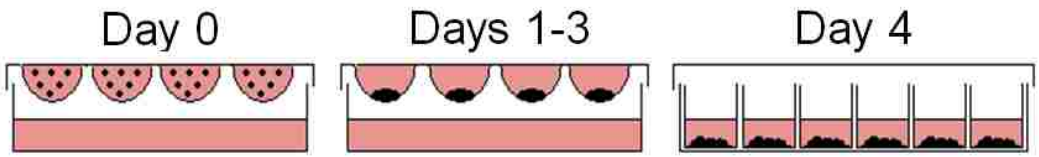

Figure 48: Method of EB formation. Cells are suspended in a 40 µl drop on day 0. Cells aggregate for 3 days and are plated onto tissue culture treated glass coverslips.

4.3.2. Immunocytochemistry

Fixation and immunocytochemical processing for sarcomeric actin, troponin T, myosin heavy chain (MHC), actinin, and tropomyosin expression were conducted using standard protocols. Mouse monoclonal anti-sarcomeric actin (1:250) was purchased from Invitrogen (Carlsbad, CA). The monoclonal antibodies MNCD2 (anti-N-cadherin, 1:100), CT3 (anti-cardiac troponin T, 1:100) and ALD-58 (anti-myosin heavy chain, 1:100), developed by Masatoshi Takeichi and Hiroaki Matsunami, Jim Jung-Ching Lin, and Donald A. Fischman, respectively, were obtained from the Developmental Studies Hybridoma Bank developed under the auspices of the NICHD and maintained by The University of Iowa, Department of Biology, Iowa City, IA 52242. Sheep polyclonal anti-tropomyosin (1:500), mouse monoclonal anti-actinin (1:200), and mouse

monoclonal anti-connexin 43 (1:200) were purchased from Millipore (Billerica, MA). Briefly, cells were fixed with 10% formalin (Sigma Aldrich) in 1 x PBS for 15 minutes. The samples were then treated with 100% methanol for 7 minutes. Non-specific binding sites were blocked with 1% bovine serum albumin (BSA) for 30 minutes at room temperature. Primary antibodies were incubated for 1 h at 37°C, followed by incubation with appropriate secondary antibodies (Alexa Fluor 488, Alexa Fluor 555, and Alexa Fluor 647, 1:1000, Invitrogen) for 1 h at room temperature. The nuclei were then counterstained with Hoechst dye (0.002 mg/ml in 1xPBS) for 5 minutes.

4.3.3. qPCR

qPCR was performed to assess mRNA expression of cardiomyocyte markers (Table 4). Total RNA was isolated using an RNeasy Plus Micro Kit (Qiagen, Valencia, CA). RNA was converted to cDNA using a Qiagen Omniscript RT Kit. Cycles were optimized for the amplicon size and primer T_m on a Qiagen Rotor-Gene qPCR system. A SYBR green qPCR kit from Qiagen was used to assess gene expression. Fold changes were determined through ΔΔCt comparison to the negative control (undifferentiated hMSCs). Primer efficiency values were empirically derived from undifferentiated hMSCs for the housekeeping gene (GAPDH) and from cardiomyogenic hMSCs for cardiomyocyte markers. The copy rate for each primer was found using the slope of the efficiency curve. Fold changes were determined through ΔΔCt comparison, and all data was subject to normalization to the housekeeping gene (GAPDH) corresponding to each experimental condition and specimen. The ΔΔCt was calculated

using the Ct of both the housekeeping gene (HKG) and the gene of interest (GOI) for the experimental and control conditions. Statistical significance was evaluated with a paired Student's t-test for comparison of t-dependent groups.

Table 4: qPCR primers for cardiomyogenic differentiation

Target/control Gene	Primer Sequence (5'-3')	Primer T_m	Amplicon Size
GAPDH	F- CGGATTTGGTCGTATTGG R- TCAAAGGTGGAGGAGTGG	F Tm = 53 R Tm = 56	861
Nkx2.5	F- CCAGCCAAGGACCCTAGAG R- AGCTCCACCGCCTTCTG	F Tm = 59 R Tm = 59	359
MEF2C	F- GACTTTCTGAAGGATGGGCAA R- AAGTGCTAAGCTTATCTCAGCA	F Tm = 58 R Tm = 59	233
GATA4	F- GATGCCTTTACACGCTGATG R- GATGTCCCCGTGAATTGGGT	F Tm = 57 R Tm = 59	400
α-Cardiac Actin	F- GCCTTCCTCATTTAAAGCTC R- AACACCACTGCTCTAGCCACG	F Tm = 54 R Tm = 63	418
β-MHC	F- GATCACCAACAACCCCTACG R- ATGCAGAGCTGCTCAAAGC	F Tm = 58 R Tm = 59	528
Desmin	F- CCAACAAGAACAACGACG R- TGGTATGGACCTCAGAACC	F Tm = 54 R Tm = 56	408
Troponin T	F- AGGCGCTGATTGAGGCTCAC R- ATAGATGCTCTGCCACAGC	F Tm = 63 R Tm = 57	407

4.4. Results and Discussion

4.4.1. Cell Proliferation

hMSCs are a heterogeneous population with two main cell types: spindle-shaped cells and large flattened cells (Figure 49a) [10,249,250]. The hanging drop procedure produces EBs that are approximately 1mm in diameter (Figure 49b). The differentiated

cells growing outward from the EBs were elongated and appeared to be a homogeneous population (Figure 49c). The cells aligned as they spread from the EB.

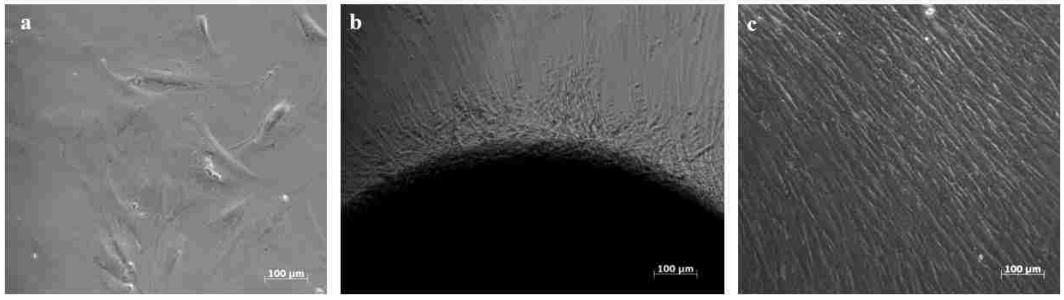

Figure 49: Phase-contrast images of a) undifferentiated hMSC cells, b) an EB with aligned cardiomyocyte-like cells, c) aligned outgrowth from EB

Cell counts were performed at days 0, 5, 10, and 18 to determine proliferation (Figure 50). The cell count at day 0 is representative of the EB alone, while the counts at days 5, 10, and 18 are representative of both the EB and the outgrowth. The average number of cells at day 0 was $2.43\pm0.19 \times 10^5$ cells, indicating that slight cell death occurred during cell aggregation, most likely due to hypoxia in the EB [251]. Significant cell growth did not occur between days 0 and 5. However, cell growth was significant ($P<0.01$) between days 5 and 10, and days 10 and 18.

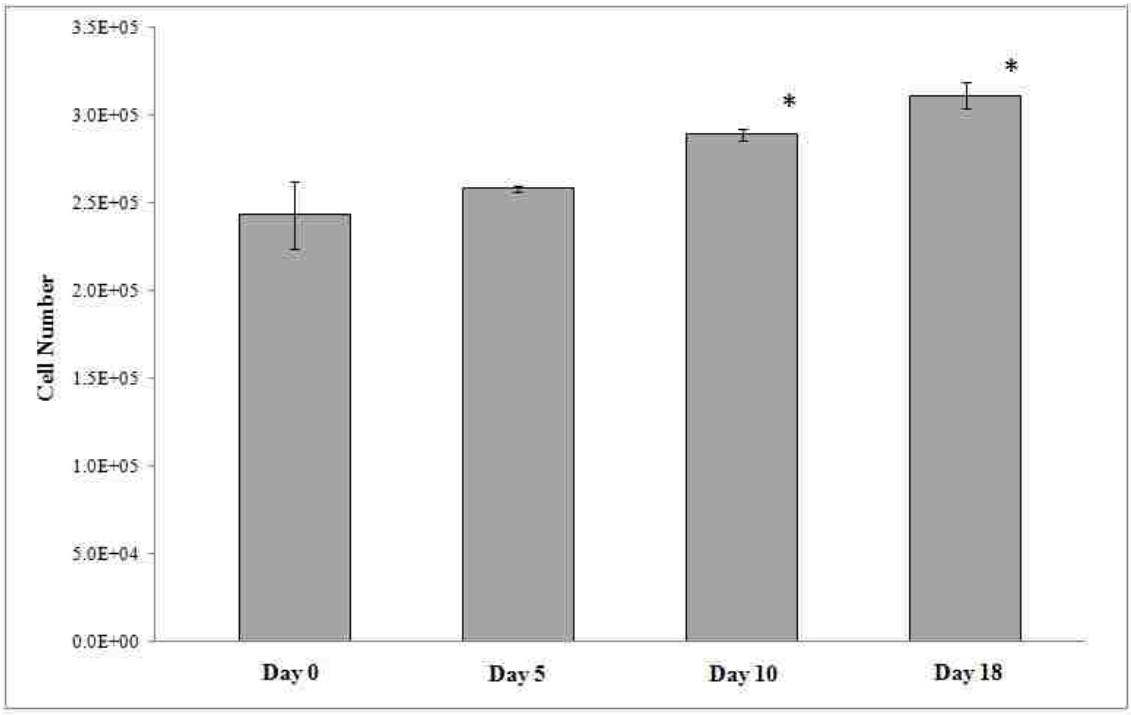

Figure 50: Proliferation of EB-derived cells from day 0 to 18 (*P<0.01 compared to previous cell count)

4.4.2. Immunocytochemistry

hMSC-derived cardiomyocytes have previously been tested for cardiac markers, but with mixed results from various differentiation procedures [220,252]. The hanging drop differentiation procedure (250,000 cells/40µl) used in this study, as reported by Potapova et al., produces cardiomyogenic cells that displayed the cardiac markers α-actinin, troponin T, atrial natiuretic peptide, cardiotin, and Ca_v 1.2 [248]. The current study examines the expression of additional cardiac markers (sarcomeric actin, tropomyosin, n-cadherin, Cx43, and β-myosin heavy chain) at 18 days post-plating. All of the cardiac markers examined will be outlined below.

Sarcomeric actin appeared as filaments in the differentiated cells (Figure 51, a-b). Sarcomeric actin is a key component of the contractile unit in cardiac muscle, the sarcomere, and appears at day 8 in developing embryo [112]. Some undifferentiated hMSCs were weakly positive for sarcomeric actin (Figure 51c), but staining was diffuse and no striations were observed. Muscle-specific proteins have previously been reported in untreated hMSCs [253]. This presence may suggest an inherent capacity for cardiomyogenic differentiation, and therefore, myocardial repair [233].

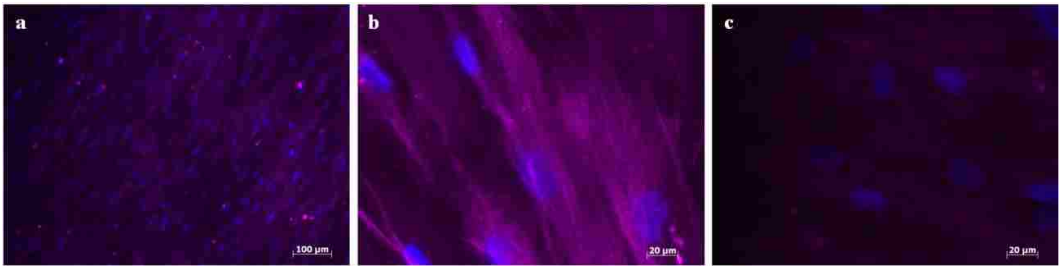

Figure 51: Sarcomeric actin in hMSC-derived cardiomyocytes (a-b) and non-induced hMSCs (c)

Clear striations were detected with tropomyosin staining (Figure 52, a-b). Tropomyosin is a protein that regulates sarcomeric contraction. Tropomyosin interacts with actin and the troponin complex to control the attachment of crossbridges to actin. Therefore, the presence of this protein indicates that the cells may have the ability to contract. Faint tropomyosin expression was observed in undifferentiated cells (Figure 52c). However, staining in undifferentiated cells was diffuse, while in cardiomyogenic cells, clearly aligned fibrils were observed. As previously stated with regard to

sarcomeric actin, the existence of tropomyosin prior to differentiation may indicate an intrinsic ability for transdifferentiation.

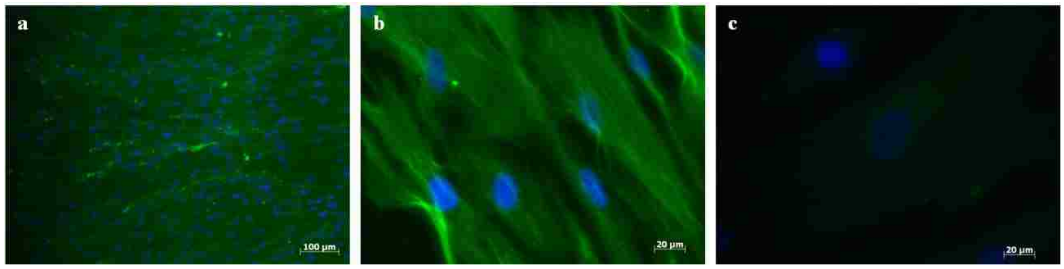

Figure 52: Tropomyosin expression in hMSC-derived cardiomyocytes (a-b) and non-induced hMSCs (c)

Troponin T was observed as punctate staining throughout the hMSC-derived cardiomyocytes (Figure 53, a-b), and was not observed in undifferentiated hMSCs (Figure 53c). Troponin T is a component of the troponin complex (along with troponin C and I) that binds to tropomyosin to form the tropomyosin-troponin complex. When Ca^{2+} binds to troponin C, a conformational change occurs in troponin I. Myosin-binding sites on actin that were previously blocked by tropomyosin are exposed. The presence of troponin T indicates the cells' ability to regulate contraction [111,254].

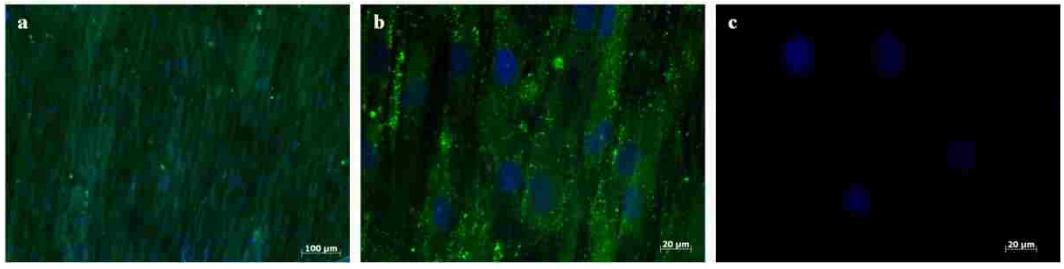

Figure 53: Troponin T expression in hMSC-derived cardiomyocytes (a-b) and non-induced hMSCs (c)

Myosin heavy chain was present in hMSC-derived cardiomyocytes (Figure 54, a-b), and was not observed in undifferentiated cells (Figure 54). Myosin is the main component of thick filaments in sarcomeres. Type II myosin, found in cardiomyocytes, has two heavy chains and four light chains. Each heavy chain is comprised of a globular head domain and a coiled tail domain [119]. Myosin is responsible for the power stroke that causes cell contraction [111]. The hMSC-derived cardiomyocytes have the structural proteins necessary for contraction: sarcomeric actin ("thin" filaments), myosin ("thick" filaments), as well as the regulatory proteins tropomyosin and troponin T.

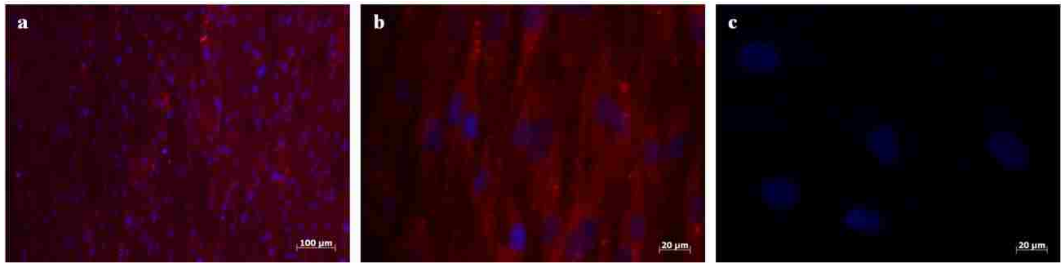

Figure 54: Myosin heavy chain expression in hMSC-derived cardiomyocytes (a-b) and non-induced hMSCs (c)

α-actinin, which plays a key role in the structure of cardiomyocytes, was present in all EB-derived cells (Figure 55, a-b). It was not observed in undifferentiated hMSCs (Figure 55c). It is a Z-band protein that crosslinks the actin/nebulin filaments in the myofibrils and also binds to titin [255]. Some cells displayed organized sarcomeres. Z-bands were evident with α-actinin staining (Figure 56), suggesting that some cells

contained mature myofibrils [256]. Additionally, Z-bands provide provide the support needed during cell contraction [255].

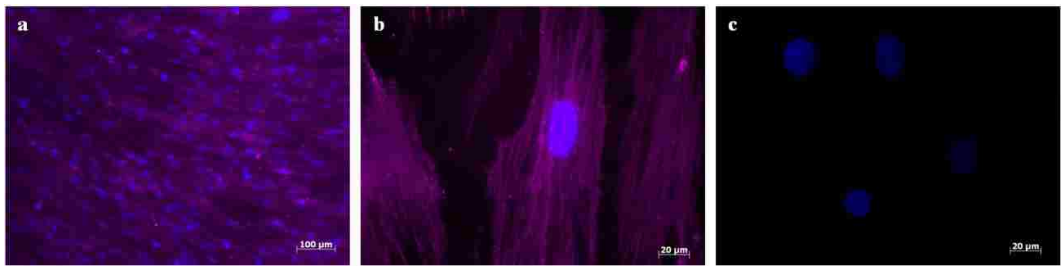

Figure 55: α-actinin expression in hMSC-derived cardiomyocytes (a-b) and non-induced hMSCs (c)

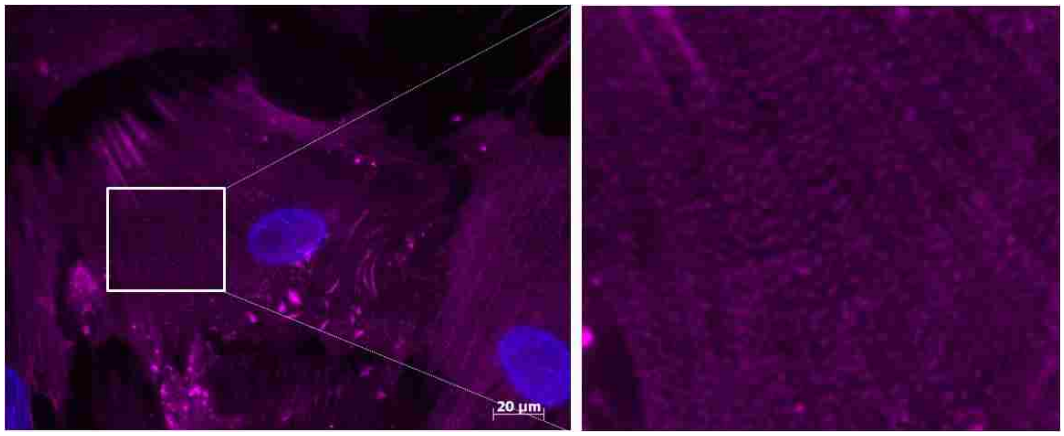

Figure 56: α-actinin staining clearly shows Z-bands in some cells

N-cadherin is a calcium-dependent glycoprotein that is present in adherens junctions in cardiac muscle [257]. The intercalated disks of cardiomyocytes contain adherens junctions and gap junctions, which mechanically and electrically link cells, respectively. While N-cadherin in mature cardiomyocytes is localized to cell-cell junctions, it was found throughout the differentiated cells (Figure 57, a-b). It was not

present in undifferentiated cells (Figure 57c). A study of knockout of N-cadherin in mouse embryos led to improper formation of the heart tube. However, cells isolated from the embryos were able to weakly aggregate and contract, demonstrating that electrical coupling is possible in the absence of N-cadherin [258]. Additionally, deletion of the N-cadherin gene in adult mice led to disassembly of intercalated discs, which led to impaired cardiac function [259]. Therefore, N-cadherin is a necessary component of cell-cell junctions in cardiomyocytes. The expression of N-cadherin in differentiated cells is promising, as it is crucial for the mechanical coupling of cardiomyocytes.

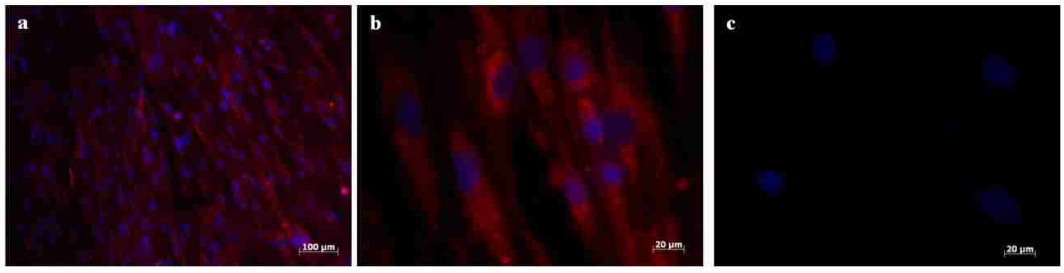

Figure 57: N-cadherin expression in hMSC-derived cardiomyocytes (a-b) and non-induced hMSCs (c)

Gap junctions of cardiomyocytes are responsible for cell-to-cell communication, intercellular propagation of electrical signals, and exchange of small signaling molecules. Connexin 43 (Cx43) is the predominant connexin expressed in cardiac tissue and is involved in the electrical coupling of the ventricles [260]. Cx43 was expressed in the aligned outgrowth (Figure 58). A membrane stain was used to

visualize the localization of the Cx43 protein to the cell-cell junctions. This localization suggests that the cells are coupled electrically.

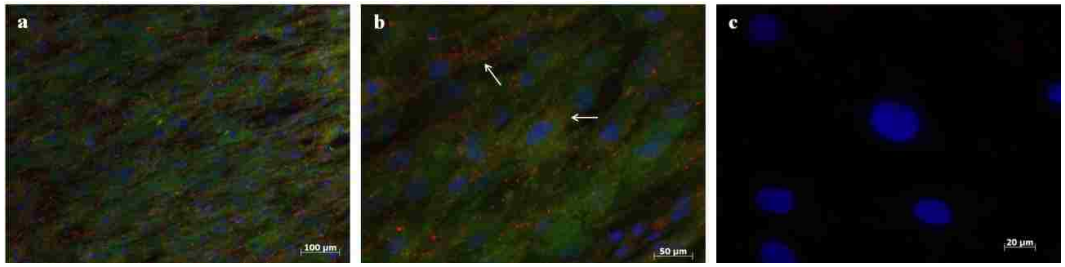

Figure 58: Cx43 expression in hMSC-derived cardiomyocytes (a-b) and non-induced hMSCs (c). Localization of Cx43 to cell junctions are denoted by white arrows in (b).

4.4.3. qPCR

mRNA was isolated from the specimens at 18 days post-plating and qPCR was performed. Fold changes of cardiac muscle markers in experimental and control samples (undifferentiated hMSCs, passage 4) were calculated compared to the housekeeping gene GAPDH (Figure 59). Three critical transcription factors were examined: Nkx2.5, MEF2C, and GATA4. In murine embryos lacking Nkx2.5, looping morphogenesis, which is critical to heart function, was not initiated [261]. Another critical transcription factor, MEF2C, is also involved in looping morphogenesis, as well as right ventricle formation and the expression of cardiac genes such as α-cardiac actin [262]. GATA4 is required for heart tube formation *in vivo* [263]. Nkx2.5, MEF2C, and GATA4 mRNA were all significantly upregulated compared to the control, indicating milestones for cardiopoiesis had been met. In early mouse embryonic development, gene expression of GATA4 is followed by β-MHC on day 4 [112]. β-MHC mRNA was

also significantly ($p<0.05$) upregulated compared to the control. Although the normal gene expression timeline for troponin T, desmin, and α-cardiac actin are not known, these genes were all upregulated compared to the control. Troponin T protein first appears on day 8 in embryonic mice [112]. Desmin is a muscle-specific intermediate filament that appears at day 9 in the developing heart. Desmin is thought to be involved in myofibrillogenesis and mechanical support for muscle cells [116]. It is not essential for cardiac differentiation, but may be necessary for normal cardiac function [264]. The expression of desmin is followed by cardiac actin in the developing embryo [265]. These results indicate that hMSC-derived cardiomyocytes are expressing key transcription factors (Nkx2.5, MEF2C, GATA4) along with several other important genes.

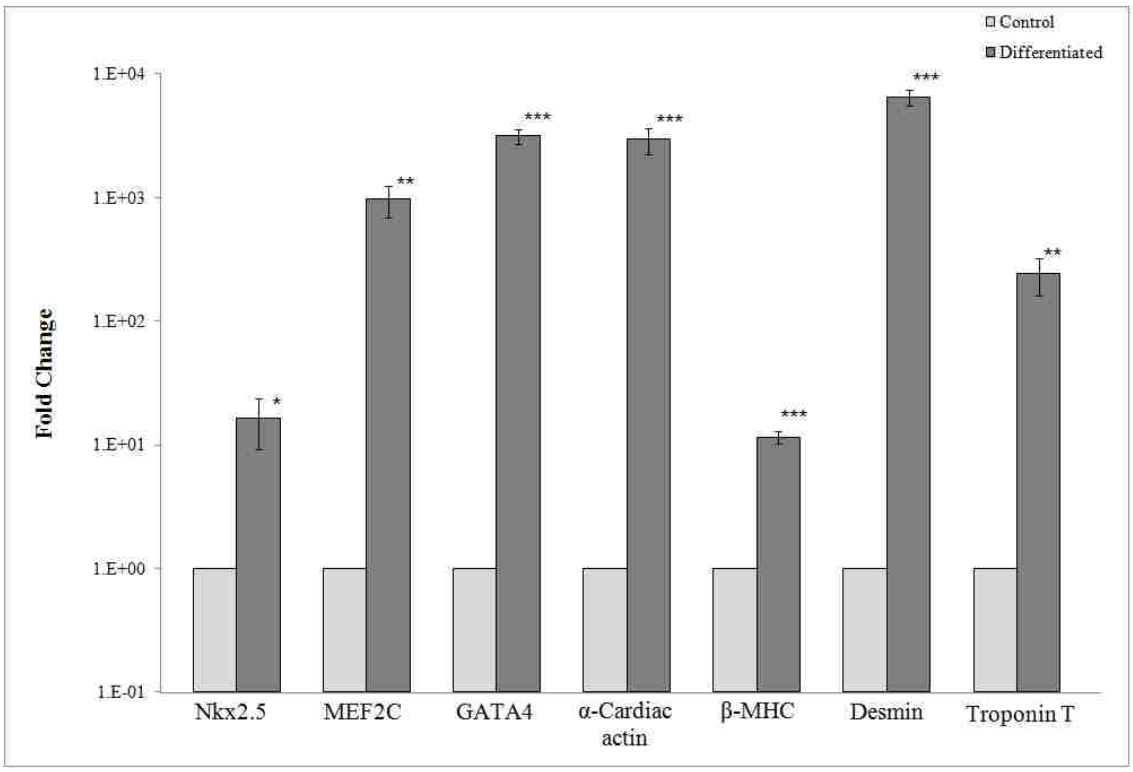

Figure 59: mRNA expression of hMSC-derived cardiomyocytes assessed by qPCR (*p<0.1, **p<0.05, ***p<0.01 upregulated over control)

While the hMSC-derived cardiomyocytes displayed numerous contractile proteins, spontaneous contractions were not observed. However, Potapova et al. patch-clamped and found that 5 of out 31 cells had an L-type calcium current. Based on the current-voltage relationship, it was determined that these cells displayed a voltage dependence and amplitude similar to adult human ventricular myocytes [248]. Therefore, it may be necessary to electrically stimulate the cells before implantation. Additionally, gap junction formation in cardiomyocytes produced by EB formation must be examined, and will be the subject of future work.

EB formation is a useful tool for producing cardiomyogenic hMSCs. However, one drawback of this differentiation method is the number of cells needed to create EBs. This method requires 250,000 cells per 40 µL drop. The authors tried using a lower number of cells per drop (100,000), but aggregates did not form (data not shown). Nevertheless, multiwell hydrogel systems [266], micropatterned substrates [240], or spinner flasks and rotating wall vessel bioreactors [243] may be used to create EBs of lower cell numbers. More work must be done to determine the optimal number of cells per EB.

While 5-aza has been used extensively to induce differentiation, success rates vary. Atonitsis et al. treated hMSCs with 10µM 5-aza for 24 hours (repeated 1x/week for 4 weeks) and found that the cells contained myofilaments that were positive for β-MHC, but no sarcomeres were observed. Using RT-PCR, they also found that the cells expressed the cardiac genes α-cardiac actin, β-MHC, and troponin T (although they were also expressed in undifferentiated cells) [222]. Xu et al. treated hMSCs with 10µM 5-aza and 10µg/L basic fibroblast growth factor. After a 24 hour treatment period, the media was replaced with normal growth media and the experiment was carried out for 2 weeks. Approximately 80% of the cells were positive for desmin, α-cardiac actin, and β-MHC. Additionally, the genes desmin, α-cardiac actin, β-MHC, and troponin T were highly expressed. The study reported that the differentiated cells contained myofilament-like structures, but no sarcomere formation were observed [223]. On the other hand, Martin-Rendon et al. treated hMSCs with 3, 5, or 10µM 5-aza for various time periods and reported that less than 1% of cells became

cardiomyocyte-like cells, suggesting that treatment of 5-aza may not be an effective differentiation method [224]. Mohanty et al. induced differentiation with TGFβ1 and compared it to treatment with 5-aza. While both treatments produced cells that expressed cardiac myosin, troponin I, and GATA4, levels were higher in the cells treated with 5-aza [221]. Therefore, the EB method may be preferred because of the presence of sarcomeres, which is indicative of mature myofibrils [256], and for the efficacy of the method, as all cells in this study were positive for the cardiac protein markers.

Another differentiation treatment that has been used is insulin, dexamethasone, and ascorbic acid [220]. Shim et al. used this differentiation media for multiple passages. RT-PCR analysis revealed the gene expression of GATA4 and MEF2, but not Nkx2.5/Csx, another critical transcription factor in cardiac differentiation. These cells stained positive for numerous cardiac muscle markers (desmin, tropomyosin, troponin I, α-cardiac actin, and α-actinin, among others) and were negative for skeletal muscle markers. Some Z bands were detected after 4-5 passages in differentiation media. The EB method may be superior since it produced cells with Z bands after only 18 days and does not use chemical induction. However, more studies should be done, specifically focused on electrical stimulation of cells to initiate the formation of functional gap junctions and spontaneous contractility.

4.5. Conclusion

The hanging drop method for EB formation is a valuable method for producing hMSC-derived cardiomyocytes, and may be superior to chemical induction methods. The EB-derived cells displayed numerous cardiac contractile protein markers and contained organized myofibrils. Some Z bands were visualized with α-actinin staining, indicating mature myofibrils. N-cadherin, an adherens junction protein necessary for mechanical coupling during cell contraction, was present, but was not localized to cell-cell junctions. However, Cx43, a gap junction protein, was localized to cell-cell junctions. Several cardiac muscle genes, α-cardiac actin, troponin T, β-MHC, and desmin, along with key transcription factors, Nkx2.5, MEF2C, and GATA4, were upregulated compared to undifferentiated cells. Given the success rate of this differentiation method, and absence of chemical induction, it may prove to be a viable clinical option for future cardiac cell therapies derived from hMSCs.

Chapter 5: *In Vitro* Comparative Biodegradation Analysis of Salt-Leached Porous Polymer Scaffolds

5.1. Chapter Overview

This study presents a comprehensive, side-by-side analysis of chemical, thermal, mechanical, and morphological changes in four polymers used in tissue engineering: poly(glycerol-sebacate) (PGS), poly(lactic acid) (PLA)/poly(ε-caprolactone) (PCL) blend, poly(lactic-*co*-glycolic acid) (PLGA), and Texin 950, a segmented polyurethane resin (PUR). Polymer foams were created using a salt-leaching technique and then analyzed over a sixteen week period. Biodegradation was analyzed by examining the morphology, thermal properties, molecular weight, chemical and mechanical properties using scanning electron microscopy, differential scanning calorimetry, gel permeation chromatography, attenuated total reflectance-Fourier transform infrared spectroscopy, thermogravimetric analysis, and compression testing. PGS underwent the most rapid degradation, and was hallmarked by a decrease in compressive modulus. PLA/PCL blend and PLGA both had rapid initial decreases in compressive modulus, coupled with large decreases in molecular weight. Surface cracks were observed in the PUR samples, accompanied by a slight decrease in compressive modulus. However, as expected, the molecular weight did not decrease. These results confirm that PUR does not undergo significant degradation, but may not be suitable for long term implants. The biodegradation rates of porous PGS, PLA/PCL blend, and PLGA found in this study can guide their use in tissue engineering and other biomedical applications.

5.2. Introduction

A wide array of porous polymeric scaffolds has been examined for tissue engineering applications. Natural materials include collagen (cardiac and cartilage tissue engineering) [267-270], gelatin [271,272], and alginate [272-274]. Synthetic polymers common in tissue engineering research are polyglycolic acid (PGA) [275-278], polylactic acid (PLA) [279-281], poly(lactic-*co*-glycolic acid) (PLGA), poly(ε-caprolactone) (PCL) [282-284], poly(lactic acid-*co*-caprolactone) (PLCL) [285-287], poly(glycerol-sebacate) (PGS) [288-291], poly(hydroxy butyrate) (PHB) [292,293], polyurethane resin (PUR) [183,184,294], and poly(propylene fumarate) (PPF) [295,296]. Many of the polymers that have been used in tissue engineering applications are biodegradable, including PCL, PLA, PGA, PLGA, PLCL and PGS (among others). Often, one goal of scaffold design and development is to ensure that the rate of tissue ingrowth and the rate of polymer biodegradation are well-matched for the application at hand. While the biodegradation kinetics of the polymers listed have been examined in depth [32,297-299], the scaffold fabrication between the various polymeric materials has been widely varied. In addition, the analytical methods for examining biodegradation are not always consistent between studies.

In this study, four polymers common in biomedical applications were examined (Figure 60): PGS, PLA/PCL blend, PLGA (all biodegradable at different rates), and a segmented PUR (not biodegradable). To illustrate the broad usage of these polymers in biomedical research, we have briefly reviewed each in the paragraphs below.

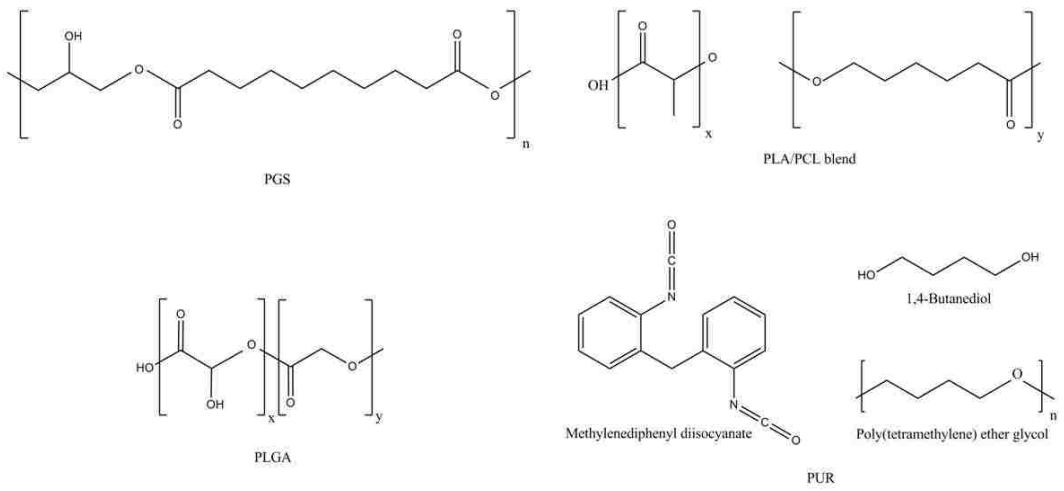

Figure 60: Chemical structures of polymers used in study.

PGS is a bioresorbable elastomer developed by Wang et al. in 2002 [300]. PGS has tunable mechanical properties, which makes it particularly interesting in tissue engineering applications. The elastic modulus and ultimate tensile strength can range from 0.056 to 1.20 MPa, and 0.23 to 0.47 MPa, respectively, depending on cure temperature [301]. PGS degrades rapidly by surface erosion, which results in a linear mass degradation profile [298], regardless of degradation media composition [300,301]. PGS has a short, but very rich history as a biomaterial, *in vivo* and *in vitro* [289,302-304], including uses in nerve guides [305] and heart valve constructs [306]. PGS has been fabricated using a number of technologies [288-291,303,304,306-309], resulting in both porous and nonporous formats. However, while the degradation kinetics of nonporous PGS have been examined [298,300,301,305,310], degradation kinetics of porous PGS have not yet been published.

PCL and PLA are commonly prepared as a blend or a copolymer. PCL is a semi-crystalline aliphatic polyester with a relatively long degradation time (2 years), due to its hydrophobicity and crystallinity [311]. PLA is an aliphatic polyester that degrades in 2-24 months [312,313]. PLA is available in both the L and D stereoisomer forms, which affects the degradation rate, crystallinity, and molecular weight [314]. PLA/PCL blends and copolymers undergo bulk degradation by hydrolysis [312,315-317]. PLA/PCL blends have been used in a variety of ways, including drug delivery [318-321] and for nerve repair [322,323]. However, biodegradation of PLA/PCL blends in a porous format has not yet been examined.

PLGA, a copolymer of PLA and PGA, is another commonly used biodegradable polymer [32,189,324-333]. PGA is a crystalline aliphatic polymer that rapidly degrades (2-12 months) because of its hydrophilic nature [313,334]. PLGA has a degradation time of 1-6 months, based on the PLA/PGA ratio, as well as the crystallinity and molecular weight [313], with a 50/50 copolymer having the most rapid degradation rate [335]. Degradation studies have also been done on PLGA porous foams *in vitro*, commonly in PBS [32,331-333], and *in vivo* [32]. While many *in vitro* and *in vivo* studies have already been performed on PLGA, the degradation rate is highly reliant on the format (porous vs. nonporous), the ratio of PLA to PGA, and the starting molecular weight, making more research in this area crucial for understanding the potential uses of PLGA in biomedical applications.

PURs have been used in many biomedical applications [183,184,294,336-338], including pacemaker lead insulation and catheters [182]. While traditionally known as

non-biodegradable, PURs are susceptible to environmental stress cracking [339]. The elastomeric properties of PUR make it a potentially useful platform in soft tissue engineering [183,184,294]. The polyether PUR used in this study is Texin 950, a segmented block copolymer. Segmented PURs are made up of soft segments (usually a polyol) and hard segments (a diisocyanate and chain extender) and can be tailored to have a wide range of mechanical properties. *In vivo* degradation studies have been performed on chemically similar PURs (based on MDI, 1,4-butanediol, and poly(tetramethylene) ether glycol) [340,341] but to our knowledge, Texin 950 has not been the subject of inquiry. In this study, we examine the *in vitro* biodegradation of Texin 950 in a porous format, presenting data that is currently not available in the literature.

This study compares four polymers relevant to tissue engineering, and presents the first biodegradation study of porous PGS, porous PLA/PCL blend, and porous PUR. While most tissue engineering scaffolds have a porous structure, many biodegradation studies do not reflect this fact. We focused our efforts on salt-leached porous scaffolds with a nominal pore size of approximately 200 μm. We performed a biodegradation analysis in simulated body fluid (SBF), under aseptic, 37°C conditions. The polymers were analyzed at specific intervals over a time course of 16 weeks, using a variety of techniques to examine chemical, thermal, mechanical, and structural changes. Our results indicate that the PGS, PLA/PCL blend, and PLGA undergo significant chemical changes indicative of biodegradation, in time periods as little as 2-4 weeks. In addition, PUR, as a non-biodegradable polymer, exhibits cracking over time, leading to altered

mechanical properties, which may impact the success of this polymer in a biomedical application. These factors are critical when considering material choice, fabrication technique, and ultimately cell integration with a biomedical device, and therefore need to be studied in a systematic fashion, as described herein.

5.3. Experimental Details

5.3.1. Materials

PUR (Texin 950) was obtained from Bayer MaterialScience (Pittsburgh, PA). PLA 3051D was purchased from Natureworks (Minnetonka, MN). PCL, glycerol, sebacic acid, and dimethyl sulfoxide (DMSO) were acquired from Sigma Aldrich. Glycolic acid was from TCI America (Portland, OR). Chloroform was purchased from VWR (West Chester, PA). Tetrahydrofuran (THF) and 1,1,1,3,3,3-hexamethyldisilazane (HMDS) were from Acros Organics (Morris Plains, NJ). Sodium chloride (NaCl) was purchased from EMD Chemicals Inc. (Gibbstown, NJ). Zinc acetate dihydrate ($Zn(CH_3CO_2)_2 \cdot 2H_2O(I)$) was obtained from Strem Chemicals (Newburyport, MA).

5.3.2. Polymer/polymer blend synthesis

The PGS pre-polymer synthesis was adapted from established methods [300]. Briefly, equimolar (1:1) amounts of anhydrous glycerol, and sebacic acid, which was purified via recrystallization in ethanol (3 times), were mixed in an airtight glass jar that was partially immersed in a heated silicone bath. The mixture was gradually heated to

120 ºC under nitrogen gas flow. The mixture was then stirred with a rotor (50 rpm) at this temperature for 24 h. The gas flow was then stopped and vacuum was applied at –20 kPa for a further 24 h.

PGA was synthesized by polycondensation, with zinc acetate dihydrate as the catalyst, as previously established [342]. This method produces a high molecular weight PGA with a number average molecular weight (M_n) of 45,000, a weight average molecular weight (M_w) of 91,000, and a crystallinity of 33%, as reported by Takahashi et al [342].

PLGA (PLA/PGA 85:15) copolymer and PLA/PCL (50:50) blend were prepared using microwave radiation [188]. Briefly, polymers were dissolved (or suspended) in chloroform at 10% (w/v). The respective polymers were mixed prior to microwaving. This method produced a PLA/PCL blend with a PCL continuous phase and PLA microspheres ranging in diameter from 0.5-1 mm.

5.3.3. Preparation of specimens

The porous specimens were prepared by a solvent casting/salt leaching method [189,290]. Polymers were dissolved in solvent to yield a solution of 5% (w/v). Chloroform was used as the solvent for PLGA and PLA/PCL blend. The solvent used for PUR and PGS was THF. NaCl particles (>125μm) (90% w/v) were added to each solution. The solution was cast into rectangular molds (45 x 13 x 3 mm). The specimens were air-dried for 48 h to allow the solvent to evaporate. The PGS specimens were then cured at 120˚C for 7 days. The specimens were subsequently

removed from the mold and immersed in distilled deionized water at 60˚C for 72 h to leach out the salt.

5.3.4. *In vitro* degradation

SBF was prepared by dissolving various reagents in ddH_20 at 37°C [343]. The SBF was filtered (0.2μm) for sterility. Porous polymer specimens (45 x 13 x 3 mm) were soaked in SBF and incubated in a controlled environment (37°C, 5% CO_2). Every two weeks, three specimens were removed from SBF. The surface liquid was removed with a Kimwipe, and the surfaces were air dried overnight in a laminar flow hood to maintain sterility. The degradation study lasted for sixteen weeks, a time period suitable for comparing polymers with variable degradation rates.

5.3.5. Porosity of the initial samples

The porosity was calculated using the densities of the porous and non-porous polymers. Ten specimens were used for porosity calculations. The densities of the porous scaffolds were measured using a pycnometer. The scaffolds were dried at 70°C for 1 h prior to measurements. First, the empty, dry pycnometer was weighed (m_0). A scaffold was inserted into the pycnometer and the weight was taken again ($m_{a,dry}$). After that, the scaffold was then soaked in distilled water and placed back into the pycnometer and measured again ($m_{b,wet}$). Distilled water was added so that the pycnometer was filled. The total weight was taken (m_2). The pycnometer was emptied and filled again with just distilled water (m_3). The difference between the weight of the

material wet versus dry was taken ($d = m_{b,wet} - m_{a,dry}$) then added to the weight of only distilled water in the pycnometer ($m_{3,corrected} = m_3 + d$). The weight of the water ($m_{H2O} = m_{3,corrected} - m_0$) and the weight of the scaffold ($m_S = m_{a,dry} - m_0$) were calculated. Then the weight of the added water was calculated ($m'_{H2O} = m_2 - m_{a,dry}$). The volume of the scaffold (V_S) was calculated using the following equation:

$$V_S = \frac{m_{H_2O} - m'_{H_2O}}{\rho_{H_2O}} \quad (35)$$

The density of the scaffold, ρ_S, was then calculated using the equation below:

$$\rho_S = \frac{m_S}{V_S} \quad (36)$$

Finally, the porosity was calculated using the density of the nonporous polymer (ρ_P) and the density of the porous scaffold:

$$Porosity = \frac{\rho_P - \rho_S}{\rho_P} \times 100 \quad (37)$$

5.3.6. SEM

SEM was conducted using a Philips XL30 ESEM. The parameters used are as indicated at the bottom of each SEM image. Prior to imaging, the samples were sputter coated with iridium using an EMS575x Turbo Sputter Coater, using a sputter current of 20 mA for 30 seconds.

5.3.7. Mechanical testing: compression tests

Compression testing is a common method for analyzing mechanical properties of porous biomedical polymers [344-346]. It has been used to evaluate biodegradation

of porous PLGA [347]. Testing was performed using a Rheometrics ARES System in compression mode at a cross-head speed of 0.083 mm/s. Porous specimens were cut into 3 mm cubes for testing. The compressive modulus was calculated as the slope of the initial linear portion of the stress-strain curve. Ten compression tests were performed for each time point.

5.3.8. Attenuated total reflectance-Fourier transform infrared spectroscopy (ATR-FTIR)

ATR-FTIR was performed on a Perkin Elmer Spectrum 100. The FTIR absorbance spectra were obtained with 16 scans per sample over the range of 4000–650 cm^{-1}, with a resolution of 4 cm^{-1}. Three samples were used for each time point.

5.3.9. GPC

GPC was performed on a Waters Associates Liquid Chromatography machine (Model #201, Milford, MA). Polymers were dissolved in THF to form 1% (w/v) solutions. The M_n and M_w data were expressed with respect to polystyrene standards. Three samples were used for each time point.

5.3.10. DSC

DSC was used to monitor thermally induced polymer processes. It was carried out on a DuPont DSC2910 at a rate of 10°C/min; each sample was re-heated. Samples weighed approximately 15mg. The polymer samples were heated based on the areas of

interest for each polymer. PGS samples were heated from -60°C to 100°C. PLA/PCL blend samples were heated from -60°C to 250°C. PLGA samples were heated from 20°C to 250°C. PUR samples were heated from -40°C to 250°C. The changes in the glass transition temperature (T_g), crystallization temperature (T_c) and melting temperature (T_m) were evaluated. One sample was used for each time point.

5.3.11. Thermogravimetric analysis (TGA)

TGA (TA Instruments Q500 Thermogravimetric Analyzer) was used to analyze thermal stability. The onset temperatures, which indicate initial temperature of mass loss, were recorded. A decrease in molecular weight is likely to be reflected in the onset temperature. The specimens were scanned from 30°C to 800°C at a heating rate of 10°C/min with a nitrogen flow rate of 40 ml/min. The weight of each sample was approximately 15mg. Three samples were used for each time point.

5.4. Results and discussion

5.4.1. Porosity of the specimens

The porosities of the scaffolds were calculated after determining the densities of the porous scaffolds using a pycnometer. Since the scaffolds were prepared with 90% sodium chloride, a porosity of 90% would indicate that all the salt had been leached out. However, the calculated porosities of the PGS, PLA/PCL blend, PLGA, and PUR scaffolds were 80.06% (±0.02), 83.28% (±0.02), 81.24% (±0.004), and 84.16% (±0.03), respectively. This suggests that some sodium chloride was still present in the scaffolds.

5.4.2. SEM

SEM was used to examine the porous scaffolds during degradation (Figure 61). The images confirm that the scaffolds are highly porous, with large pores (approximately 200 μm), indicative of the salt-leaching process used to create the scaffolds. The solvent casting/salt leaching method does not give complete interconnectivity, but this method is straightforward and simple. The surface of PGS samples no longer exhibited appreciable surface porosity by week 6. However, the cross section showed that the porous structure was still maintained in the core of the sample. These pores disappeared by week 10. Cracks could be seen on both the surface and in the cross section, most likely the result of the shrunken pores. By week 16, the PGS samples became gel-like. The fast degradation rate of PGS is beneficial for tissue engineering, but the loss of surface porosity early during degradation may prevent nutrient diffusion to the underlying cells. In addition, the loss of surface porosity could limit diffusion of degradation byproducts out of the scaffolds, possibly leading to toxic effects. Therefore, further testing needs to be completed with a PGS/cell hybrid to determine if cells maintained deep in the scaffolds are able to survive past the 6 week time frame.

While the pore structure of the PLA/PCL samples was maintained on the surface and throughout the bulk for all 16 weeks, holes and increased roughness can be seen starting at week 2 of degradation. This type of structural change could be beneficial in allowing nutrient diffusion into the scaffolds (and degradation byproduct

diffusion out), as well as allowing for cell-cell contact in the bulk of the scaffolds, critical to tissue engineering applications.

On the PLGA samples, cracking can be seen at week 6, and by week 10, large cracks are seen on the surface and in the bulk. Week 16 samples did not have sufficient mechanical integrity to allow for SEM preparation and imaging. Similar to the PLA/PCL blends, these changes in the structure of scaffold could improve performance with regards to cell-cell communication and diffusion. However, with both the PLA/PCL blend and the PLGA, further long-term biodegradation testing with cells would be necessary to determine how these structural changes affect cell and tissue-level integrity.

The PUR samples seemed to have an increased number of holes by week 8, and cracks can be seen by week 10. This was unexpected, given that PUR is a non-biodegradable polymer. However, similar PUR chemistries have been shown to undergo significant surface cracking *in vivo* [341]. While the holes would possibly be beneficial for cell integration and diffusion, it is unclear if the structural changes are a result of handling or other factors. Therefore, we chose to examine chemical, thermal and mechanical changes that result in each of the polymers chosen.

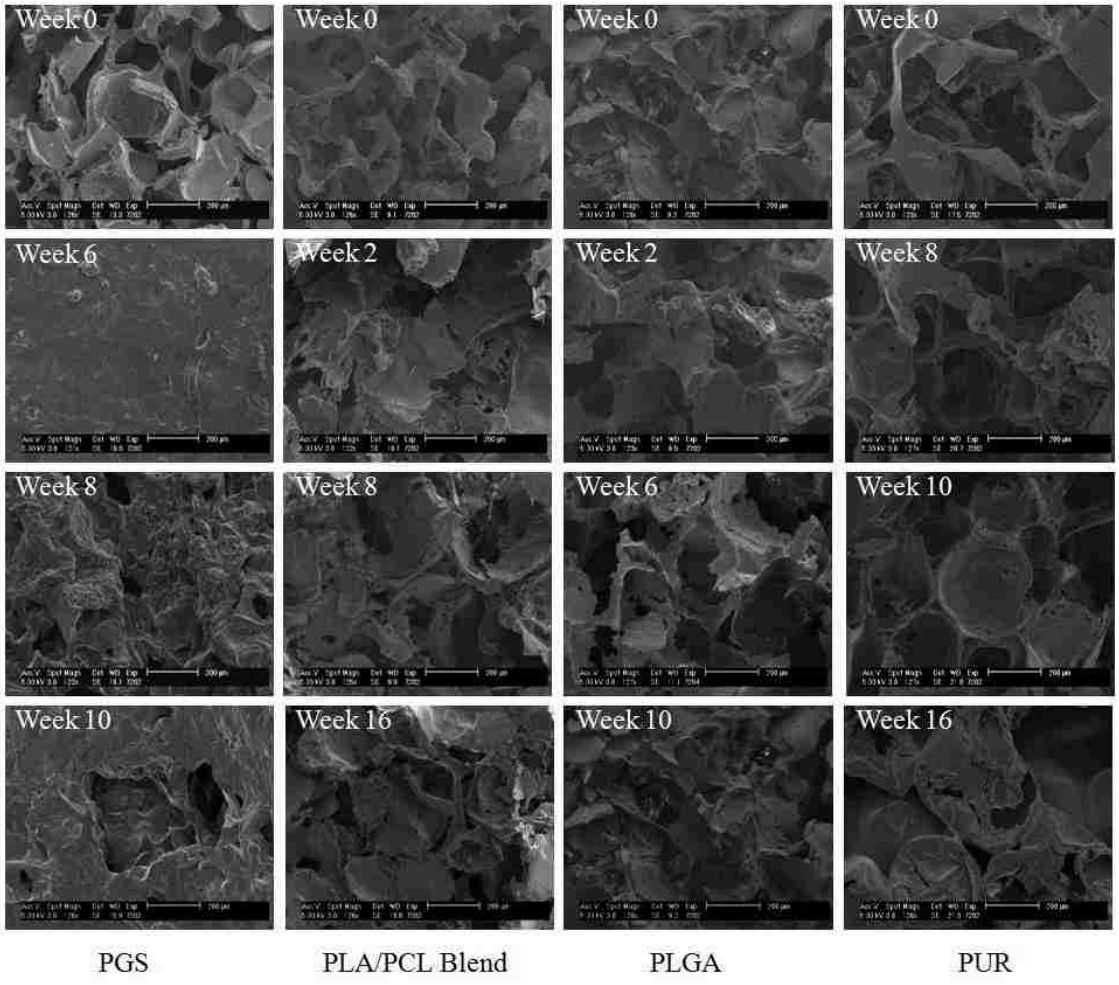

Figure 61: SEM micrographs of polymers at various timepoints of degradation.

5.4.3. Mechanical testing: compression tests

The compressive modulus of each polymer was examined during the degradation study (Figure 62). Examining the initial compressive modulus indicates that some salt may have been left behind in the scaffolds prior to placing in degradation buffer. Therefore, each polymer exhibited a dramatic drop-off in compressive strength after the first 2 weeks in culture. Initially, porous PGS had a compressive modulus of

7.24±0.93 kPa. The modulus decreased by approximately 50% at week 6 (3.25±0.61 kPa), which is attributed to the leaching out of any remaining salt in the scaffold. The modulus increased at week 8 to 7.61±0.89 kPa, which corresponds to the substantial loss of porosity (Figure 61) then decreased again at week 10 to 5.53±1.20 kPa. After 16 weeks, the PGS samples became gel-like, and therefore, the modulus could not be tested. Wang et al. reported that after 5 weeks *in vivo*, the compressive modulus of PGS implants decreased by 50% [298], similar to the results seen here.

Porous PLA/PCL blend had an initial compressive modulus of 136.53±34.86 kPa. The modulus rapidly decreased, more than 70%, to 36.98±6.28 kPa at week 2, likely due to salt leaching. It further decreased to 11.34±2.55 kPa by week 16. This decrease is significant and could impact the functional ability of the scaffold during cell growth. The macroscopic structure of the scaffold did not appear significantly different, indicating that there may not have been significant pore collapse. Therefore, the degradation is attributed to bulk degradation [313], which is usually accompanied by a rapid loss in mechanical properties, consistent with the results seen here.

The compressive modulus of the initial porous PLGA sample was 230.39±59.66 kPa. From week 0 to week 6, the modulus decreased by 85% to 34.49±5.08 kPa, likely due to leftover leached salt. By week 16, the modulus had decreased to 17.37±3.13 kPa, a 50% further drop from the week 6 values. Similar to PLA/PCL, PLGA is known to undergo bulk degradation, therefore, the rapid loss of mechanical integrity was expected. In addition, the PLGA macroscopic structure underwent significant changes

during the degradation period, indicating a pore breakdown and ultimate collapse of the scaffold structure.

The initial compressive modulus of porous PUR was 28.08±6.00 kPa. Over the course of the degradation study, the modulus decreased more than 30%, to 18.44±3.81 kPa at week 16. This was a surprising finding, given that PUR does not undergo chemical degradation. However, the loss of mechanical integrity indicates that there are other factors at work in PUR incubation, which are further discussed in the data below. Regardless, the loss of mechanical integrity indicates that PUR may not be an ideal scaffold material for applications requiring a porous structure with continued mechanical integrity.

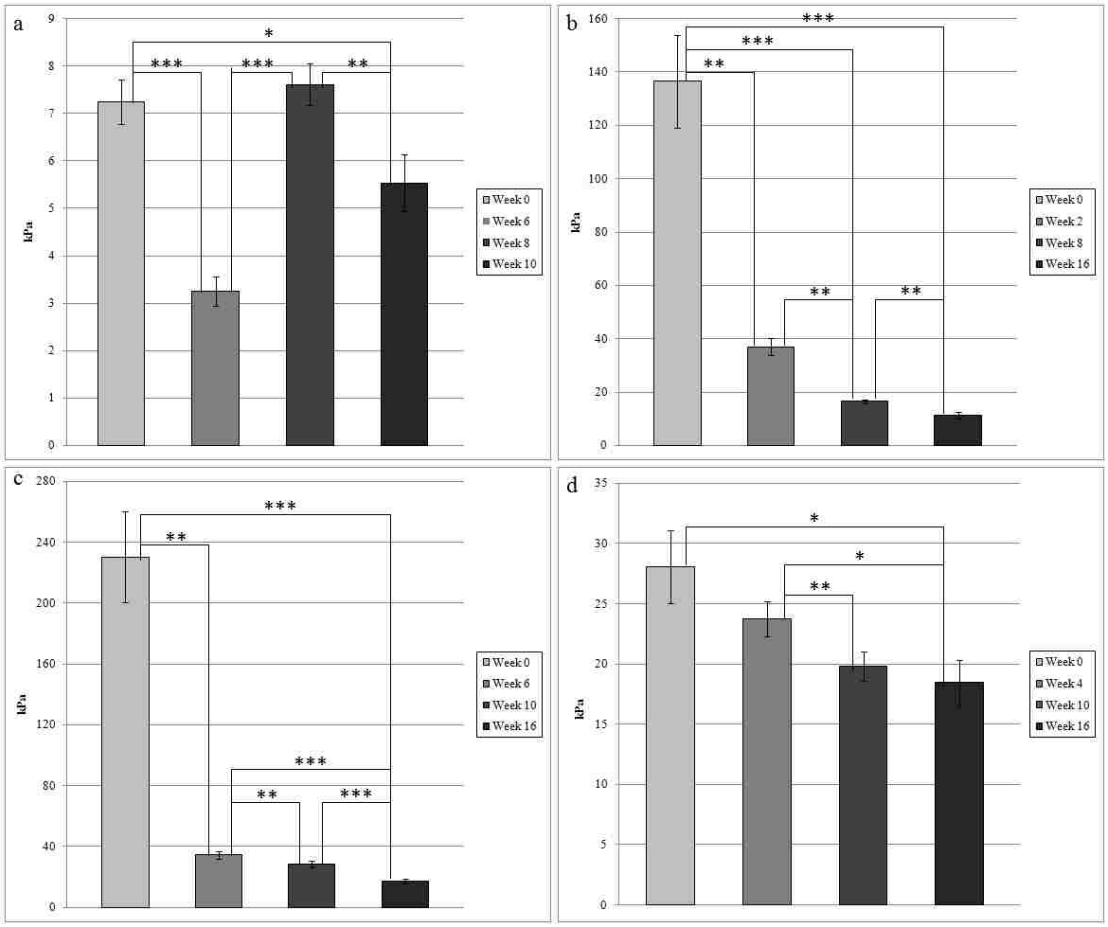

Figure 62: Compressive modulus values of a) PGS, b) PLA/PCL blend, c) PLGA, and d) PUR. PGS samples had an increase in compressive modulus from week 6 to 8, a result of the collapsed pores in the scaffold. PLA/PCL blend and PLGA had a rapid decrease in mechanical strength. PUR had a more linear decrease in compressive modulus. Error bars represent Standard Error (SE). (*P<0.1, **P<0.05, ***P<0.01)

5.4.4. ATR-FTIR

ATR-FTIR was used to assess chemical changes occurring in the specimens during biodegradation. Each polymer was examined 3 times at each time point and averaged. Specific regions of interest are discussed below.

PGS has an intense stretch at approximately 1740 cm^{-1} for the double bond, C=O (Figure 63). The prepolymer displays another peak at approximately 1700 cm^{-1} for unsaturated carboxylic acids. As the crosslinks between the PGS strands break down, the peak starts to form at 1700 cm^{-1} (noticeably at week 16). This indicates breakdown of crosslinks at week 16.

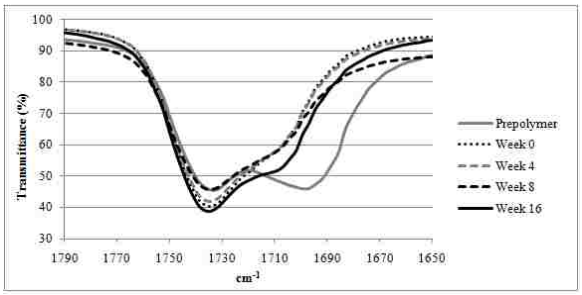

Figure 63: ATR-FTIR C=O stretch in PGS as a function of degradation time.

PLA/PCL blend, prior to degradation, exhibits C=O stretching at 1750 cm^{-1} (due to PLA rich phase) and 1728 (due to PCL rich phase) (Figure 64). The blend also has peaks at 3000 cm^{-1} (due to PLA), 2945 cm^{-1}, and 2870 cm^{-1} (due to both PLA and PCL), representing the alkyl groups [348]. As the PLA/PCL blend degrades, the peaks due to the alkyl vibrations are maintained. A new peak forms at 3200 cm^{-1}, likely due to the increase in O-H groups as the polymer chains break. In addition, the C=O stretch exhibits an increase in the peak absorbance associated with the PLA and PCL. At week 16, the PLA/PCL blend C=O vibrational stretch indicates the evolution of increased free PLA and PCL. However, the slight shift of the peak near 1750 cm^{-1} indicates

noncovalent interactions between the molecules as the polymer undergoes biodegradation.

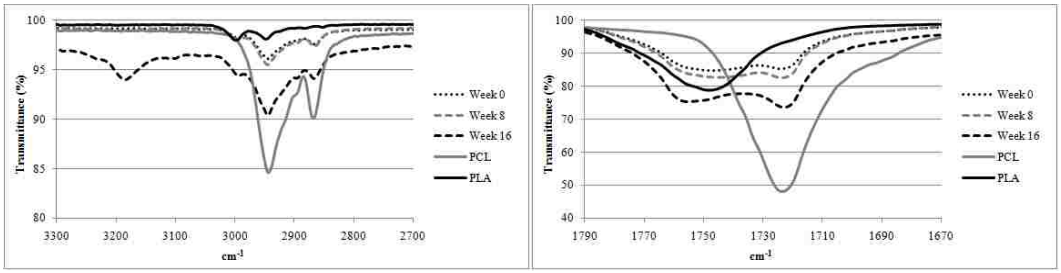

Figure 64: ATR-FTIR regions of interest for PLA/PCL blend as a function of degradation time.

PLGA FTIR spectra can be seen in Figure 65. During the first 6 weeks of PLGA degradation, a broad peak forms at 3400 cm^{-1}, indicating an increase in hydroxyl groups because of chain scission [349]. By week 10, the peak shifts to 3200 cm^{-1}. This indicates a decrease in hydroxyl groups, as the soluble hydroxyl end groups are leached out of the polymer. Likewise, the peak at 1750 cm^{-1}, which represents the C=O bond, increases from week 0 to 6, as chain scission occurs and carboxylic acid groups are formed. It then decreases from week 6 to 10, indicating that the carboxylic acids are being leached out, which results in significant mass loss [349]. From week 10 to 16 the C=O bond increases, most likely the result of more chain scission.

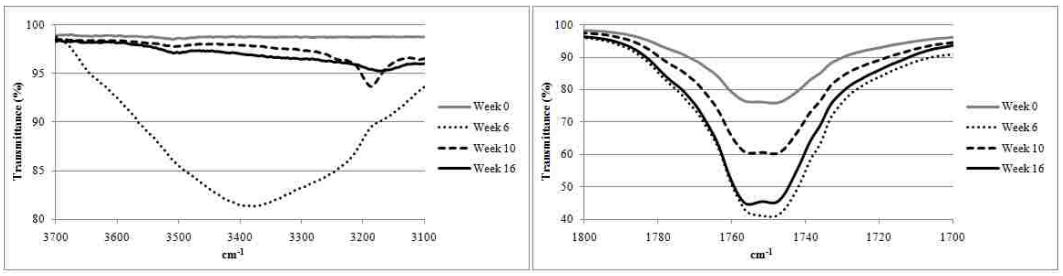

Figure 65: ATR-FTIR regions of interest for PLGA as a function of degradation time.

PUR has peaks at 2855 cm^{-1} and 2941 cm^{-1} for the C-H stretch (Figure 66). It also displays peaks at 1700 cm^{-1} and 1733 cm^{-1} for the C=O bond. No significant changes were seen in the C-H and C=O stretches of PUR, indicating no major changes are occurring to the chemical bonding structure of the polymer. PUR, an MDI-based polyurethane, has semicrystalline hard segments which generally protect the urethane linkages [340].

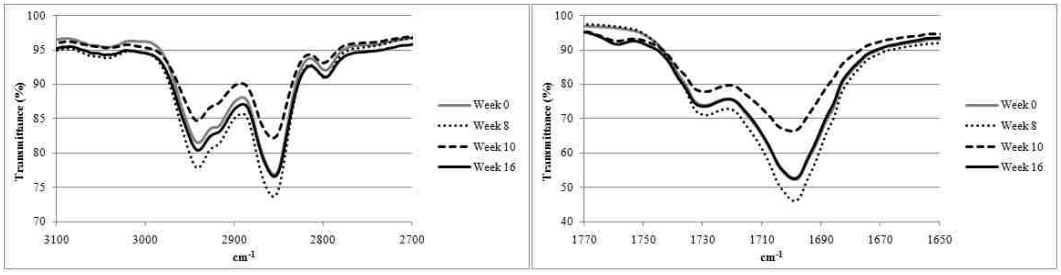

Figure 66: ATR-FTIR spectral regions for PUR as a function of degradation time.

5.4.5. GPC

The molecular weights and polydispersity index (PDI) of the polymer samples were analyzed using GPC. In specimens that undergo bulk degradation (PLGA and PLA/PCL), a reduction in molecular weight is indicative of degradation in the absence of bulk weight loss. All results can be seen in Table 5. For the PGS samples, only the prepolymer and week 16 were analyzed by GPC, due to the cross-linked nature of cured PGS. PGS samples through week 10 would not dissolve in THF, but the week 16 samples did dissolve, confirming that the crosslinks had entirely broken down. Additionally, the M_n and M_w decreased 14% and 12%, respectively, indicating that polymer chain length decreased compared to the prepolymer.

Because PLA/PCL is a polymer blend, two distinct peaks were expected. However, the starting molecular weights of the two polymers are similar: the M_n and M_w of PLA are 80,000 and 125,000, and the M_n and M_w of PCL are 84,000 and 119,000, respectively, as measured by GPC. Consequently, only one broad peak was found for all samples, consistent with Zhang et al.'s findings [115]. This peak became broader over the course of the biodegradation study, which is reflected in the increase in the PDI. Because only one peak was observed for the blend, the PDI does not distinguish between the two polymers and is intended to be an approximation. It is hypothesized that if the biodegradation study had been carried out longer, eventually two peaks would have become evident, as PLA is known to degrade faster than PCL. Overall, the M_n and M_w of the PLA/PCL blend decreased 45% and 29%, respectively, in the 16 week study.

The PLGA samples experienced a rapid decrease in M_n and M_w of 53% and 75%, respectively, by week 2. By week 16, the M_n and M_w had decreased 92% and 97%, respectively, from the initial samples. Interestingly, the PDI decreased throughout the experiment to a value of 1.00 by week 16, indicating that polymer chain scission had occurred very uniformly.

The PUR samples did not exhibit any decreases in M_n and M_w after 16 weeks, and the small variations seen are considered to be within the expected GPC error range of <10%. This was an expected result, given the known properties of PUR; however, it does not help to explain the loss of compressive strength that was observed.

Table 5: Change in molecular weight for polymer samples.

PGS				**PLA/PCL blend**			
Week	M_n	M_w	PDI	Week	M_n	M_w	PDI
Prepolymer	600	2500	4.17	0	92,900	174,000	1.87
16	500	2200	4.40	4	86,300	166,500	1.93
				8	76,200	160,300	2.10
				16	51,200	123,000	2.40
PLGA				**PUR**			
Week	M_n	M_w	PDI	Week	M_n	M_w	PDI
0	17,900	51,200	2.86	0	77,000	235,300	3.06
2	8300	12,900	1.55	8	79,600	221,200	2.78
10	1600	1600	1.00	10	79,600	227,700	2.86
16	1400	1400	1.00	16	81,600	237,400	2.91

5.4.6. DSC

The thermal properties of the polymer samples were analyzed using DSC. All T_g, T_m, and T_c values can be seen in Table 6. All PGS samples have a T_g of approximately -30ºC [350]. The prepolymer displays one melting temperature (T_m =

10ºC) and one crystallization temperature (T_c = -18ºC), as does the week 0 sample (T_m = 1ºC, T_m = -21ºC). At week 8, another melting peak is observed at 32ºC. By week 16, three melting peaks are evident, at 2 ºC, 33ºC, and 75ºC. These additional peaks are attributed to the breakdown of PGS into its monomers, consistent with the ATR-FTIR and GPC data.

The T_g of PCL has been reported to be approximately -60°C [351], while the T_g of PLA was measured as 51°C. No discernible T_g was observed in the PLA/PCL blend samples. However, the samples display two distinct melting regions, one at approximately 60°C for the PCL regions, and another at approximately 155°C, for the PLA regions, which is consistent with other reports [352-354]. An interesting finding is that the week 0 samples display one broad endotherm at 154°C for the melting of the PLA regions, while weeks 4, 8, and 16 display two endothermic peaks at approximately 150°C and 155°C, possibly indicating microphase separation. The PLA/PCL blend samples also display two distinct recrystallization temperatures, one at approximately 30°C for the PCL regions, and another at approximately 120°C for the PLA regions. The presence of two distinct melting and recrystallization regions confirm that PLA/PCL is a polymer blend.

Only one melting and crystallization region is observed in the PLGA DSC results, confirming that PLGA is a copolymer. Large decreases in the T_g, T_c, and T_m of PLGA can be seen by week 10. These observations confirm the chain scission that occurs during degradation, which results in increased chain mobility [355], and is consistent with the GPC and ATR-FTIR results.

The glass transition temperature of the PUR samples is not easily discernable. PUR has endotherms at approximately 180ºC and 200 ºC. Hiltz reported that the endotherm at 180ºC indicates the presence of microcrystalline hard segments, while the endotherm at 200ºC is due to melting of crystalline hard segments resulting from increased phase separation [356]. From week 0 to week 4, the melting and crystallization temperatures shifted to the right, suggesting that the microcrystalline hard segments may have become slightly more ordered [356].

Table 6: Changes in thermal properties of polymers during degradation (PP = prepolymer).

PGS					**PLA/PCL blend**					
Week	T_{m1} (°C)	T_{m2} (°C)	T_{m3} (°C)	T_c (°C)	Week	T_{m1} (°C)	T_{m2} (°C)	T_{m3} (°C)	T_{c1} (°C)	T_{c2} (°C)
PP	10	-	-	-18	0	60	-	154	31	123
0	1	-	-	-21	4	58	148	154	27	118
8	4	32	-	-22	8	60	150	156	27	119
16	2	33	75	-13	16	58	147	155	30	117
PLGA					**PUR**					
Week	T_g (°C)	T_c (°C)	T_m (°C)		Week	T_{m1} (°C)	T_{m2} (°C)	T_c (°C)		
0	52	118	148		0	178	187	117		
2	53	113	151		4	184	203	151		
10	38	103	136		10	188	200	150		
16	39	99	129		16	184	199	155		

5.4.7. TGA

Thermal stability was evaluated by TGA (Figure 67). As biodegradation occurs, thermal stability decreases, which is reflected in the onset temperature. The high weight percentage at the end of the test for the week 0 samples indicates unleached salt

present in the samples and residual salt from the SBF. The onset temperatures, which indicate initial temperature of mass loss, can be seen in Table 7. The onset temperature of the PGS prepolymer is 198°C. The onset temperature increases until week 8, as the weight loss curve shifts to the right. From weeks 8 to 16, the onset temperature decreases, as the curve shifts back to the left and more closely matches that of the prepolymer. All onset temperature changes are statistically significant ($p<0.01$) between the weeks analyzed. The onset temperature of PLGA decreased significantly ($p<0.01$) over the 16 week degradation period by approximately 12%, indicating it became less thermally stable as it degraded. The onset temperature of the PLA/PCL blend samples significantly decreased ($p<0.05$) between weeks 0 and 16 by approximately 6%. No significant decrease of onset temperature was observed for PUR over the 16 week degradation period, indicating it maintained its thermal stability.

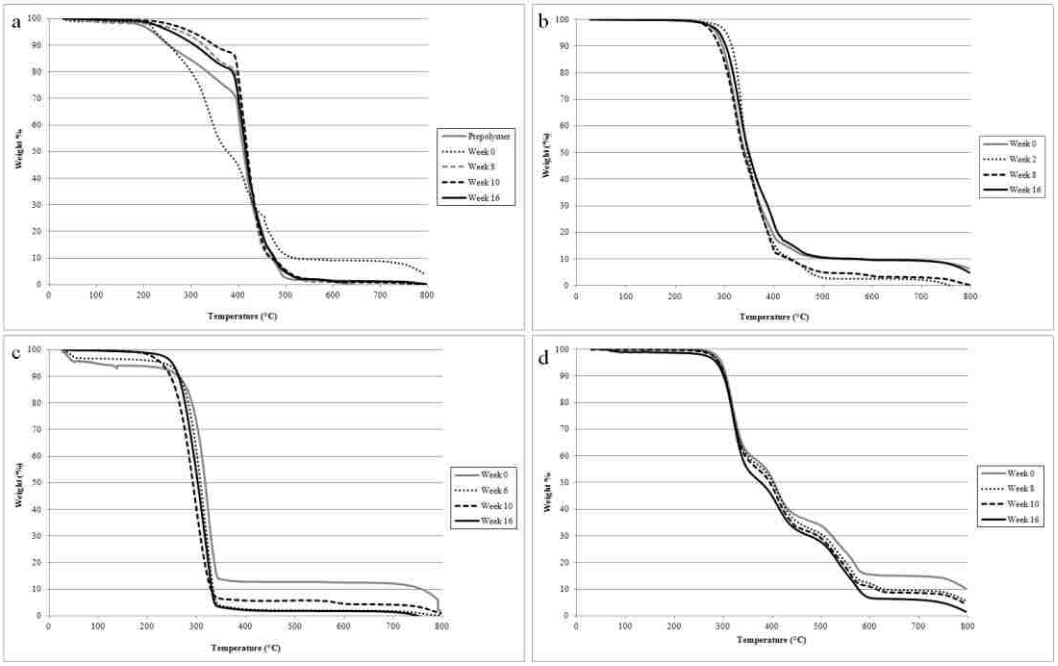

Figure 67: TGA curves of a) PGS, b) PLA/PCL blend, c) PLGA, and d) PUR.

Table 7: Changes in thermal stability of polymers during degradation, as indicated by onset temperature (T_o).

PGS		**PLA/PCL blend**		**PLGA**		**PUR**	
Week	T_o (°C)	Week	T_o (°C)	Week	T_o (°C)	Week	T_o (°C)
0	210	0	312	0	301	0	295
8	283	2	312	6	277	8	292
10	257	8	293	10	263	10	295
16	227	16	294	16	264	16	299

PGS exhibited the fastest biodegradation rate of the 4 polymers tested. By week 6, the surface of the samples was no longer porous, and by week 16, the polymer became gel-like. The crosslinks completely disappeared by week 16, marked by the appearance of a peak at 1700 cm^{-1}. The M_n and M_w of the prepolymer decreased from 600 and 2500, respectively, to 500 and 2200, respectively, at week 16. Additionally,

two extra melting peaks were observed at week 16, which indicate monomer presence. The rapid degradation rate of PGS and the loss of porosity must be taken into account for the chosen application and structure.

The PLA/PCL blend underwent substantial degradation during the 16 week study. Increased surface roughness was observed by SEM, starting at week 2. The M_n and M_w decreased 45% and 29%, respectively, by week 16. A drastic decrease in compressive modulus of approximately 70% was observed by week 2, which can be attributed to bulk degradation and the loss of residual salt. By week 16, the compressive modulus had decreased by approximately 89%. A new peak at 3200 cm^{-1} also formed by week 16, which indicates an increase in hydroxyl groups due to chain scission.

PLGA had a major loss of mechanical integrity and molecular weight during the study. An increase in hydroxyl groups was observed during the first 6 weeks of the study, indicating chain scission. By week 16, the M_n and M_w decreased 92% and 97%. PLGA showed decreased thermal stability, as the onset temperature decreased approximately 13% by week 16. Large decreases in the T_g, T_c, and T_m of PLGA were also observed. Like the PLA/PCL blend, the PLGA samples had a drastic decrease of compressive modulus initially. By week 16, the compressive modulus decreased by approximately 92%. The severe loss of mechanical integrity may prevent its use in some applications.

PUR, a nonbiodegradable polymer, had a slight decrease in compressive modulus over the 16 week study, which may limit its use for long-term applications.

An increased number of surface cracks was also observed by SEM. A shift in the T_m and T_c from weeks 0 to 4 may have signified increased order in the microcrystalline hard segments. However, no changes were observed in the chemical bonds. No decrease in thermal stability was observed.

5.5. Conclusions

This study presents a comprehensive, side-by-side analysis of chemical, thermal, mechanical, and morphological changes in four polymers used in tissue engineering. This study also presents the first report of biodegradation in porous PGS, PLA/PCL blend, and PUR. During the 16 week biodegradation study, all four polymers showed signs of degradation. PGS degraded the quickest, with complete breakdown of its crosslinks by week 16. Additionally, DSC results indicated monomer presence. Since PGS has the fastest degradation rate of the polymers tested, it may be the most appropriate for many tissue engineering applications. However, the fact that the pores collapsed after 10 weeks must be taken into consideration. The PLA/PCL blend quickly experienced a rapid decrease in compressive modulus and had significant molecular weight decrease. PLGA degraded more rapidly, with significant chain scission occurring in the first 6 weeks, and showed a larger decrease in both compressive modulus and molecular weight. By week 16, the PLGA samples also lost most of their mechanical integrity and were difficult to handle. The rapid loss of mechanical properties of the PLA/PCL blend and PLGA copolymer make them unattractive candidates for tissue engineering scaffolds. Cracks and pits were seen in the SEM

images of the PUR samples at week 16, which explain the 30% decrease in compressive modulus. However, its molecular weight and thermal stability did not decrease. PUR will not biodegrade in a timely manner, but it also may not be suitable for long-term implants, due to the surface flaws that result after long-term incubation. This comprehensive study presents the biodegradation properties of four polymers and can serve as a guide for their use in biomedical applications.

Chapter 6: Conclusions and Recommendations

6.1. Research Summary

6.1.1. Effect of *In Vitro* Aging on Mechanical Properties and Differentiation Capacity of Human Mesenchymal Stem Cells

This study investigated the effect of *in vitro* aging on the mechanical properties of cells, and the relation of the mechanical properties to differentiation ability. The average elastic modulus approximately tripled during extended culture (P4-P11, ~17 population doublings). The differentiation capacity seemed reliant of the elastic modulus of cells prior to differentiation. The most successful myogenic differentiation occurred when the elastic modulus of the cells matched that of native tissue. Osteogenic differentiations were more successful in earlier passages, when the elastic modulus of the cells was lower. **While many *in vitro* aging studies of hMSCs exist, this is the first to examine myogenic differentiation in extended culture.** Furthermore, this investigation is one of the few to look at mRNA expression of lineage markers in both undifferentiated and differentiated cells as they age. These results may guide researchers using hMSCs in extended culture.

6.1.2. Mechanical Loading on Polymeric Foams: Effect on hMSC Differentiation

hMSCs were subjected to cyclic loading to stimulate differentiation in the absence of chemical induction. Cells on PUR and PLA/PCL were stretched (5%, 10%, 15%, 20%) and compressed (2.5%, 5%, 7.5%, 10%) to induce myogenesis and osteogenesis, respectively. Similar upregulation of myogenic mRNA was observed

with 10% stretch and static loading on PUR. Compressive loading at every condition appeared to enhance osteogenesis, with upregulation of Runx2 and Col 1, early osteogenic markers. Loading at 2.5% had the highest upregulation of a late osteogenic marker, OC, which may indicate the most mature cells. **This investigation is the first that examines cyclic loading of hMSCs in 3-D synthetic scaffolds in the absence of chemical induction.** The results of this study indicate that hMSC differentiation can be accelerated by mechanical loading.

6.1.3. Cardiogenic Potential of hMSCs by Embryoid Body Formation

The 3-D cell culture technique of EB formation was used to differentiate hMSCs into cardiomyocytes. The chemical frequently used to induce cardiomyogenic differentiation, 5-azacytidine, may also induce non-specific DNA methylation, and therefore, may not be a clinical option. The aligned cells that grew from the EB expressed various cardiac protein markers (including MHC, troponin T, and α-actinin). Several Z bands, which are indicative or mature sarcomeres, were also observed. A gap junction protein, Cx43, that is necessary for electrical coupling of cardiomyocytes, was observed at cell-cell junctions. **This study is the first to examine the mRNA expression of cardiomyocytes produced by EB formation, and results show that the cells expressed key transcription factors (Nkx2.5, MEF2X, and GATA4).** Given the presence of key transcription factors and various cardiomyogenic proteins, EB formation may be a viable clinical alternative to chemical induction.

6.1.4. *In Vitro* Comparative Biodegradation Analysis of Salt-Leached Porous Polymer Scaffolds

This biodegradation study presented a comprehensive, side-by-side analysis of chemical, thermal, mechanical, and morphological changes in four polymers used in tissue engineering: PGS, PLA/PCL blend, PLGA, and PUR. Frequently these polymers are used in a porous format, but the biodegradation rates had not been extensively studied. The four polymers were submerged in simulated body fluid, and examined every 2 weeks up to 16 weeks. Various changes in morphologies, molecular weights, and melting and recystallization temperatures were found. The crosslinks of PGS had completely broken down by week 16, and the polymer became gel-like. Despite being marketed as "non-biodegradable," decreases in compressive modulus values, as well as cracks and pitting, were observed for PUR. **This study presented the first report of biodegradation in porous PGS, PLA/PCL blend, and PUR, and may guide those researchers using these polymers in a porous format for tissue engineering applications.**

6.2. Future Recommendations

6.2.1. Effect of *In Vitro* Aging on Mechanical Properties and Differentiation Capacity of Human Mesenchymal Stem Cells

While this study gave tremendous insight into the effects of aging on the myogenic lineage, the study must be repeated with hMSCs from multiple donors to verify the observed trend. It is also of great interest to see how the change in mechanical properties affects the adipogenic and chondrogenic lineages, and how the expression of adipogenic/chondrogenic lineage markers change during extended culture. Additionally, the expression of Rho GTPases (RhoA, Rac1, Rock) in aging hMSCs should be examined, as these are likely a part of the aging phenomenon.

In addition to tracking the changes of hMSCs during extended passaging, efforts must be made to prevent this cell aging. One way to prevent aging may be by culturing cells on a softer substrate. A material of interest is a thermoplastic polyurethane (TexinRxT85A) with an elastic modulus of approximately 12.5MPa. Studies are already underway using injection molded PUR samples. Cell elastic modulus will be measured using AFM to see if this material can prevent age-related stiffening.

6.2.2. Mechanical Loading on Polymeric Foams: Effect on hMSC Differentiation

In the mechanical loading investigation, 3 days of cyclic loading was able to upregulate the mRNA of differentiation markers. This study must be carried out longer to examine the protein expression. Additionally, specific late-stage differentiation markers must be observed to deem a differentiation "successful" (i.e. calcium

deposition for osteogenesis, which can be assessed by Von Kossa staining- Section 2.4.6). Optimization studies may also be done for loading regimen.

6.2.3. Cardiogenic Potential of hMSCs by Embryoid Body Formation

The hanging drop method utilized in this study uses 250,000 cells per EB. More studies must be conducted to determine the optimal number of cells per EB. Other EB formation methods may also be investigated, such as hydrogel microwells. While this hanging drop method produces an aligned cell outgrowth that express cardiac proteins, other cell types may be present in the actual EB, as is known to be the case with ESC EBs. More work must be done to characterize the cells in the EB. One obstacle associated with hMSC-derived cardiomyocytes is the lack of spontaneous contraction. Electrical stimulation may be one way to generate spontaneous contraction, and should be investigated.

References

1. Doetschman TC, Eistetter H, Katz M, Schmidt W, Kemler R. (1985) The invitro development of blastocyst-derived embryonic stem-cell lines - formation of visceral yolk-sac, blood islands and myocardium. J Embryol Exp Morphol 87: 27-&.
2. Wobus AM, Wallukat G, Hescheler J. (1991) Pluripotent mouse embryonic stem-cells are able to differentiate into cardiomyocytes expressing chronotropic responses to adrenergic and cholinergic agents and Ca2+ channel blockers. Differentiation 48: 173-182.
3. Takahashi K, Yamanaka S. (2006) Induction of pluripotent stem cells from mouse embryonic and adult fibroblast cultures by defined factors. Cell 126: 663-676.
4. Yamashita T, Kawai H, Tian F, Ohta Y, Abe K. (2011) Tumorigenic development of induced pluripotent stem cells in ischemic mouse brain. Cell Transplant 20: 883-891.
5. Spangrude G, Heimfeld S, Weissman I. (1988) Purification and characterization of mouse hematopoietic stem-cells. Science 241: 58-62.
6. Caplan A. (1991) Mesenchymal stem cells. Journal of Orthopaedic Research 9: 641-650.
7. Haynesworth S, Goshima J, Goldberg V, Caplan A. (1992) Characterization of cells with osteogenic potential from human marrow. Bone 13: 81-88.
8. Wakitani S, Saito T, Caplan AI. (1995) Myogenic cells derived from rat bone-marrow mesenchymal stem-cells exposed to 5-azacytidine. Muscle Nerve 18: 1417-1426.
9. Saito T, Dennis JE, Lennon DP, Young RG, Caplan AI. (1995) Myogenic expression of mesenchymal stem cells within myotubes of mdx mice in vitro and in vivo. Tissue Eng. 1: 1076-3279.
10. Bruder SP, Jaiswal N, Haynesworth SE. (1997) Growth kinetics, self-renewal, and the osteogenic potential of purified human mesenchymal stem cells during extensive subcultivation and following cryopreservation. J Cell Biochem 64: 278-294.
11. Jaiswal N, Haynesworth S, Caplan A, Bruder S. (1997) Osteogenic differentiation of purified, culture-expanded human mesenchymal stem cells in vitro. J Cell Biochem 64: 295-312.
12. Young R, Butler D, Weber W, Caplan A, Gordon S, et al. (1998) Use of mesenchymal stem cells in a collagen matrix for achilles tendon repair. Journal of Orthopaedic Research 16: 406-413.
13. Mackay A, Beck S, Murphy J, Barry F, Chichester C, et al. (1998) Chondrogenic differentiation of cultured human mesenchymal stem cells from marrow. Tissue Eng 4: 415-428.
14. Ferrari G, Cusella-De Angelis G, Coletta M, Paolucci E, Stornaiuolo A, et al. (1998) Muscle regeneration by bone marrow derived myogenic progenitors. Science 279: 1528-1530.

15. Pittenger MF, Mackay AM, Beck SC, Jaiswal RK, Douglas R, et al. (1999) Multilineage potential of adult human mesenchymal stem cells. Science 284: 143-147.
16. Sanchez-Ramos J, Song S, Cardozo-Pelaez F, Hazzi C, Stedeford T, et al. (2000) Adult bone marrow stromal cells differentiate into neural cells in vitro. Exp Neurol 164: 247-256.
17. Woodbury D, Schwarz E, Prockop D, Black I. (2000) Adult rat and human bone marrow stromal cells differentiate into neurons. J Neurosci Res 61: 364-370.
18. Toma C, Pittenger MF, Cahill KS, Byrne BJ, Kessler PD. (2002) Human mesenchymal stem cells differentiate to a cardiomyocyte phenotype in the adult murine heart. Circulation 105: 93-98.
19. Friedenstein AJ, Petrakov KV, Kuroleso AI, Frolova GP. (1968) Heterotopic transplants of bone marrow - analysis of precursor cells for osteogenic and hematopoietic tissues. Transplantation 6: 230-&.
20. Erices A, Conget P, Minguell J. (2000) Mesenchymal progenitor cells in human umbilical cord blood. Br J Haematol 109: 235-242.
21. Zuk P, Zhu M, Mizuno H, Huang J, Futrell J, et al. (2001) Multilineage cells from human adipose tissue: Implications for cell-based therapies. Tissue Eng 7: 211-228.
22. Dominici M, Le Blanc K, Mueller I, Slaper-Cortenbach I, Marini FC, et al. (2006) Minimal criteria for defining multipotent mesenchymal stromal cells. the international society for cellular therapy position statement. Cytotherapy 8: 315-317.
23. Le Blanc K, Tammik C, Rosendahl K, Zetterberg E, Ringden O. (2003) HLA expression and immunologic properties of differentiated and undifferentiated mesenchymal stem cells. Exp Hematol 31: 890-896.
24. Zhang Y, Khan D, Delling J, Tobiasch E. (2012) Mechanisms underlying the osteo- and adipo-differentiation of human mesenchymal stem cells. Scientific World Journal : 793823.
25. Horwitz E, Prockop D, Gordon P, Koo W, Fitzpatrick L, et al. (2001) Clinical responses to bone marrow transplantation in children with severe osteogenesis imperfecta. Blood 97: 1227-1231.
26. Wakitani S, Imoto K, Yamamoto T, Saito M, Murata N, et al. (2002) Human autologous culture expanded bone marrow mesenchymal cell transplantation for repair of cartilage defects in osteoarthritic knees. Osteoarthritis Cartilage 10: 199-206.
27. Quarto R, Mastrogiacomo M, Cancedda R, Kutepov S, Mukhachev V, et al. (2001) Repair of large bone defects with the use of autologous bone marrow stromal cells. N Engl J Med 344: 385-386.
28. Chen S, Fang W, Qian J, Ye F, Liu Y, et al. (2004) Improvement of cardiac function after transplantation of autologous bone marrow mesenchymal stem cells in patients with acute myocardial infarction. Chin Med J 117: 1443-1448.
29. Caplan AI. (2007) Adult mesenchymal stem cells for tissue engineering versus regenerative medicine. J Cell Physiol 213: 341-347.

30. Grove J, Bruscia E, Krause D. (2004) Plasticity of bone marrow-derived stem cells. Stem Cells 22: 487-500.
31. Eschenhagen T, Zimmermann WH. (2005) Engineering myocardial tissue. Circ Res 97: 1220-1231.
32. Lu L, Peter SJ, Lyman MD, Lai HL, Leite SM, et al. (2000) In vitro and in vivo degradation of porous poly(DL-lactic-co-glycolic acid) foams. Biomaterials 21: 1837-1845.
33. Li WJ, Laurencin CT, Caterson EJ, Tuan RS, Ko FK. (2002) Electrospun nanofibrous structure: A novel scaffold for tissue engineering. J Biomed Mater Res 60: 613-621.
34. Nam Y, Park T. (1999) Porous biodegradable polymeric scaffolds prepared by thermally induced phase separation. J Biomed Mater Res 47: 8-17.
35. Discher DE, Janmey P, Wang YL. (2005) Tissue cells feel and respond to the stiffness of their substrate. Science 310: 1139-1143.
36. Ingber DE. (2006) Cellular mechanotransduction: Putting all the pieces together again. FASEB J 20: 811-827.
37. Ingber D. (2003) Mechanobiology and diseases of mechanotransduction. Ann Med 35: 564-577.
38. Chen C, Tan J, Tien J. (2004) Mechanotransduction at cell-matrix and cell-cell contacts. Annu Rev Biomed Eng 6: 275-302.
39. Docheva D, Popov C, Mutschler W, Schieker M. (2007) Human mesenchymal stem cells in contact with their environment: Surface characteristics and the integrin system. J Cell Mol Med 11: 21-38.
40. Hynes R. (2002) Integrins: Bidirectional, allosteric signaling machines. Cell 110: 673-687.
41. Burridge K, Fath K, Kelly T, Nuckolls G, Turner C. (1988) Focal adhesions - transmembrane junctions between the extracellular-matrix and the cytoskeleton. Annu Rev Cell Biol 4: 487-525.
42. Kanchanawong P, Shtengel G, Pasapera AM, Ramko EB, Davidson MW, et al. (2010) Nanoscale architecture of integrin-based cell adhesions. Nature 468: 580-U262.
43. Lo C, Wang H, Dembo M, Wang Y. (2000) Cell movement is guided by the rigidity of the substrate. Biophys J 79: 144-152.
44. Peyton S, Putnam A. (2005) Extracellular matrix rigidity governs smooth muscle cell motility in a biphasic fashion RID E-8643-2010. J Cell Physiol 204: 198-209.
45. Zaman MH, Trapani LM, Siemeski A, MacKellar D, Gong H, et al. (2006) Migration of tumor cells in 3D matrices is governed by matrix stiffness along with cell-matrix adhesion and proteolysis. Proc Natl Acad Sci U S A 103: 10889-10894.
46. Song G, Ju Y, Shen X, Luo Q, Shi Y, et al. (2007) Mechanical stretch promotes proliferation of rat bone marrow mesenchymal stem cells. Colloids and Surfaces B-Biointerfaces 58: 271-277.

47. Engler A, Griffin M, Sen S, Bonnetnann C, Sweeney H, et al. (2004) Myotubes differentiate optimally on substrates with tissue-like stiffness: Pathological implications for soft or stiff microenvironments. J Cell Biol 166: 877-887.
48. Engler AJ, Sen S, Sweeney HL, Discher DE. (2006) Matrix elasticity directs stem cell lineage specification. Cell 126: 677-689.
49. Engler AJ, Carag-Krieger C, Johnson CP, Raab M, Tang HY, et al. (2008) Embryonic cardiomyocytes beat best on a matrix with heart-like elasticity: Scar-like rigidity inhibits beating. Journal of Cell Science 121: 3794-3802.
50. Rowlands AS, George PA, Cooper-White JJ. (2008) Directing osteogenic and myogenic differentiation of MSCs: Interplay of stiffness and adhesive ligand presentation. American Journal of Physiology-Cell Physiology 295: C1037-C1044.
51. Winer JP, Janmey PA, McCormick ME, Funaki M. (2009) Bone marrow-derived human mesenchymal stem cells become quiescent on soft substrates but remain responsive to chemical or mechanical stimuli. Tissue Eng Part A 15: 147-154.
52. Yim EKF, Darling EM, Kulangara K, Guilak F, Leong KW. (2010) Nanotopography-induced changes in focal adhesions, cytoskeletal organization, and mechanical properties of human mesenchymal stem cells RID A-7270-2009. Biomaterials 31: 1299-1306.
53. Yu H, Lui YS, Xiong S, Leong WS, Wen F, et al. (2013) Insights into the role of focal adhesion modulation in myogenic differentiation of human mesenchymal stem cells. Stem Cells and Development 22: 136-147.
54. Yim EKF, Pang SW, Leong KW. (2007) Synthetic nanostructures inducing differentiation of human mesenchymal stem cells into neuronal lineage. Exp Cell Res 313: 1820-1829.
55. McBeath R, Pirone D, Nelson C, Bhadriraju K, Chen C. (2004) Cell shape, cytoskeletal tension, and RhoA regulate stem cell lineage commitment. Developmental Cell 6: 483-495.
56. Kilian KA, Bugarija B, Lahn BT, Mrksich M. (2010) Geometric cues for directing the differentiation of mesenchymal stem cells. Proc Natl Acad Sci U S A 107: 4872-4877.
57. Gao L, McBeath R, Chen CS. (2010) Stem cell shape regulates a chondrogenic versus myogenic fate through Rac1 and N-cadherin. Stem Cells 28: 564-572.
58. Jaffe A, Hall A. (2005) Rho GTPases: Biochemistry and biology. Annu Rev Cell Dev Biol 21: 247-269.
59. Sordella R, Jiang W, Chen G, Curto M, Settleman J. (2003) Modulation of rho GTPase signaling regulates a switch between adipogenesis and myogenesis. Cell 113: 147-158.
60. Woods A, Wang G, Dupuis H, Shao Z, Beier F. (2007) Rac1 signaling stimulates N-cadherin expression, mesenchymal condensation, and chondrogenesis. J Biol Chem 282: 23500-23508.
61. Patwari P, Lee RT. (2008) Mechanical control of tissue morphogenesis. Circ Res 103: 234-243.

62. Ashkin A. (1992) Forces of a single-beam gradient laser trap on a dielectric sphere in the ray optics regime. Biophys J 61: 569-582.
63. Hochmuth R. (2000) Micropipette aspiration of living cells. J Biomech 33: 15-22.
64. Radmacher M. (1997) Measuring the elastic properties of biological samples with the AFM. IEEE Eng Med Biol Mag 16: 47-57.
65. Ingber D. (1997) Tensegrity: The architectural basis of cellular mechanotransduction. Annu Rev Physiol 59: 575-599.
66. Theret D, Levesque M, Sato M, Nerem R, Wheeler L. (1988) The application of a homogeneous half-space model in the analysis of endothelial-cell micropipette measurements. J Biomech Eng -Trans ASME 110: 190-199.
67. Tan SCW, Pan WX, Ma G, Cai N, Leong KW, et al. (2008) Viscoelastic behaviour of human mesenchymal stem cells. BMC Cell Biol 9: 40.
68. Schmid-Schonbein G, Sung K, Tozeren H, Skalak R, Chien S. (1981) Passive mechanical-properties of human-leukocytes. Biophys J 36: 243-256.
69. Lim C, Zhou E, Quek S. (2006) Mechanical models for living cells - A review. J Biomech 39: 195-216.
70. Evans E, Yeung A. (1989) Apparent viscosity and cortical tension of blood granulocytes determined by micropipet aspiration. Biophys J 56: 151-160.
71. Maloney JM, Nikova D, Lautenschlaeger F, Clarke E, Langer R, et al. (2010) Mesenchymal stem cell mechanics from the attached to the suspended state. Biophys J 99: 2479-2487.
72. Titushkin I, Cho M. (2007) Modulation of cellular mechanics during osteogenic differentiation of human mesenchymal stem cells. Biophys J 93: 3693-3702.
73. Yourek G, Hussain MA, Mao JJ. (2007) Cytoskeletal changes of mesenchymal stem cells during differentiation. ASAIO J 53: 219-228.
74. Yu H, Tay CY, Leong WS, Tan SCW, Liao K, et al. (2010) Mechanical behavior of human mesenchymal stem cells during adipogenic and osteogenic differentiation. Biochem Biophys Res Commun 393: 150-155.
75. Hertz H. (1882) On the contact of elastic solids. J. reine und angewandte Mathematik 92: 156–171.
76. Sneddon IN. (1965) The relation between load and penetration in the axisymmetric boussinesq problem for a punch of arbitrary profile. International Journal of Engineering Science 3: 47-57.
77. Mathur AB, Collinsworth AM, Reichert WM, Kraus WE, Truskey GA. (2001) Endothelial, cardiac muscle and skeletal muscle exhibit different viscous and elastic properties as determined by atomic force microscopy. J Biomech 34: 1545-1553.
78. Carl P, Schillers H. (2008) Elasticity measurement of living cells with an atomic force microscope: Data acquisition and processing. Pflugers Arch 457: 551-559.
79. Vichare S, Inamdar MM, Sen S. (2012) Influence of cell spreading and contractility on stiffness measurements using AFM. Soft Matter 8: 10464-10471.
80. Dimitriadis E, Horkay F, Maresca J, Kachar B, Chadwick R. (2002) Determination of elastic moduli of thin layers of soft material using the atomic force microscope. Biophys J 82: 2798-2810.

81. Darling E, Zauscher S, Guilak F. (2006) Viscoelastic properties of zonal articular chondrocytes measured by atomic force microscopy. Osteoarthritis and Cartilage 14: 571-579.
82. Svoboda K, Block S. (1994) Biological applications of optical forces. Annu Rev Biophys Biomol Struct 23: 247-285.
83. Titushkin I, Cho M. (2006) Distinct membrane mechanical properties of human mesenchymal stem cells determined using laser optical tweezers. Biophys J 90: 2582-2591.
84. Friedenstein A, Latzinik N, Grosheva A, Gorskaya U. (1982) Marrow micro-environment transfer by heterotopic transplantation of freshly isolated and cultured-cells in porous sponges. Exp Hematol 10: 217-227.
85. Radmacher M, Fritz M, Kacher C, Cleveland J, Hansma P. (1996) Measuring the viscoelastic properties of human platelets with the atomic force microscope. Biophys J 70: 556-567.
86. Darling EM, Topel M, Zauscher S, Vail TP, Guilak F. (2008) Viscoelastic properties of human mesenchymally-derived stem cells and primary osteoblasts, chondrocytes, and adipocytes. J Biomech 41: 454-464.
87. Bonab M, Alimoghaddam K, Talebian F, Ghaffari S, Ghavamzadeh A, et al. (2006) Aging of mesenchymal stem cell in vitro. BMC Cell Biol 7: 14.
88. Banfi A, Muraglia A, Dozin B, Mastrogiacomo M, Cancedda R, et al. (2000) Proliferation kinetics and differentiation potential of ex vivo expanded human bone marrow stromal cells: Implications for their use in cell therapy RID B-8720-2008. Exp Hematol 28: 707-715.
89. Zhou S, Greenberger JS, Epperly MW, Goff JP, Adler C, et al. (2008) Age-related intrinsic changes in human bone-marrow-derived mesenchymal stem cells and their differentiation to osteoblasts. Aging Cell 7: 335-343.
90. Kim J, Kang JW, Park JH, Choi Y, Choi KS, et al. (2009) Biological characterization of long-term cultured human mesenchymal stem cells. Arch Pharm Res 32: 117-126.
91. Zaim M, Karaman S, Cetin G, Isik S. (2012) Donor age and long-term culture affect differentiation and proliferation of human bone marrow mesenchymal stem cells. Ann Hematol 91: 1175-1186.
92. Hofmann UG, Rotsch C, Parak WJ, Radmacher M. (1997) Investigating the cytoskeleton of chicken cardiocytes with the atomic force microscope. J Struct Biol 119: 84-91.
93. DiGirolamo C, Stokes D, Colter D, Phinney D, Class R, et al. (1999) Propagation and senescence of human marrow stromal cells in culture: A simple colony-forming assay identifies samples with the greatest potential to propagate and differentiate. Br J Haematol 107: 275-281.
94. Baxter M, Wynn R, Jowitt S, Wraith J, Fairbairn L, et al. (2004) Study of telomere length reveals rapid aging of human marrow stromal cells following in vitro expansion RID B-4405-2009. Stem Cells 22: 675-682.

95. Binnig G, Quate C, Gerber C. (1986) Atomic force microscope. Phys Rev Lett 56: 930-933.
96. Engler AJ, Rehfeldt F, Sen S, Discher DE. (2007) Microtissue elasticity: Measurements by atomic force microscopy and its influence on cell differentiation. Cell Mechanics 83: 521-+.
97. Ikai A. (2010) A review on: Atomic force microscopy applied to nano-mechanics of the cell. Adv Biochem Eng Biotechnol 119: 47-61.
98. Hutter J, Bechhoefer J. (1993) Calibration of atomic-force microscope tips. Rev Sci Instrum 64: 1868-1873.
99. Chaudhuri T, Rehfeldt F, Sweeney HL, Discher DE. (2010) Preparation of collagen-coated gels that maximize in vitro myogenesis of stem cells by matching the lateral elasticity of in vivo muscle. 621.
100. Heid C, Stevens J, Livak K, Williams P. (1996) Real time quantitative PCR. Genome Res 6: 986-994.
101. Livak K, Schmittgen T. (2001) Analysis of relative gene expression data using real-time quantitative PCR and the 2(T)(-delta delta C) method. Methods 25: 402-408.
102. Halvorsen Y, Franklin D, Bond A, Hitt D, Auchter C, et al. (2001) Extracellular matrix mineralization and osteoblast gene expression by human adipose tissue-derived stromal cells. Tissue Eng 7: 729-741.
103. Sethe S, Scutt A, Stolzing A. (2006) Aging of mesenchymal stem cells. Ageing Research Reviews 5: 91-116.
104. Lieber S, Aubry N, Pain J, Diaz G, Kim S, et al. (2004) Aging increases stiffness of cardiac myocytes measured by atomic force microscopy nanoindentation. American Journal of Physiology-Heart and Circulatory Physiology 287: H645-H651.
105. Zahn JT, Louban I, Jungbauer S, Bissinger M, Kaufmann D, et al. (2011) Age-dependent changes in microscale stiffness and mechanoresponses of cells. Small 7: 1480-1487.
106. Docheva D, Padula D, Popov C, Mutschler W, Clausen-Schaumann H, et al. (2008) Researching into the cellular shape, volume and elasticity of mesenchymal stem cells, osteoblasts and osteosarcoma cells by atomic force microscopy. J Cell Mol Med 12: 537-552.
107. Sugitate T, Kihara T, Liu X, Miyake J. (2009) Mechanical role of the nucleus in a cell in terms of elastic modulus. Curr Appl Phys 9: E291-E293.
108. Rico F, Roca-Cusachs P, Gavara N, Farre R, Rotger M, et al. (2005) Probing mechanical properties of living cells by atomic force microscopy with blunted pyramidal cantilever tips. Phys Rev E 72: 021914.
109. Collinsworth AM, Zhang S, Kraus WE, Truskey GA. (2002) Apparent elastic modulus and hysteresis of skeletal muscle cells throughout differentiation. Am J Physiol -Cell Physiol 283: C1219-C1227.

110. Takai E, Costa K, Shaheen A, Hung C, Guo X. (2005) Osteoblast elastic modulus measured by atomic force microscopy is substrate dependent. Ann Biomed Eng 33: 963-971.
111. Gordon A, Homsher E, Regnier M. (2000) Regulation of contraction in striated muscle. Physiol Rev 80: 853-924.
112. Boheler KR, Czyz J, Tweedie D, Yang HT, Anisimov SV, et al. (2002) Differentiation of pluripotent embryonic stem cells into cardiomyocytes. Circ Res 91: 189-201.
113. Young P, Ferguson C, Banuelos S, Gautel M. (1998) Molecular structure of the sarcomeric Z-disk: Two types of titin interactions lead to an asymmetrical sorting of alpha-actinin. EMBO J 17: 1614-1624.
114. Chiron S, Tomczak C, Duperray A, Laine J, Bonne G, et al. (2012) Complex interactions between human myoblasts and the surrounding 3D fibrin-based matrix. Plos One 7: e36173.
115. Zhang L, Xiong C, Deng X. (1995) Biodegradable polyester blends for biomedical application. J Appl Polym Sci 56: 103-112.
116. Costa M, Escaleira R, Cataldo A, Oliveira F, Mermelstein C. (2004) Desmin: Molecular interactions and putative functions of the muscle intermediate filament protein. Brazilian Journal of Medical and Biological Research 37: 1819-1830.
117. Sugi Y, Lough J. (1992) Onset of expression and regional deposition of alpha-smooth and sarcomeric actin during avian heart development. Developmental Dynamics 193: 116-124.
118. Frid M, Shekhonin B, Koteliansky V, Glukhova M. (1992) Phenotypic changes of human smooth-muscle cells during development - late expression of heavy caldesmon and calponin. Dev Biol 153: 185-193.
119. Wick M. (1999) Filament assembly properties of the sarcomeric myosin heavy chain. Poult Sci 78: 735-742.
120. Siegel G, Krause P, Woehrle S, Nowak P, Ayturan M, et al. (2012) Bone marrow-derived human mesenchymal stem cells express cardiomyogenic proteins but do not exhibit functional cardiomyogenic differentiation potential. Stem Cells Dev 21: 2457-2470.
121. Kelm R, Swords N, Orfeo T, Mann K. (1994) Osteonectin in matrix remodeling - a plasminogen-osteonectin-collagen complex. J Biol Chem 269: 30147-30153.
122. Lian J, Stein G, Stein J, Van Wijnen A. (1999) Regulated expression of the bone-specific osteocalcin gene by vitamins and hormones. Vitamins and Hormones - Advances in Research and Applications 55: 443-509.
123. Hessle L, Johnson K, Anderson H, Narisawa S, Sali A, et al. (2002) Tissue-nonspecific alkaline phosphatase and plasma cell membrane glycoprotein-1 are central antagonistic regulators of bone mineralization. Proc Natl Acad Sci U S A 99: 9445-9449.
124. Sila-Asna M, Bunyaratvej A, Maeda S, Kitaguchi H, Bunyaratavej N. (2007) Osteoblast differentiation and bone formation gene expression in strontium-inducing bone marrow mesenchymal stem cell. Kobe J Med Sci 53: 25-35.

125. Ducy P, Geoffroy V, Karsenty G. (1996) Study of osteoblast-specific expression of one mouse osteocalcin gene: Characterization of the factor binding to OSE2. Connect Tissue Res 35: 7-14.
126. Banfi A, Bianchi G, Notaro R, Luzzatto L, Cancedda R, et al. (2002) Replicative aging and gene expression in long-term cultures of human bone marrow stromal cells RID B-8720-2008. Tissue Eng 8: 901-910.
127. Khoo MLM, Shen B, Tao H, Ma DDF. (2008) Long-term serial passage and neuronal differentiation capability of human bone marrow mesenchymal stem cells. Stem Cells Dev 17: 883-896.
128. Muraglia A, Cancedda R, Quarto R. (2000) Clonal mesenchymal progenitors from human bone marrow differentiate in vitro according to a hierarchical model. J Cell Sci 113: 1161-1166.
129. Stenderup K, Justesen J, Clausen C, Kassem M. (2003) Aging is associated with decreased maximal life span and accelerated senescence of bone marrow stromal cells. Bone 33: 919-926.
130. Gonzalez-Cruz RD, Fonseca VC, Darling EM. (2012) Cellular mechanical properties reflect the differentiation potential of adipose-derived mesenchymal stem cells. Proc Natl Acad Sci U S A 109: E1523-E1529.
131. Wang Y, Yu X, Cohen DM, Wozniak MA, Yang MT, et al. (2012) Bone morphogenetic protein-2-induced signaling and osteogenesis is regulated by cell shape, RhoA/ROCK, and cytoskeletal tension. Stem Cells Dev 21: 1176-1186.
132. Beqaj S, Jakkaraju S, Mattingly R, Pan D, Schuger L. (2002) High RhoA activity maintains the undifferentiated mesenchymal cell phenotype, whereas RhoA down-regulation by laminin-2 induces smooth muscle myogenesis. J Cell Biol 156: 893-903.
133. Kim M, Kino-oka M, Maruyama N, Saito A, Sawa Y, et al. (2010) Cardiomyogenic induction of human mesenchymal stem cells by altered rho family GTPase expression on dendrimer-immobilized surface with D-glucose display. Biomaterials 31: 7666-7677.
134. Castellani L, Salvati E, Alema S, Falcone G. (2006) Fine regulation of RhoA and rock is required for skeletal muscle differentiation. J Biol Chem 281: 15249-15257.
135. Taber LA. (2006) Biophysical mechanisms of cardiac looping. Int J Dev Biol 50: 323-332.
136. Cheshire AM, Kerman BE, Zipfel WR, Spector AA, Andrew DJ. (2008) Kinetic and mechanical analysis of live tube morphogenesis. Developmental Dynamics 237: 2874-2888.
137. Moore KA, Polte T, Huang S, Shi B, Alsberg E, et al. (2005) Control of basement membrane remodeling and epithelial branching morphogenesis in embryonic lung by rho and cytoskeletal tension. Developmental Dynamics 232: 268-281.
138. Williams B. (1998) Mechanical influences on vascular smooth muscle cell function. J Hypertens 16: 1921-1929.
139. Zerath E. (1998) Effects of microgravity on bone and calcium homeostasis. Life Sciences: Microgravity Research 21: 1049-1058.

140. Simmons CA, Matlis S, Thornton AJ, Chen SQ, Wang CY, et al. (2003) Cyclic strain enhances matrix mineralization by adult human mesenchymal stem cells via the extracellular signal-regulated kinase (ERK1/2) signaling pathway. J Biomech 36: 1087-1096.
141. Park JS, Chu JSF, Cheng C, Chen FQ, Chen D, et al. (2004) Differential effects of equiaxial and uniaxial strain on mesenchymal stem cells. Biotechnol Bioeng 88: 359-368.
142. Huang CYC, Hagar KL, Frost LE, Sun YB, Cheung HS. (2004) Effects of cyclic compressive loading on chondrogenesis of rabbit bone-marrow derived mesenchymal stem cells. Stem Cells 22: 313-323.
143. Elder SH, Goldstein SA, Kimura JH, Soslowsky LJ, Spengler DM. (2001) Chondrocyte differentiation is modulated by frequency and duration of cyclic compressive loading. Ann Biomed Eng 29: 476-482.
144. Angele P, Schumann D, Angele M, Kinner B, Englert C, et al. (2004) Cyclic, mechanical compression enhances chondrogenesis of mesenchymal progenitor cells in tissue engineering scaffolds. Biorheology 41: 335-346.
145. Sim WY, Park SW, Park SH, Min BH, Park SR, et al. (2007) A pneumatic micro cell chip for the differentiation of human mesenchymal stem cells under mechanical stimulation. Lab Chip 7: 1775-1782.
146. Mauney J, Sjostorm S, Blumberg J, Horan R, O'Leary J, et al. (2004) Mechanical stimulation promotes osteogenic differentiation of human bone marrow stromal cells on 3-D partially demineralized bone scaffolds in vitro. Calcif Tissue Int 74: 458-468.
147. Datta N, Pham Q, Sharma U, Sikavitsas V, Jansen J, et al. (2006) In vitro generated extracellular matrix and fluid shear stress synergistically enhance 3D osteoblastic differentiation. Proc Natl Acad Sci U S A 103: 2488-2493.
148. Knippenberg M, Helder M, Doulabi B, Semeins C, Wuisman P, et al. (2005) Adipose tissue-derived mesenchymal stem cells acquire bone cell-like responsiveness to fluid shear stress on osteogenic stimulation. Tissue Eng 11: 1780-1788.
149. Braccini A, Wendt D, Jaquiery C, Jakob M, Heberer M, et al. (2005) Three-dimensional perfusion culture of human bone marrow cells and generation of osteoinductive grafts. Stem Cells 23: 1066-1072.
150. Jagodzinski M, Breitbart A, Wehmeier M, Hesse E, Haasper C, et al. (2008) Influence of perfusion and cyclic compression on proliferation and differentiation of bone marrow stromal cells in 3-dimensional culture. J Biomech 41: 1885-1891.
151. Angele P, Yoo J, Smith C, Mansour J, Jepsen K, et al. (2003) Cyclic hydrostatic pressure enhances the chondrogenic phenotype of human mesenchymal progenitor cells differentiated in vitro. Journal of Orthopaedic Research 21: 451-457.
152. Hamilton D, Maul T, Vorp D. (2004) Characterization of the response of bone marrow-derived progenitor cells to cyclic strain: Implications for vascular tissue-engineering applications. Tissue Eng 10: 361-369.

153. Ghazanfari S, Tafazzoli-Shadpour M, Shokrgozar MA. (2009) Effects of cyclic stretch on proliferation of mesenchymal stem cells and their differentiation to smooth muscle cells. Biochem Biophys Res Commun 388: 601-605.
154. Nieponice A, Maul TM, Cumer JM, Soletti L, Vorp DA. (2007) Mechanical stimulation induces morphological and phenotypic changes in bone marrow-derived progenitor cells within a three-dimensional fibrin matrix. Journal of Biomedical Materials Research Part a 81A: 523-530.
155. Kurpinski K, Chu J, Hashi C, Li S. (2006) Anisotropic mechanosensing by mesenchymal stem cells. Proc Natl Acad Sci U S A 103: 16095-16100.
156. Campbell JJ, Lee DA, Bader DL. (2006) Dynamic compressive strain influences chondrogenic gene expression in human mesenchymal stem cells. Biorheology 43: 455-470.
157. Haudenschild AK, Hsieh AH, Kapila S, Lotz JC. (2009) Pressure and distortion regulate human mesenchymal stem cell gene expression. Ann Biomed Eng 37: 492-502.
158. Huang AH, Farrell MJ, Kim M, Mauck RL. (2010) Long-term dynamic loading improves the mechanical properties of chondrogenic mesenchymal stem cell-laden hydrogels. Eur Cells Mater 19: 72-85.
159. Mouw JK, Connelly JT, Wilson CG, Michael KE, Levenston ME. (2007) Dynamic compression regulates the expression and synthesis of chondrocyte-specific matrix molecules in bone marrow stromal cells. Stem Cells 25: 655-663.
160. Sittichokechaiwut A, Edwards JH, Scutt AM, Reilly GC. (2010) Short bouts of mechanical loading are as effective as dexamethasone at inducing matrix production by human bone marrow mesenchymal stem cells. Eur Cells Mater 20: 45-57.
161. Waldman SD, Couto DC, Grynpas MD, Pilliar RM, Kandel RA. (2006) A single application of cyclic loading can accelerate matrix deposition and enhance the properties of tissue-engineered cartilage. Osteoarthritis Cartilage 14: 323-330.
162. Bhang SH, Gwak S, Lee T, Kim S, Park HH, et al. (2010) Cyclic mechanical strain promotes transforming-growth-factor-beta I-mediated cardiomyogenic marker expression in bone-marrow-derived mesenchymal stem cells in vitro. Biotechnol Appl Biochem 55: 191-197.
163. David V, Martin A, Lafage-Proust M, Malaval L, Peyroche S, et al. (2007) Mechanical loading down-regulates peroxisome proliferator-activated receptor gamma in bone marrow stromal cells and favors osteoblastogenesis at the expense of adipogenesis. Endocrinology 148: 2553-2562.
164. Huang C, Chen M, Young T, Jeng J, Chen Y. (2009) Interactive effects of mechanical stretching and extracellular matrix proteins on initiating osteogenic differentiation of human mesenchymal stem cells. J Cell Biochem 108: 1263-1273.
165. Jagodzinski M, Drescher M, Zeichen J, Hankemeier S, Krettek C, et al. (2004) Effects of cyclic longitudinal mechanical strain and dexamethasone on osteogenic differentiation of human bone marrow stromal cells. European Cells & Materials 7: 35-41.

166. Kearney EM, Farrell E, Prendergast PJ, Campbell VA. (2010) Tensile strain as a regulator of mesenchymal stem cell osteogenesis. Ann Biomed Eng 38: 1767-1779.
167. Sumanasinghe RD, Bernacki SH, Loboa EG. (2006) Osteogenic differentiation of human mesenchymal stem cells in collagen matrices: Effect of uniaxial cyclic tensile strain on bone morphogenetic protein (BMP-2) mRNA expression. Tissue Eng 12: 3459-3465.
168. Kurpinski K, Chu J, Wang D, Li S. (2009) Proteomic profiling of mesenchymal stem cell responses to mechanical strain and TGF-beta 1. Cell Mol Bioeng 2: 606-614.
169. Ward DF, Jr., Salasznyk RM, Klees RF, Backiel J, Agius P, et al. (2007) Mechanical strain enhances extracellular matrix-induced gene focusing and promotes osteogenic differentiation of human mesenchymal stem cells through an extracellular-related kinase-dependent pathway. Stem Cells and Development 16: 467-479.
170. Shi Y, Li H, Zhang X, Fu Y, Huang Y, et al. (2011) Continuous cyclic mechanical tension inhibited Runx2 expression in mesenchymal stem cells through RhoA-ERK1/2 pathway. J Cell Physiol 226: 2159-2169.
171. Morita Y, Mukai T, Ju Y, Watanabe S. (2013) Evaluation of stem cell-to-tenocyte differentiation by atomic force microscopy to measure cellular elastic moduli. Cell Biochem Biophys 66: 73-80.
172. Huang CYC, Reuben PM, Cheung HS. (2005) Temporal expression patterns and corresponding protein inductions of early responsive genes in rabbit bone marrow-derived mesenchymal stem cells under cyclic compressive loading. Stem Cells 23: 1113-1121.
173. Thorpe SD, Buckley CT, Vinardell T, O'Brien FJ, Campbell VA, et al. (2008) Dynamic compression can inhibit chondrogenesis of mesenchymal stem cells. Biochem Biophys Res Commun 377: 458-462.
174. Pelaez D, Huang CC, Cheung HS. (2009) Cyclic compression maintains viability and induces chondrogenesis of human mesenchymal stem cells in fibrin gel scaffolds. Stem Cells Dev 18: 93-102.
175. Thorpe SD, Buckley CT, Vinardell T, O'Brien FJ, Campbell VA, et al. (2010) The response of bone marrow-derived mesenchymal stem cells to dynamic compression following TGF-beta 3 induced chondrogenic differentiation. Ann Biomed Eng 38: 2896-2909.
176. Zeiter S, Lezuo P, Ito K. (2009) Effect of TGF beta(1), BMP-2 and hydraulic pressure on chondrogenic differentiation of bovine bone marrow mesenchymal stromal cells. Biorheology 46: 45-55.
177. Meyer EG, Buckley CT, Thorpe SD, Kelly DJ. (2010) Low oxygen tension is a more potent promoter of chondrogenic differentiation than dynamic compression. J Biomech 43: 2516-2523.
178. Au-yeung KL, Sze KY, Sham MH, Chan BP. (2010) Development of a micromanipulator-based loading device for mechanoregulation study of human

mesenchymal stem cells in three-dimensional collagen constructs. Tissue Engineering Part C-Methods 16: 93-107.
179. Elder SH, Shim JW, Borazjani A, Robertson HM, Smith KE, et al. (2008) Influence of hydrostatic and distortional stress on chondroinduction. Biorheology 45: 479-486.
180. Liu C, Abedian R, Meister R, Haasper C, Hurschler C, et al. (2012) Influence of perfusion and compression on the proliferation and differentiation of bone mesenchymal stromal cells seeded on polyurethane scaffolds. Biomaterials 33: 1052-1064.
181. LeBlon CE, Pai R, Fodor CR, Golding AS, Coulter JP, et al. (2013) In vitro comparative biodegradation analysis of salt-leached porous polymer scaffolds. J Appl Polym Sci 128: 2701-2712.
182. Zdrahala RJ, Zdrahala IJ. (1999) Biomedical applications of polyurethanes: A review of past promises, present realities, and a vibrant future. J Biomater Appl 14: 67-90.
183. Mulder MM, Hitchcock RW, Tresco PA. (1998) Skeletal myogenesis on elastomeric substrates: Implications for tissue engineering. J Biomater Sci -Polym Ed 9: 731-748.
184. Schnell AM, Hoerstrup SP, Zund G, Kolb S, Sodian R, et al. (2001) Optimal cell source for cardiovascular tissue engineering: Venous vs. aortic human myofibroblasts. Thorac Cardiovasc Surg 49: 221-225.
185. Li J, Zhao Q, Wang E, Zhang C, Wang G, et al. (2012) Transplantation of Cbfa1-overexpressing adipose stem cells together with vascularized periosteal flaps repair segmental bone defects. J Surg Res 176: E13-E20.
186. Jegal S, Park J, Kim J, Kim T, Shin US, et al. (2011) Functional composite nanofibers of poly(lactide-co-caprolactone) containing gelatin-apatite bone mimetic precipitate for bone regeneration. Acta Biomaterialia 7: 1609-1617.
187. Kim J, Kim M, Park J, Won J, Kim T, et al. (2011) Performance of novel nanofibrous biopolymer membrane for guided bone regeneration within rat mandibular defect. In Vivo 25: 589-595.
188. Pandey A, Pandey GC, Aswath PB. (2008) Synthesis of polylactic acid-polyglycolic acid blends using microwave radiation. J Mech Behav Biomed Mater 1: 227-233.
189. Mikos AG, Thorsen AJ, Czerwonka LA, Bao Y, Langer R, et al. (1994) Preparation and characterization of poly(L-lactic acid) foams. Polymer 35: 1068-1077.
190. Huang Y, Zheng L, Gong X, Jia X, Song W, et al. (2012) Effect of cyclic strain on cardiomyogenic differentiation of rat bone marrow derived mesenchymal stem cells. Plos One 7: e34960.
191. Rensen SSM, Doevendans PAFM, van Eys GJJM. (2007) Regulation and characteristics of vascular smooth muscle cell phenotypic diversity. Netherlands Heart Journal 15: 100-108.
192. Dobrin PB. (1978) Mechanical-properties of arteries. Physiol Rev 58: 397-460.

193. Haghighipour N, Heidarian S, Shokrgozar MA, Amirizadeh N. (2012) Differential effects of cyclic uniaxial stretch on human mesenchymal stem cell into skeletal muscle cell. Cell Biol Int 36: 669-675.
194. Lian J, Javed A, Zaidi S, Lengner C, Montecino M, et al. (2004) Regulatory controls for osteoblast growth and differentiation: Role of Runx/Cbfa/AML factors. Crit Rev Eukaryot Gene Expr 14: 1-41.
195. Karsenty G, Wagner E. (2002) Reaching a genetic and molecular understanding of skeletal development. Dev Cell 2: 389-406.
196. Rubin CT, Lanyon LE. (1985) Regulation of bone mass by mechanical strain magnitude. Calcif Tissue Int 37: 411-417.
197. Michalopoulos E, Knight RL, Korossis S, Kearney JN, Fisher J, et al. (2012) Development of methods for studying the differentiation of human mesenchymal stem cells under cyclic compressive strain. Tissue Engineering Part C-Methods 18: 252-262.
198. Banes A, Tsuzaki M, Yamamoto J, Fischer T, Brigman B, et al. (1995) Mechanoreception at the cellular level: The detection, interpretation, and diversity of responses to mechanical signals. Biochem Cell Biol 73: 349-365.
199. Guharay F, Sachs F. (1984) Stretch-activated single ion channel currents in tissue-cultured embryonic chick skeletal-muscle. Journal of Physiology-London 352: 685-701.
200. Hytoenen VP, Vogel V. (2008) How force might activate talin's vinculin binding sites: SMD reveals a structural mechanism. PLoS Comput Biol 4: e24.
201. Ji B, Bao G. (2011) Cell and molecular biomechanics: Perspectives and challenges. Acta Mechanica Solida Sinica 24: 27-51.
202. McMahon LA, Campbell VA, Prendergast PJ. (2008) Involvement of stretch-activated ion channels in strain-regulated glycosaminoglycan synthesis in mesenchymal stem cell-seeded 3D scaffolds. J Biomech 41: 2055-2059.
203. Lloyd-Jones D, Adams RJ, Brown TM, Carnethon M, Dai S, et al. (2010) Executive summary: Heart disease and stroke statistics-2010 update A report from the american heart association. Circulation 121: 948-954.
204. Pfeffer MA, Braunwald E. (1990) Ventricular remodeling after myocardial-infarction - experimental-observations and clinical implications. Circulation 81: 1161-1172.
205. Gaudron P, Eilles C, Kugler I, Ertl G. (1993) Progressive left-ventricular dysfunction and remodeling after myocardial-infarction - potential mechanisms and early predictors. Circulation 87: 755-763.
206. Cohn J, Ferrari R, Sharpe N, Int Forum Cardiac Remodeling. (2000) Cardiac remodeling-concepts and clinical implications: A consensus paper from an international forum on cardiac remodeling. J Am Coll Cardiol 35: 569-582.
207. Beltrami AP, Barlucchi L, Torella D, Baker M, Limana F, et al. (2003) Adult cardiac stem cells are multipotent and support myocardial regeneration. Cell 114: 763-776.

208. Laugwitz K, Moretti A, Lam J, Gruber P, Chen Y, et al. (2005) Postnatal isl1+cardioblasts enter fully differentiated cardiomyocyte lineages. Nature 433: 647-653.
209. Bearzi C, Rota M, Hosoda T, Tillmanns J, Nascirnbene A, et al. (2007) Human cardiac stem cells. Proc Natl Acad Sci U S A 104: 14068-14073.
210. Qyang Y, Martin-Puig S, Chiravuri M, Chen S, Xu H, et al. (2007) The renewal and differentiation of Isl1(+) cardiovascular progenitors are controlled by a Wnt/beta-catenin pathway. Cell Stem Cell 1: 165-179.
211. Chen S, Fang W, Ye F, Liu Y, Qian J, et al. (2004) Effect on left ventricular function of intracoronary transplantation of autologous bone marrow mesenchymal stem cell in patients with acute myocardial infarction. Am J Cardiol 94: 92-95.
212. Berry MF, Engler AJ, Woo YJ, Pirolli TJ, Bish LT, et al. (2006) Mesenchymal stem cell injection after myocardial infarction improves myocardial compliance. Am J Physiol -Heart Circul Physiol 290: H2196-H2203.
213. Zhang S, Ge J, Sun A, Xu D, Qian J, et al. (2006) Comparison of various kinds of bone marrow stem cells for the repair of infarcted myocardium: Single clonally purified non-hematopoietic mesenchymal stem cells serve as a superior source. J Cell Biochem 99: 1132-1147.
214. Hou M, Yang K, Zhang H, Zhu W, Duan F, et al. (2007) Transplantation of mesenchymal stem cells from human bone marrow improves damaged heart function in rats. Int J Cardiol 115: 220-228.
215. Simpson D, Liu H, Fan TM, Nerem R, Dudley SC, Jr. (2007) A tissue engineering approach to progenitor cell delivery results in significant cell engraftment and improved myocardial remodeling. Stem Cells 25: 2350-2357.
216. Gaebel R, Furlani D, Sorg H, Polchow B, Frank J, et al. (2011) Cell origin of human mesenchymal stem cells determines a different healing performance in cardiac regeneration. PLoS One 6: e15652.
217. Grinnemo K, Mansson-Broberg A, Leblanc K, Corbascio M, Wardell E, et al. (2006) Human mesenchymal stem cells do not differentiate into cardiomyocytes in a cardiac ischemic xenomodel. Ann Med 38: 144-153.
218. Yoon Y, Park J, Tkebuchava T, Luedeman C, Losordo D. (2004) Unexpected severe calcification after transplantation of bone marrow cells in acute myocardial infarction. Circulation 109: 3154-3157.
219. Breitbach M, Bostani T, Roell W, Xia Y, Dewald O, et al. (2007) Potential risks of bone marrow cell transplantation into infarcted hearts. Blood 110: 1362-1369.
220. Shim WSN, Jiang S, Wong P, Tan J, Chua YL, et al. (2004) Ex vivo differentiation of human adult bone marrow stem cells into cardiomyocyte-like cells. Biochem Biophys Res Commun 324: 481-488.
221. Mohanty S, Bose S, Jain KG, Bhargava B, Airan B. (2013) TGF beta 1 contributes to cardiomyogenic-like differentiation of human bone marrow mesenchymal stem cells. Int J Cardiol 163: 93-99.

222. Antonitsis P, Loannidou-Papagiannaki E, Kaidogou A, Charokopos N, Kalogeridis A, et al. (2008) Cardiomyogenic potential of human adult bone marrow mesenchymal stem cells in vitro. Thorac Cardiovasc Surg 56: 77-82.
223. Xu WR, Zhang XR, Qian H, Zhu W, Sun XC, et al. (2004) Mesenchymal stem cells from adult human bone marrow differentiate into a cardiomyocyte phenotype in vitro. Exp Biol Med 229: 623-631.
224. Martin-Rendon E, Sweeney D, Lu F, Girdlestone J, Navarrete C, et al. (2008) 5-azacytidine-treated human mesenchymal Stem/progenitor cells derived from umbilical cord, cord blood and bone marrow do not generate cardiomyocytes in vitro at high frequencies. Vox Sang 95: 137-148.
225. Balana B, Nicoletti C, Zahanich I, Graf EM, Christ T, et al. (2006) 5-azacytidine induces changes in electrophysiological properties of human mesenchymal stem cells. Cell Res 16: 949-960.
226. Liu Y, Song J, Liu W, Wan Y, Chen X, et al. (2003) Growth and differentiation of rat bone marrow stromal cells: Does 5-azacytidine trigger their cardiomyogenic differentiation? Cardiovasc Res 58: 460-468.
227. Fukuhara S, Tomita S, Yamashiro S, Morisaki T, Yutani C, et al. (2003) Direct cell-cell interaction of cardiomyocytes is key for bone marrow stromal cells to go into cardiac lineage in vitro. J Thorac Cardiovasc Surg 125: 1470-1480.
228. Rangappa S, Entwistle JWC, Wechsler AS, Kresh JY. (2003) Cardiomyocyte-mediated contact programs human mesenchymal stem cells to express cardiogenic phenotype. J Thorac Cardiovasc Surg 126: 124-132.
229. Plotnikov EY, Khryapenkova TG, Vasileva AK, Marey MV, Galkina SI, et al. (2008) Cell-to-cell cross-talk between mesenchymal stem cells and cardiomyocytes in co-culture. J Cell Mol Med 12: 1622-1631.
230. Genovese JA, Spadaccio C, Chachques E, Schussler O, Carpentier A, et al. (2009) Cardiac pre-differentiation of human mesenchymal stem cells by electrostimulation. Front Biosci 14: 2996-3002.
231. Mooney E, Mackle JN, Blond DJP, O'Cearbhaill E, Shaw G, et al. (2012) The electrical stimulation of carbon nanotubes to provide a cardiomimetic cue to MSCs. Biomaterials 33: 6132-6139.
232. Motamedi R, Azadbakht M, Fathi F, Amini A, Ghaidari MI, et al. (2010) In vitro differentiation of human bone marrow-derived mesenchymal stem cells into cardiomyocyte-like cells. Yakhteh 12: 387-394.
233. Behfar A, Yamada S, Crespo-Diaz R, Nesbitt JJ, Rowe LA, et al. (2010) Guided cardiopoiesis enhances therapeutic benefit of bone marrow human mesenchymal stem cells in chronic myocardial infarction. J Am Coll Cardiol 56: 721-734.
234. Keller G, Kennedy M, Papayannopoulou T, Wiles M. (1993) Hematopoietic commitment during embryonic stem-cell differentiation in culture. Mol Cell Biol 13: 473-486.
235. Wartenberg M, Gunther J, Hescheler J, Sauer H. (1998) The embryoid body as a novel in vitro assay system for antiangiogenic agents. Lab Invest 78: 1301-1314.

236. Wobus AM, Kleppisch T, Maltsev V, Hescheler J. (1994) Cardiomyocyte-like cells differentiated in-vitro from embryonic carcinoma-cells P19 are characterized by functional expression of adrenoceptors and Ca2+ channels. In Vitro Cellular & Developmental Biology-Animal 30A: 425-434.
237. Keller GM. (1995) In-vitro differentiation of embryonic stem-cells. Curr Opin Cell Biol 7: 862-869.
238. Itskovitz-Eldor J, Schuldiner M, Karsenti D, Eden A, Yanuka O, et al. (2000) Differentiation of human embryonic stem cells into embryoid bodies comprising the three embryonic germ layers. Mol Med 6: 88-95.
239. Saleh FA, Genever PG. (2011) Turning round: Multipotent stromal cells, a three-dimensional revolution? Cytotherapy 13: 903-912.
240. Wang WJ, Itaka K, Ohba S, Nishiyama N, Chung UI, et al. (2009) 3D spheroid culture system on micropatterned substrates for improved differentiation efficiency of multipotent mesenchymal stem cells. Biomaterials 30: 2705-2715.
241. Burns JS, Rasmussen PL, Larsen KH, Schroder HD, Kassem M. (2010) Parameters in three-dimensional osteospheroids of telomerized human mesenchymal (stromal) stem cells grown on osteoconductive scaffolds that predict in vivo bone-forming potential. Tissue Engineering Part a 16: 2331-2342.
242. Hildebrandt C, Bueth H, Cho S, Impidjati, Thielecke H. (2010) Detection of the osteogenic differentiation of mesenchymal stem cells in 2D and 3D cultures by electrochemical impedance spectroscopy. J Biotechnol 148: 83-90.
243. Frith JE, Thomson B, Genever PG. (2010) Dynamic three-dimensional culture methods enhance mesenchymal stem cell properties and increase therapeutic potential. Tissue Engineering Part C-Methods 16: 735-749.
244. Hildebrandt C, Bueth H, Thielecke H. (2011) A scaffold-free in vitro model for osteogenesis of human mesenchymal stem cells. Tissue Cell 43: 91-100.
245. Kabiri M, Kul B, Lott WB, Futrega K, Ghanavi P, et al. (2012) 3D mesenchymal stem/stromal cell osteogenesis and autocrine signalling. Biochem Biophys Res Commun 419: 142-147.
246. Hermann A, Gastl R, Liebau S, Popa M, Fiedler J, et al. (2004) Efficient generation of neural stem cell-like cells from adult human bone marrow stromal cells. J Cell Sci 117: 4411-4422.
247. Bartosh TJ, Ylostalo JH, Mohammadipoor A, Bazhanov N, Coble K, et al. (2010) Aggregation of human mesenchymal stromal cells (MSCs) into 3D spheroids enhances their antiinflammatory properties. Proc Natl Acad Sci U S A 107: 13724-13729.
248. Potapova IA, Doronin SV, Kelly DJ, Rosen AB, Schuldt AJT, et al. (2008) Enhanced recovery of mechanical function in the canine heart by seeding an extracellular matrix patch with mesenchymal stem cells committed to a cardiac lineage. American Journal of Physiology-Heart and Circulatory Physiology 295: H2257-H2263.

249. Kuznetsov S, Krebsbach P, Satomura K, Kerr J, Riminucci M, et al. (1997) Single-colony derived strains of human marrow stromal fibroblasts form bone after transplantation in vivo. J Bone Miner Res 12: 1335-1347.
250. Mets T, Verdonk G. (1981) In vitro aging of human-bone marrow derived stromal cells. Mech Ageing Dev 16: 81-89.
251. Carmeliet P, Dor Y, Herbert J, Fukumura D, Brusselmans K, et al. (1998) Role of HIF-1 alpha or in hypoxia-mediated apoptosis, cell proliferation and tumour angiogenesis. Nature 394: 485-490.
252. Mastitskaya S, Denecke B. (2009) Human spongiosa mesenchymal stem cells fail to generate cardiomyocytes in vitro. J Negat Results Biomed 8: 11.
253. Bayes-Genis A, Roura S, Soler-Botija C, Farre J, Hove-Madsen L, et al. (2005) Identification of cardiomyogenic lineage markers in untreated human bone marrow-derived mesenchymal stem cells. Transplant Proc 37: 4077-4079.
254. Jagatheesan G, Rajan S, Wieczorek DF. (2010) Investigations into tropomyosin function using mouse models. J Mol Cell Cardiol 48: 893-898.
255. Wang J, Shaner N, Mittal B, Zhou Q, Chen J, et al. (2005) Dynamics of Z-band based proteins in developing skeletal muscle cells. Cell Motil Cytoskeleton 61: 34-48.
256. Sanger JW, Kang S, Siebrands CC, Freeman N, Du A, et al. (2005) How to build a myofibril. J Muscle Res Cell Motil 26: 343-354.
257. Volk T, Geiger B. (1984) A 135-kd-membrane protein of intercellular adherens junctions. EMBO J 3: 2249-2260.
258. Radice G, Rayburn H, Matsunami H, Knudsen K, Takeichi M, et al. (1997) Developmental defects in mouse embryos lacking N-cadherin. Dev Biol 181: 64-78.
259. Kostetskii I, Li J, Xiong Y, Zhou R, Ferrari V, et al. (2005) Induced deletion of the N-cadherin gene in the heart leads to dissolution of the intercalated disc structure. Circ Res 96: 346-354.
260. Reaume A, Desousa P, Kulkarni S, Langille B, Zhu D, et al. (1995) Cardiac malformation in neonatal mice lacking Connexin43. Science 267: 1831-1834.
261. Lyons I, Parsons L, Hartley L, Li R, Andrews J, et al. (1995) Myogenic and morphogenetic defects in the heart tubes of murine embryos lacking the homeo box gene Nkx2-5. Genes Dev 9: 1654-1666.
262. Lin Q, Schwarz J, Bucana C, Olson E. (1997) Control of mouse cardiac morphogenesis and myogenesis by transcription factor MEF2C. Science 276: 1404-1407.
263. Kuo C, Morrisey E, Anandappa R, Sigrist K, Lu M, et al. (1997) GATA4 transcription factor is required for ventral morphogenesis and heart tube formation. Genes Dev 11: 1048-1060.
264. Weitzer G, Milner D, Kim J, Bradley A, Capetanaki Y. (1995) Cytoskeletal control of myogenesis: A desmin null mutation blocks the myogenic pathway during embryonic stem cell differentiation. Dev Biol 172: 422-439.

265. Furst D, Osborn M, Weber K. (1989) Myogenesis in the mouse embryo - differential onset of expression of myogenic proteins and the involvement of titin in myofibril assembly. J Cell Biol 109: 517-527.
266. Wang C, Chen C, Hwang S, Lin W, Huang C, et al. (2009) Spherically symmetric mesenchymal stromal cell bodies inherent with endogenous extracellular matrices for cellular cardiomyoplasty. Stem Cells 27: 724-732.
267. Eschenhagen T, Fink C, Remmers U, Scholz H, Wattchow J, et al. (1997) Three-dimensional reconstitution of embryonic cardiomyocytes in a collagen matrix: A new heart muscle model system. Faseb Journal 11: 683-694.
268. Frenkel SR, Toolan B, Menche D, Pitman MI, Pachence JM. (1997) Chondrocyte transplantation using a collagen bilayer matrix for cartilage repair. J Bone Joint Surg -Br Vol 79B: 831-836.
269. Wakitani S, Goto T, Young RG, Mansour JM, Goldberg VM, et al. (1998) Repair of large full-thickness articular cartilage defects with allograft articular chondrocytes embedded in a collagen gel. Tissue Eng 4: 429-444.
270. Radisic M, Park H, Shing H, Consi T, Schoen FJ, et al. (2004) Functional assembly of engineered myocardium by electrical stimulation of cardiac myocytes cultured on scaffolds. Proc Natl Acad Sci U S A 101: 18129-18134.
271. Li RK, Jia ZQ, Weisel RD, Mickle DA, Choi A, et al. (1999) Survival and function of bioengineered cardiac grafts. Circulation 100: II63-9.
272. Awad HA, Wickham MQ, Leddy HA, Gimble JM, Guilak F. (2004) Chondrogenic differentiation of adipose-derived adult stem cells in agarose, alginate, and gelatin scaffolds. Biomaterials 25: 3211-3222.
273. Rowley JA, Madlambayan G, Mooney DJ. (1999) Alginate hydrogels as synthetic extracellular matrix materials. Biomaterials 20: 45-53.
274. Leor J, Aboulafia-Etzion S, Dar A, Shapiro L, Barbash IM, et al. (2000) Bioengineered cardiac grafts: A new approach to repair the infarcted myocardium? Circulation 102: III56-61.
275. Cao YL, Vacanti JP, Paige KT, Upton J, Vacanti CA. (1997) Transplantation of chondrocytes utilizing a polymer-cell construct to produce tissue-engineered cartilage in the shape of a human ear. Plast Reconstr Surg 100: 297-302.
276. Freed LE, Vunjaknovakovic G, Biron RJ, Eagles DB, Lesnoy DC, et al. (1994) Biodegradable polymer scaffolds for tissue engineering. Bio-Technology 12: 689-693.
277. Carrier RL, Papadaki M, Rupnick M, Schoen FJ, Bursac N, et al. (1999) Cardiac tissue engineering: Cell seeding, cultivation parameters, and tissue construct characterization. Biotechnol Bioeng 64: 580-589.
278. Vunjak-Novakovic G, Martin I, Obradovic B, Treppo S, Grodzinsky AJ, et al. (1999) Bioreactor cultivation conditions modulate the composition and mechanical properties of tissue-engineered cartilage. J Orthop Res 17: 130-138.
279. Chu CR, Coutts RD, Yoshioka M, Harwood FL, Monosov AZ, et al. (1995) Articular-cartilage repair using allogeneic perichondrocyte-seeded biodegradable

porous polylactic acid (pla) - a tissue-engineering study. J Biomed Mater Res 29: 1147-1154.
280. Sittinger M, Reitzel D, Dauner M, Hierlemann H, Hammer C, et al. (1996) Resorbable polyesters in cartilage engineering: Affinity and biocompatibility of polymer fiber structures to chondrocytes. J Biomed Mater Res 33: 57-63.
281. Lu HH, Cooper JA, Manuel S, Freeman JW, Attawia MA, et al. (2005) Anterior cruciate ligament regeneration using braided biodegradable scaffolds: In vitro optimization studies. Biomaterials 26: 4805-4816.
282. Hutmacher DW, Schantz T, Zein I, Ng KW, Teoh SH, et al. (2001) Mechanical properties and cell cultural response of polycaprolactone scaffolds designed and fabricated via fused deposition modeling. J Biomed Mater Res 55: 203-216.
283. Ishii O, Shin M, Sueda T, Vacanti JP. (2005) In vitro tissue engineering of a cardiac graft using a degradable scaffold with an extracellular matrix-like topography. Journal of Thoracic and Cardiovascular Surgery 130: 1358-1363.
284. Williams JM, Adewunmi A, Schek RM, Flanagan CL, Krebsbach PH, et al. (2005) Bone tissue engineering using polycaprolactone scaffolds fabricated via selective laser sintering. Biomaterials 26: 4817-4827.
285. Xu CY, Inai R, Kotaki M, Ramakrishna S. (2004) Aligned biodegradable nanofibrous structure: A potential scaffold for blood vessel engineering. Biomaterials 25: 877-886.
286. Jeong SI, Kim SH, Kim YH, Jung Y, Kwon JH, et al. (2004) Manufacture of elastic biodegradable PLCL scaffolds for mechano-active vascular tissue engineering. J Biomater Sci -Polym Ed 15: 645-660.
287. Bhang SH, Lim JS, Choi CY, Kwon YK, Kim B. (2007) The behavior of neural stem cells on biodegradable synthetic polymers. Journal of Biomaterials Science-Polymer Edition 18: 223-239.
288. Fidkowski C, Kaazempur-Mofrad MR, Borenstein J, Vacanti JP, Langer R, et al. (2005) Endothelialized microvasculature based on a biodegradable elastomer. Tissue Eng 11: 302-309.
289. Bettinger CJ, Weinberg EJ, Kulig KM, Vacanti JP, Wang YD, et al. (2006) Three-dimensional microfluidic tissue-engineering scaffolds using a flexible biodegradable polymer. Adv Mater 18: 165-169.
290. Gao J, Crapo PM, Wang YD. (2006) Macroporous elastomeric scaffolds with extensive micropores for soft tissue engineering. Tissue Engineering 12: 917-925.
291. Engelmayr GC, Cheng MY, Bettinger CJ, Borenstein JT, Langer R, et al. (2008) Accordion-like honeycombs for tissue engineering of cardiac anisotropy. Nature Materials 7: 1003-1010.
292. Yang C, Sodian R, Fu P, Luders C, Lemke T, et al. (2006) In vitro fabrication of a tissue engineered human cardiovascular patch for future use in cardiovascular surgery. Ann Thorac Surg 81: 57-64.
293. Asran AS, Razghandi K, Aggarwal N, Michler GH, Groth T. (2010) Nanofibers from blends of polyvinyl alcohol and polyhydroxy butyrate as potential scaffold material for tissue engineering of skin. Biomacromolecules 11: 3413-3421.

294. Grad S, Kupcsik L, Gorna K, Gogolewski S, Alini M. (2003) The use of biodegradable polyurethane scaffolds for cartilage tissue engineering: Potential and limitations. Biomaterials 24: 5163-5171.
295. Fisher JP, Vehof JWM, Dean D, van der Waerden JPCM, Holland TA, et al. (2002) Soft and hard tissue response to photocrosslinked poly(propylene fumarate) scaffolds in a rabbit model. J Biomed Mater Res 59: 547-556.
296. Vehof JWM, Fisher JP, Dean D, van der Waerden JPCM, Spauwen PHM, et al. (2002) Bone formation in transforming growth factor beta-1-coated porous poly(propylene fumarate) scaffolds. J Biomed Mater Res 60: 241-251.
297. Kenley RA, Lee MO, Mahoney TR, Sanders LM. (1987) Poly(lactide-co-glycolide) decomposition kinetics invivo and invitro. Macromolecules 20: 2398-2403.
298. Wang YD, Kim YM, Langer R. (2003) In vivo degradation characteristics of poly(glycerol sebacate). Journal of Biomedical Materials Research Part A 66A: 192-197.
299. Jeong SI, Kim BS, Kang SW, Kwon JH, Lee YM, et al. (2004) In vivo biocompatibilty and degradation behavior of elastic poly(L-lactide-co-epsilon-caprolactone) scaffolds. Biomaterials 25: 5939-5946.
300. Wang Y, Ameer GA, Sheppard BJ, Langer R. (2002) A tough biodegradable elastomer. Nat Biotechnol 20: 602-606.
301. Chen QZ, Bismarck A, Hansen U, Junaid S, Tran MQ, et al. (2008) Characterisation of a soft elastomer poly(glycerol sebacate) designed to match the mechanical properties of myocardial tissue. Biomaterials 29: 47-57.
302. Sun Z, Chen C, Sun M, Ai C, Lu X, et al. (2009) The application of poly (glycerol-sebacate) as biodegradable drug carrier. Biomaterials 30: 5209-5214.
303. Motlagh D, Yang J, Lui KY, Webb AR, Ameer GA. (2006) Hemocompatibility evaluation of poly(glycerol-sebacate) in vitro for vascular tissue engineering. Biomaterials 27: 4315-4324.
304. Kemppainen JM, Hollister SJ. (2010) Tailoring the mechanical properties of 3D-designed poly(glycerol sebacate) scaffolds for cartilage applications. J Biomed Mater Res Part A 94A: 9-18.
305. Sundback CA, Shyu JY, Wang YD, Faquin WC, Langer RS, et al. (2005) Biocompatibility analysis of poly(glycerol sebacate) as a nerve guide material. Biomaterials 26: 5454-5464.
306. Sales VL, Engelmayr GC, Jr., Johnson JA, Jr., Gao J, Wang Y, et al. (2007) Protein precoating of elastomeric tissue-engineering scaffolds increased cellularity, enhanced extracellular matrix protein production, and differentially regulated the phenotypes of circulating endothelial progenitor cells. Circulation 116: I55-I63.
307. Yi F, LaVan DA. (2008) Poly(glycerol sebacate) nanofiber scaffolds by core/shell electrospinning. Macromol Biosci 8: 803-806.
308. Radisic M, Park H, Chen F, Salazar-Lazzaro JE, Wang Y, et al. (2006) Biomirnetic approach to cardiac tissue engineering: Oxygen carriers and channeled scaffolds. Tissue Eng 12: 2077-2091.

309. Bettinger CJ, Orrick B, Misra A, Langer R, Borenstein JT. (2006) Micro fabrication of poly (glycerol-sebacate) for contact guidance applications. Biomaterials 27: 2558-2565.
310. Pomerantseva I, Krebs N, Hart A, Neville CM, Huang AY, et al. (2009) Degradation behavior of poly(glycerol sebacate). J Biomed Mater Res Part A 91A: 1038-1047.
311. Middleton JC, Tipton AJ. (2000) Synthetic biodegradable polymers as orthopedic devices. Biomaterials 21: 2335-2346.
312. Pitt CG, Gratzl MM, Kimmel GL, Surles J, Schindler A. (1981) Aliphatic polyesters II. the degradation of poly(dl-lactide), poly(epsilon-caprolactone), and their copolymers in vivo. Biomaterials 2: 215-220.
313. Gunatillake PA, Adhikari R. (2003) Biodegradable synthetic polymers for tissue engineering. Eur Cell Mater 5: 1-16; discussion 16.
314. Garlotta D. (2001) A literature review of poly(lactic acid). Journal of Polymers and the Environment 9: 63-84.
315. Gan ZH, Yu DH, Zhong ZY, Liang QZ, Jing XB. (1999) Enzymatic degradation of poly(epsilon-caprolactone)/poly(DL-lactide) blends in phosphate buffer solution. Polymer 40: 2859-2862.
316. Liu LJ, Li SM, Garreau H, Vert M. (2000) Selective enzymatic degradations of poly(L-lactide) and poly(epsilon-caprolactone) blend films. Biomacromolecules 1: 350-359.
317. Wang L, Ma W, Gross R, McCarthy S. (1998) Reactive compatibilization of biodegradable blends of poly(lactic acid) and poly(epsilon-caprolactone). Polym Degrad Stab 59: 161-168.
318. Chandy T, Wilson R, Rao G, Das G. (2002) Changes in cisplatin delivery due to surface-coated poly (lactic acid)-poly(epsilon-caprolactone) microspheres. J Biomater Appl 16: 275-291.
319. Cai Q, Bei J, Wang S. (2002) In vitro study on the drug release behavior from polylactide-based blend matrices. Polym Adv Technol 13: 534-540.
320. Fialho SL, Prado LMF, Ferreira DS, Pereira BG, Faraco AAG, et al. (2010) Evaluation of biodegradable implants based on polymer blends: Development, characterization and in vitro release studies. Lat Am J Pharm 29: 694-700.
321. Shen Y, Sun W, Zhu K, Shen Z. (2000) Regulation of biodegradability and drug release behavior of aliphatic polyesters by blending. J Biomed Mater Res 50: 528-535.
322. Sun M, Downes S. (2009) Physicochemical characterisation of novel ultra-thin biodegradable scaffolds for peripheral nerve repair. J Mater Sci -Mater Med 20: 1181-1192.
323. Sun M, Kingham PJ, Reid AJ, Armstrong SJ, Terenghi G, et al. (2010) In vitro and in vivo testing of novel ultrathin PCL and PCL/PLA blend films as peripheral nerve conduit. J Biomed Mater Res Part A 93A: 1470-1481.

324. Ishaug SL, Crane GM, Miller MJ, Yasko AW, Yaszemski MJ, et al. (1997) Bone formation by three-dimensional stromal osteoblast culture in biodegradable polymer scaffolds. J Biomed Mater Res 36: 17-28.
325. Stitzel J, Liu L, Lee SJ, Komura M, Berry J, et al. (2006) Controlled fabrication of a biological vascular substitute. Biomaterials 27: 1088-1094.
326. Lu L, Garcia C, Mikos A. (1999) In vitro degradation of thin poly(DL-lactic-co-glycolic acid) films. J Biomed Mater Res 46: 236-244.
327. Ishaug-Riley SL, Okun LE, Prado G, Applegate MA, Ratcliffe A. (1999) Human articular chondrocyte adhesion and proliferation on synthetic biodegradable polymer films. Biomaterials 20: 2245-2256.
328. Fu K, Pack DW, Klibanov AM, Langer R. (2000) Visual evidence of acidic environment within degrading poly(lactic-co-glycolic acid) (PLGA) microspheres. Pharm Res 17: 100-106.
329. Cohen S, Yoshioka T, Lucarelli M, Hwang L, Langer R. (1991) Controlled delivery systems for proteins based on poly(lactic glycolic acid) microspheres. Pharm Res 8: 713-720.
330. Park TG. (1995) Degradation of poly(lactic-co-glycolic acid) microspheres - effect of copolymer composition. Biomaterials 16: 1123-1130.
331. Thomson RC, Yaszemski MJ, Powers JM, Mikos AG. (1995) Fabrication of biodegradable polymer scaffolds to engineer trabecular bone. Journal of Biomaterials Science-Polymer Edition 7: 23-38.
332. Widmer M, Gupta P, Lu L, Meszlenyi R, Evans G, et al. (1998) Manufacture of porous biodegradable polymer conduits by an extrusion process for guided tissue regeneration. Biomaterials 19: 1945-1955.
333. Wu XS, Wang N. (2001) Synthesis, characterization, biodegradation, and drug delivery application of biodegradable lactic/glycolic acid polymers. part II: Biodegradation. Journal of Biomaterials Science-Polymer Edition 12: 21-34.
334. Webb AR, Yang J, Ameer GA. (2004) Biodegradable polyester elastomers in tissue engineering. Expert Opinion on Biological Therapy 4: 801-812.
335. Miller RA, Brady JM, Cutright DE. (1977) Degradation rates of oral resorbable implants (polylactates and polyglycolates) - rate modification with changes in pla-pga copolymer ratios. J Biomed Mater Res 11: 711-719.
336. Gorna K, Gogolewski S. (2006) Biodegradable porous polyurethane scaffolds for tissue repair and regeneration. J Biomed Mater Res Part A 79A: 128-138.
337. McDevitt TC, Woodhouse KA, Hauschka SD, Murry CE, Stayton PS. (2003) Spatially organized layers of cardiomyocytes on biodegradable polyurethane films for myocardial repair. Journal of Biomedical Materials Research Part A 66A: 586-595.
338. Alperin C, Zandstra PW, Woodhouse KA. (2005) Polyurethane films seeded with embryonic stem cell-derived cardiomyocytes for use in cardiac tissue engineering applications. Biomaterials 26: 7377-7386.
339. Stokes K, McVenes R, Anderson JM. (1995) Polyurethane elastomer biostability. J Biomater Appl 9: 321-354.

340. Hergenrother R, Wabers H, Cooper S. (1993) Effect of hard segment chemistry and strain on the stability of polyurethanes - invivo biostability. Biomaterials 14: 449-458.
341. Brandwood A, Meijs G, Gunatillake P, Noble K, Schindhelm K, et al. (1994) In-vivo evaluation of polyurethanes based on novel macrodiols and mdi rid A-1375-2008. J Biomater Sci -Polym Ed 6: 41-54.
342. Takahashi K, Taniguchi I, Miyamoto M, Kimura Y. (2000) Melt/solid polycondensation of glycolic acid to obtain high-molecular-weight poly(glycolic acid). Polymer 41: 8725-8726, 8727, 8728.
343. Kokubo T, Kushitani H, Sakka S, Kitsugi T, Yamamuro T. (1990) Solutions able to reproduce in vivo surface-structure changes in bioactive glass-ceramic A-W. J Biomed Mater Res 24: 721-734.
344. Lam C, Mo X, Teoh S, Hutmacher D. (2002) Scaffold development using 3D printing with a starch-based polymer Mater Sci Eng C-Biomimetic Supramol Syst 20: 49-56.
345. Mathieu L, Mueller T, Bourban P, Pioletti D, Muller R, et al. (2006) Architecture and properties of anisotropic polymer composite scaffolds for bone tissue engineering. Biomaterials 27: 905-916.
346. Kang Y, Yang J, Khan S, Anissian L, Ameer G. (2006) A new biodegradable polyester elastomer for cartilage tissue engineering Journal of Biomedical Materials Research Part a 77A: 331-339.
347. Wu LB, Ding JD. (2004) In vitro degradation of three-dimensional porous poly(D,L-lactide-co-glycolide) scaffolds for tissue engineering. Biomaterials 25: 5821-5830.
348. Garkhal K, Verma S, Jonnalagadda S, Kumar N. (2007) Fast degradable poly(L-lactide-co-epsilon-caprolactone) microspheres for tissue engineering: Synthesis, characterization, and degradation behavior. Journal of Polymer Science Part A-Polymer Chemistry 45: 2755-2764.
349. Tan HY, Widjaja E, Boey F, Loo SCJ. (2009) Spectroscopy techniques for analyzing the hydrolysis of PLGA and PLLA. Journal of Biomedical Materials Research Part B-Applied Biomaterials 91B: 433-440.
350. Jaafar IH, Ammar MM, Jedlicka SS, Pearson RA, Coulter JP. (2010) Spectroscopic evaluation, thermal, and thermomechanical characterization of poly(glycerol-sebacate) with variations in curing temperatures and durations. J Mater Sci 45: 2525-2529.
351. Ye WP, Du FS, Jin JY, Yang JY, Xu Y. (1997) In vitro degradation of poly(caprolactone), poly(lactide) and their block copolymers: Influence of composition, temperature and morphology. React Funct Polym 32: 161-168.
352. Chen C, Chueh J, Tseng H, Huang H, Lee S. (2003) Preparation and characterization of biodegradable PLA polymeric blends. Biomaterials 24: 1167-1173.

353. Lopez-Rodriguez N, Lopez-Arraiza A, Meaurio E, Sarasua JR. (2006) Crystallization, morphology, and mechanical behavior of polylactide/poly(epsilon-caprolactone) blends. Polym Eng Sci 46: 1299-1308.
354. Park J, Todo M. (2011) Compressive mechanical properties and deformation behavior of porous polymer blends of poly(epsilon-caprolactone) and poly(l-lactic acid). J Mater Sci 46: 7850-7857.
355. Mehta R, Thanoo B, DeLuca P. (1996) Peptide containing microspheres from low molecular weight and hydrophilic poly(d,l-lactide-co-glycolide). J Controlled Release 41: 249-257.
356. Hiltz JA. (1998) Characterization of poly(ether)urethane thermoplastic elastomers. Defence Research Establishment Atlantic TM98/222, Grant 1GH: 1-38.

Vita

Courtney LeBlon was born on May 16, 1986 in New Brunswick, NJ to Vincent and Deirdre LeBlon. She earned a B.S. in Engineering Science- Biomedical Engineering from The College of New Jersey in May 2008 where she received the Armstrong Award for the highest grade point average in her major. She received her M.S. in Mechanical Engineering in 2010 from Lehigh. She plans to obtain her doctorate in Mechanical Engineering from Lehigh University in 2013.

Publications and Proceedings Papers

LeBlon, C. E., Fodor, C. R., Zhang, T., Zhang, X., Jedlicka, S.S. (2013) "Human Mesenchymal Stem Cell Elastic Modulus directs Differentiation Capacity." Submitted to BMC Cell Biology.

LeBlon, C. E., Jedlicka, S.S. (2013) "Cardiogenic Potential of Human Mesenchymal Stem Cells by Embryoid Body Formation." Submitted to *PLOS ONE*, in revision.

LeBlon, C. E., Pai, R., Fodor, C. R., Golding, A. S., Coulter, J. P., Jedlicka, S. S. (2013). "In Vitro Comparative Biodegradation Analysis of Salt-Leached Porous Polymer Scaffolds." Journal of Applied Polymer Science, 128(5), 2701-2712.

LeBlon, C. E., Fodor, C. R., Zhang, T., Zhang, X., Jedlicka, S. S. (2012) "Effect of Substrate Elasticity on *In Vitro* Aging of Human Mesenchymal Stem Cells." Materials Research Society 2012 Fall Meeting Proceedings.

Casey, M. E., Rodgers, J. W., **LeBlon, C. E.**, Coulter, J. P., Jedlicka, S. S. (2012) "Micro-injection Molded Polymeric Surfaces for the Maintenance of Human Mesenchymal Stem Cells (hMSCs)." Materials Research Society 2012 Fall Meeting Proceedings.

Przybylowski, C., Quinn, T., Callahan, A., Kaplan, M., Golding, A. S., Alesi, C., Ammar, M., **LeBlon, C. E.**, Guo, Y., Zhang, X., Jedlicka, S. S. (2012). "MC3T3 Preosteoblast Differentiation on Bone Morphogenetic Protein-2 Peptide Ormosils." Journal of Materials Chemistry, 22(21), 10672-10683.

Jaafar, I. H., **LeBlon, C. E.**, Wei, M., Ou-Yang, D., Coulter, J. P., & Jedlicka, S. S. (2011). "Improving fluorescence imaging of biological cells on biomedical polymers." Acta Biomaterialia, 7(4), 1588-1598.